



TECHNISCHE  
UNIVERSITÄT  
WIEN

Vienna University of Technology

# DIPLOMARBEIT

## **Electrochemische Stabilität der Stromableiter in protischen organischen Lösungsmitteln für Magnesium aufladbare Batterien**



**AUSTRIAN INSTITUTE  
OF TECHNOLOGY**

Ausgeführt am AIT Austrian Institute of Technology  
Giefinggasse 2, 1210 Wien

Unter Anleitung von  
Ao. Univ. Prof. Dipl.-Ing. Dr. Tech. Günter FAFILEK  
Assoc. Prof. Dipl. Ing. Dr. rer. nat. Atanaska TRIFONOVA

durch  
Seyma KILIC, BSc.  
Gerasdorferstraße 147/17 1210 Wien

Wien, November 2016

The true sign of intelligence is not knowledge  
but imagination.  
*Albert Einstein*

## **EIDESSTATTLICHE ERKLÄRUNG**

---

Hiermit erkläre ich an Eides statt, dass ich die vorliegende Diplomarbeit selbstständig verfasst, andere als die angegebenen Quellen und Hilfsmittel nicht benutzt und die den benutzten Quellen wörtlich und inhaltlich entnommenen Stellen als solche erkenntlich gemacht habe.

## **STATUTORY DECLARATION**

---

I declare that I have authored this thesis independently, that I have not used other than the declared sources / resources, and that I have explicitly marked all material which has been quoted either literally or by content from the used sources.

## ACKNOWLEDGEMENT

---

I want to thank ...

... Prof. Dr. G. Fafilek for being my thesis' supervisor and for his suggestion to work within this research group.

... Prof. Dr. A. Trifonova for giving me the chance to work within her research group and for giving me the opportunity to work on an interesting, up-to-date topic, for her guidance, and supervision.

... the Federal Ministry for Transport, Innovation and Technology (BMVIT) for the financial support for this project.

... Dr. Hristina Vasilchina for her guidance, patience, sharing her knowledge and experimental expertise.

... my husband Eser Kilic for his patience, encouragement and without him my study and this work would not have been possible.

... parents (especially mother) for their encouragement and trust. I will always be grateful for their financial support throughout my studies.

... God for giving me my well-behaved daughter Esma Kilic. At first I thought that I could not achieve my targets if I had a child. But I arrived at a snail`s pace in the end.

... my colleagues; Ilian Popov, Simeon Stankov, Zoltan Fakete, Raad Hamid, Joong-Hee Han, Ningxin Zhang at the Austrian Institute of Materials Technology for their helps.

... Ilian P. for his patience, sharing who always knows where to find everything and for the set up of my experiments.

... Simeon S. for his tips and helps regarding synthesis.

... Raad H. for XRD and XRF measurements.

## **KURZFASSUNG**

---

Im Rahmen dieser Masterarbeit wurde die elektrochemische Stabilität der Stromableiter in protischen organischen Lösungsmitteln für Magnesium aufladbare Batterien untersucht und optimiert. Diese Arbeit wurde am Materiallabor der AIT Austrian Institute of Technology ausgeführt. Ziel der Untersuchungen war es, die elektrochemische Aktivität potenzieller Insertionsmaterialien für ein neues Magnesium Energiespeichersystem zu entwickeln. Zuerst wurden die Korrosionsprozesse an Stromableitern für die positive Elektrode in verschiedenen protischen organischen Lösungsmitteln charakterisiert. Aufgrund dieser Ergebnisse wurden die besten geeigneten Stromableiter für die Elektrode gewählt und Elektroden mit einigen Kathodenmaterialien hergestellt. Diese Elektroden wurden in weiterer Folge elektrochemisch charakterisiert. Die Elektrodenpräparation, der Zellenbau in der Glovebox, Zyklovoltammetrie und galvanostatische Tests wurden durchgeführt.

## **ABSTRACT**

---

Within this master thesis, the electrochemical stability of current collectors in different protic organic solvents has been investigated and optimized. This work was executed at the Material Laboratory of Austrian Institute of Technology (AIT). The aim of this study is to develop the electrochemical activity of the potential insertion materials for new magnesium energy storage systems. First, the corrosion processes on the current collectors for the positive electrode in different protic organic solvents were characterized. The most appropriate current collectors were selected and electrodes with some cathode materials were fabricated. Then, the electrochemical characterization of the different compounds was carried out. The electrode preparation, the cell assembly in the glove box, the cyclic voltammetry and the galvanostatic tests were performed.

# TABLE OF CONTENTS

---

<b>1 Introduction</b> .....	1
1.1 Comparison of Mg, Li and other battery systems.....	2
1.2 Functional principle of a rechargeable Magnesium ion battery.....	4
1.3 Electrolytes of Magnesium ion batteries.....	6
1.3.1 All Phenyl Complex (APC) electrolyte.....	7
1.3.2 Magnesium hexamethyldisilazide (Mg-HMDS) electrolyte.....	9
1.3.3 Magnesium Aluminum Chloride Complex (MACC) electrolyte.....	11
1.4 Negative electrodes.....	12
1.5 Positive electrodes.....	13
1.5.1 Tunneled Manganese Oxides ( $\alpha\text{MnO}_2$ ).....	14
1.6 Current collectors.....	15
1.6.1 Corrosion.....	16
1.7 Electrochemical charecterization methods.....	20
1.7.1 Cyclic voltammetry.....	20
1.7.2 Evans diagrams.....	24
1.7.3 Galvanostatic cyclic voltammetry .....	24
1.7.4 Chronoamperometry (Stability test).....	26
<b>2 Experimental Section</b> .....	28
2.1 Corrosion processes of current collectors.....	28
2.1.1 Corrosion test with APC electrolyte.....	29
2.1.1.1 Glassy carbon with APC electrolyte.....	29
2.1.1.2 Titanium with APC electrolyte.....	31
2.1.1.3 Stainless steel with APC electrolyte.....	33
2.1.1.4 Copper with APC electrolyte.....	35
2.1.1.5 Nickel with APC electrolyte.....	37
2.1.1.6 Graphite foil with APC electrolyte.....	39
2.1.1.7 Carbon paper 1 with APC electrolyte.....	41

2.1.1.8 Carbon paper 2 with APC electrolyte.....	43
2.1.1.9 Carbon textile 1 with APC electrolyte.....	45
2.1.1.10 Carbon textile 2 (sorbent) with APC electrolyte.....	47
2.1.2 Comparison of current collectors with APC electrolyte.....	49
2.1.3 Stability tests of current collectors with APC electrolyte.....	51
2.1.3.1 Nickel.....	52
2.1.3.2 Glassy carbon.....	54
2.1.3.3 Graphite foil.....	56
2.1.3.4 Carbon textile 2 .....	58
2.1.4 Corrosion test with Mg-HMDS electrolyte.....	60
2.1.4.1 Glassy carbon.....	60
2.1.4.2 Graphite foil.....	62
2.1.4.3 Nickel.....	64
2.1.5 Corrosion test with MACC electrolyte.....	66
2.1.5.1 Glassy carbon.....	66
2.1.5.2 Graphite foil.....	68
2.1.5.3 Nickel.....	70
2.2 Electrochemical performance of cathode materials.....	72
2.2.1 Electrodes preparation.....	72
2.2.1.1 Slurry.....	72
2.2.1.1 Dry electrode .....	73
2.2.2 Comparison of results with literature.....	73
<b>4 Conclusions.....</b>	<b>75</b>
List of References .....	76





# 1 INTRODUCTION

---

Advanced energy storage systems like ion transfer batteries are required for use in electric vehicle and other applications. Most of the current electrochemical studies are relating to the promising lithium systems because of its low electrode potential and high specific charge. The complicated behavior of magnesium batteries can be better understood by comparison with lithium batteries.

The interest for rechargeable magnesium (Mg) batteries have rapidly increased because of being low cost batteries with high safety, having large theoretical capacity (2205 mAh/g), having very low standard electrode potential, being environment friendly and reliable[1].

One of the greatest success stories in electrochemistry is the development and commercialization of the lithium ion battery. In the future the rechargeable Mg battery is considered as a potential replacement for the lithium ion battery. In particular, consumer want better batteries for smart phones and other wearable gadgets that last longer at lower prize but also batteries for long range Electric Vehicles (EV). Especially the volumetric energy density of the battery is very important when considering applications where there is a limited space to accommodate it [2]. As in Table 1 showed, Mg has higher volumetric energy density (3837 Ah/l) than other metals. Moreover, magnesium is less flammable and explosive than lithium (Li). Therefore it would be a better choice for electric vehicles.

Another big advantage is that Mg reserves are over a hundred times larger in the earth's crust than for lithium. Unlike Li ion batteries, Mg ion batteries do not heat so much during fast charging or overcharging [3].

Nevertheless, the development of Mg ion batteries suffers from difficult problems related to the thermodynamic stable electrolyte systems up to 3V, the proper choice for current collector materials with high stability against corrosion. The big challenge currently is the finding of suitable cathode materials that can insert bivalent Mg ion [3].

In the first part of the theoretical part of this thesis, Magnesium, Lithium and other batteries are compared with respect to their theoretical properties and the main cell components of Mg ion cell are explained. Then the drawbacks of Mg ion battery development are described. Electrochemical characterization methods that are used in this study are also presented.

## 1.1 Comparison of Magnesium, Lithium and other battery systems

These properties are the fundamental parameters for comparison of the batteries.

- **Energy density** (kWh/l) or **Specific energy** (kWh/kg): is the amount of energy stored in a battery per unit volume or mass.
- **Cycleability** means that not to lose too much capacity after many cycles. It is measured in number of cycles until the normalized capacity falls under a defined threshold.
- **Battery capacity**: is a reference to the total amount of electric charge stored within a battery. It is rated in Ampere-hours (Ah), which is the product of:

$$\text{Ah} = \text{Current} \times \text{Hours to Total Discharge}$$

- **Specific capacity** (mAh/g) =  $(N \times F) / (\text{Atomic Weight})$  where,  
 N = Valency of the Material  
 F = Faraday constant = 96485 Coulombs/Mole  
 If this has to be expressed in terms of current, divide that by 3600  
 F = 26.801Ah/Mole

Theoretical Values	Lithium	Magnesium	Sodium
Cation Valence	1+	2+	1+
Atomic Weight(g/mol)	6.94	24.3	22.98
Specific Capacity (mAh/g)	3861	2205	1166
Specific Charge Anode (Ah/l)	2046	3837	1131
Electrode Potential (V)	-3.04	-2.38	-2.71
Natural Abundance (%)	0.006	1.94 (8th)	2.6 (6th)
Raw Material (\$/ton)	64000	2260	1200

**Table 1:** The comparison of theoretical parameters of Li, Mg, Na batteries

Due to thermodynamic reasons for the selection of the negative electrode (anode) material, light metals lithium, magnesium and sodium are preferred to common heavy battery metals, as zinc and cadmium because they have high specific charges. The most successful (rechargeability) of the Li battery was the use of lithium insertion electrode materials contrary to lithium metal, that called “lithium ion cells”. Li ion batteries have high cell voltages, high specific energies (>130Wh/kg), energy densities (>300 Wh/L) as well as the long cycle life (500 - 1000 charge/discharge cycles) that make their utilization admirable [4].

Figure 1 illustrates the evolution of Li ion technology and it is compared with nickel-metal hydride, nickel-cadmium and lead acid batteries. Also some new battery technologies are also defined. These are lithium-oxygen, lithium-sulphur, magnesium ion and advanced Li ion batteries. The predictions of the average energy density are also determined [5].

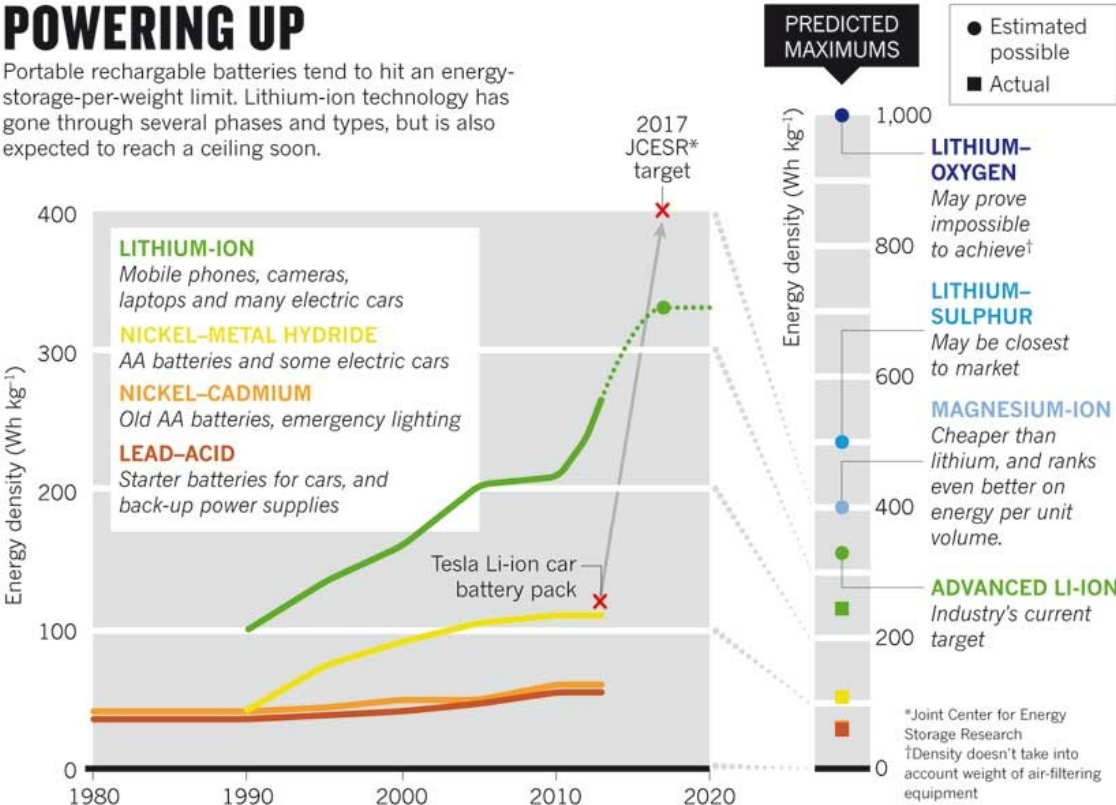


**Figure 1:** The comparison of energy density of Li ion, Ni-metal hydride, Ni-Cd, Lead acid, Mg ion, Li-S and Li-O batteries [5]

Lithium ion batteries have not enough energy density for electric vehicles (EV) development. In consideration of EVs development with a range and cost competitive to those of

conventional combustion engines, the advanced Li batteries will be required. As a result, post Li ion batteries (PLiB) were defined as batteries with a theoretical energy density higher than that of a Li ion battery concluding a carbon anode and a lithium cobalt oxide cathode (2000 Wh/l) [5]. The Holy Grail in battery research is the development of PLiB which may require shifting from alloys to pure metal anodes. Because of the inherent instability of Li metal (especially during charging), the commercializing a rechargeable battery containing a Li metal anode have been deterred. Unsuccessfully, batteries including Li metal anodes suffer from thermal runaway, which is characterized by temperatures quickly rising above the melting point of metallic Li [6]. This inherent safety problem can be related to dendrite formation on the Li metal anode which short-circuits the battery [7]. In order to moderate this intrinsic instability of batteries containing a Li metal anode, research shifted towards lithiated graphites and alloy-based anodes containing Si and Sn [8,9]. Therefore, one of the important challenges in the commercialization of PLiBs including a Li metal anode will be the prevention of dendritic growth; this is not a trivial task [7].

In contrast to Li metal, magnesium (Mg) metal anodes are not plagued by dendritic formation [10]. For example THF solutions of Grignard-based Mg compounds are used and it makes possible of using metallic Mg as an anode in rechargeable Mg batteries.

## **1.2 Functional principle of a rechargeable Magnesium ion battery**

The rechargeable magnesium battery is working functionally similar to the lithium ion battery and includes a reversible insertion / extraction of metal ions into / from a host matrix (electrode material) during the discharge / charge process.

This process is accompanied by a flow of ions through the electrolyte and is supported by a reduction / oxidation (redox reaction) of the host matrix with an electron flow through the external circuit (current collector) (Figure 2).

During the charging process, the molybdenum ions are oxidized and  $Mg^{2+}$  ions move to the anode side, where they deposit [11]. When the cell discharges and generates electricity, the  $Mg^{2+}$  ions move from the anode (dissolving) to the cathode and cause an electron flow through the external circuit. The open circuit voltage (OCV) of such a cell is given by the

difference in the chemical potential of magnesium in the cathode ( $\mu_{Mg(K)}$ ) and the anode ( $\mu_{Mg(A)}$ ):

$$V_{oc} = [(\mu_{Mg(K)}) - (\mu_{Mg(A)})] / nF, \text{ where } F = \text{Faraday constant and } n=2$$

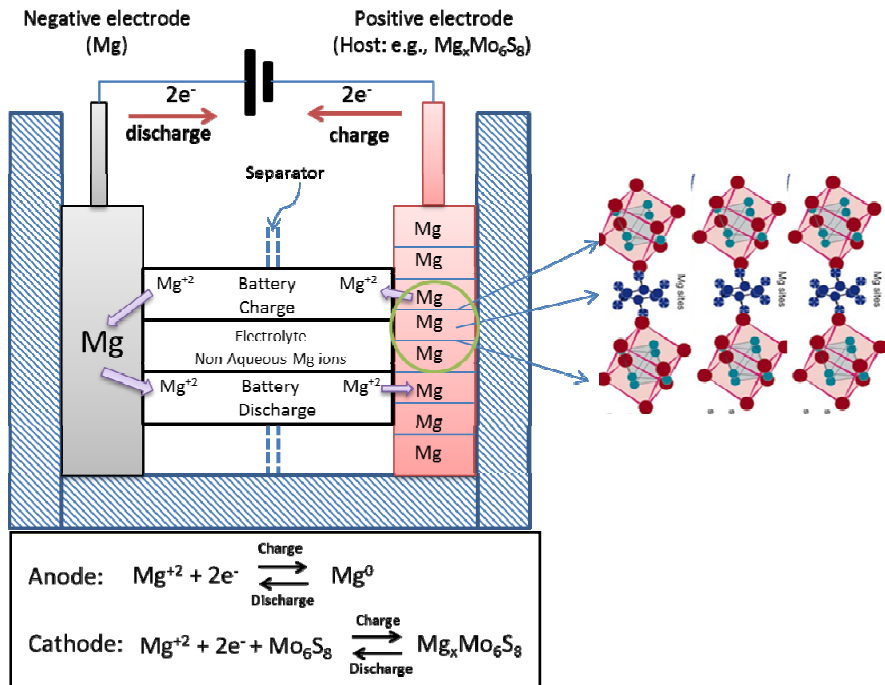


**Figure 2:** Schematic representation of a rechargeable magnesium ion battery [22]

Figure 2 shows the schematic energy diagram of a cell at open circuit voltage ( $V_{oc}$ ). The cell voltage  $V_{oc}$  is determined by the energies involved in both electron and  $Mg^{2+}$  ion transfer.

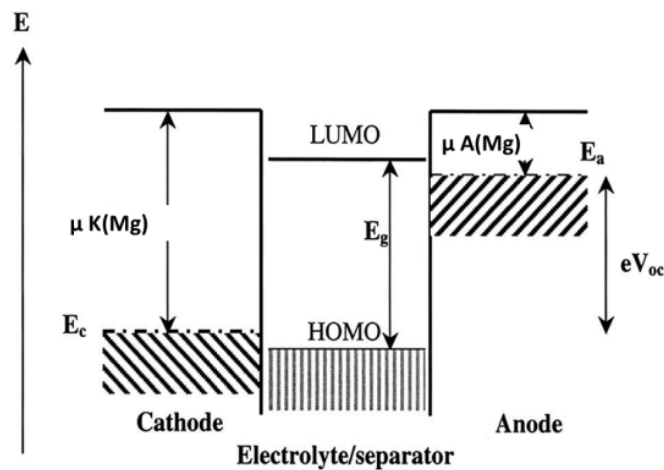


**Figure 3:** Schematic energy diagram of a magnesium cell at open circuit: HOMO and LUMO refer, respectively, to the highest occupied molecular orbital and the lowest unoccupied molecular orbital in the electrolyte;  $eV_{oc} < E_g$  [22].

The energy involved in electron transfer is related to the redox potential of the ion involved in  $\text{Mg}^{2+}$  ion transfer which is determined by the crystal structure and the coordination geometry of the host compound (the site into/from which the  $\text{Mg}^{2+}$  ions are inserted/extracted) [12].

The thermodynamic stability of the cell requires that the redox energies of the cathode and the anode lie within the band gap of the electrolyte (Figure 3). This does not result in any undesired side processes, such as reduction or oxidation of the electrolyte during the charge-discharge process.

### 1.3 Electrolytes of Magnesium ion batteries

The first report about a magnesium battery electrolyte that enables reversible electrochemical deposition-dissolution of magnesium was given in 1990s. Gregory et al introduced various electrolytes for a rechargeable magnesium battery initially guided by earlier reports on successful deposition of magnesium metal from the electrolysis of Grignard reagents [13].

In order to advance high energy density rechargeable Mg batteries, it is very essential to find an electrolyte system operating within a wide electrochemical window up to 3V with high coulombic efficiency for Mg deposition–dissolution processes [14]. Owing to the high chemical reactivity of Mg metal, only polar aprotic solvents are appropriate for preparation of the electrolytes for rechargeable Mg batteries [15].

The major difficulty in Mg ion battery is that unintended reduction of electrolyte components (organic solvents and impurities like water, oxygen, organics) precipitate as insoluble products that passivate the Mg electrode surface and block transport of both ions and electrons. This property is different from Li metal and Li-ion anodes that form passivating layers with electrolyte solution components which usually supply adequate Li ion transport between the solid and liquid phases (solid electrolyte interface – SEI) [16]. From this reason, passivating of the surface Mg cannot be plated reversible from an aprotic solution including simple ionic salts such as  $\text{MgCl}_2$ ,  $\text{Mg}(\text{ClO}_4)_2$ ,  $\text{Mg}(\text{CF}_3\text{SO}_2)_2$ , etc. [17]. The Mg electrode behaves reversible in tetrahydrofuran (THF) solution including Grignard salts

(RMgX, R=alkyl, aryl groups and X=Cl, Br, I) as it was reported by Gregory et al. [18]. There is no passivation layer that blocks the electrodes in these THF solutions. However, the electrochemical window of common RMgX/THF solutions is limited for their use as electrolytes in rechargeable Mg batteries [19].

In 2007 Aurbach et al. established an appropriate electrolyte system based on the reaction of PhMgCl and AlCl<sub>3</sub> [20]. Hereby the structural and electronic effects of a Grignard reagent on the electrochemical properties are understood. However, this electrolyte is not stable at higher potential and is quite corrosive for many metals.

In this study, the electrochemical stability of different metal substrates in three different electrolytes was investigated. These electrolytes are All Phenyl Complex (APC), Magnesium Hexamethyldisilazide (Mg-HMDS) and Magnesium Aluminum Chloride Complex (MACC) – 1,2-dimethoxyethane (DME). In the next chapters, these electrolytes are described in details.

### 1.3.1 All Phenyl Complex (APC) Electrolyte

THF is a solvent which is unacceptable in practical applications owing to its high vaporousness and inclination to form peroxides. As above described Aurbach et al. illustrated improved electrolytes and they also developed solvents with less volatile ethers such as tetraglymes [21]. Nevertheless, RMgX/THF (where R: alkyl, aryl, phenyl... and X: Cl, Br) is still part of the best operating electrolytes.

Chloride is an essential component to form complexes (PhMgCl or AlCl<sub>3</sub>). It was found that it causes corrosion of non-noble metals above about 2V vs. Mg [2]. Hence, the aluminum foil is not appropriate as a current collector with APC electrolyte.

From previous studies, it was supposed that using complex salt solutions with phenyl instead of alkyl ligands might allow the widening of their electrochemical window and raise their specific conductivity. Uncomplicated and commercial reagents have been used, i.e., phenylmagnesium chloride (C<sub>6</sub>H<sub>5</sub>MgCl (PhMgCl)) and aluminum chloride (AlCl<sub>3</sub>), as salts. The best performance of the APC solutions were prepared with the PhMgCl and AlCl<sub>3</sub> at a ratio of 2:1 and consists of Ph<sub>2</sub>AlCl<sub>2</sub><sup>-</sup>, AlPh<sub>4</sub><sup>-</sup>, MgCl<sup>+</sup> and/or Mg<sub>2</sub>Cl<sub>3</sub><sup>+</sup> as main active species.

1.  $\text{AlCl}_3 + 2\text{PhMgCl} \rightarrow \text{Ph}_2\text{AlCl} + 2\text{MgCl}_2\text{Ph}_2\text{AlCl} + 2\text{MgCl}_2 = \text{Ph}_2\text{AlCl}_2^- + \text{MgCl}^+ + \text{MgCl}_2$  (or  $\text{Mg}_2\text{Cl}_3^+$ )
2.  $2\text{AlCl}_3 + 4\text{PhMgCl} \rightarrow \text{AlPh}_3 + 0.5\text{Al}_2\text{Cl}_6 + 3\text{MgCl}_2 + \text{PhMgClAlPh}_3 + 0.5\text{Al}_2\text{Cl}_6 + 3\text{MgCl}_2 + \text{PhMgCl} = \text{AlPh}_4^- + 0.5\text{Al}_2\text{Cl}_6 + 3\text{MgCl}_2 + \text{MgCl}^+$

The Mg-C bonds provide an acceptable anodic stability for APC solutions that is about 1 V higher compared to solutions depending on complexes with alkyl ligands [23].

Organoaluminate species in which the ligands are aromatic form stronger Al-C bonds, compared to aliphatic systems. It can be concluded that the  $\text{AlCl}_{4-n}\text{Ph}_n^-$  ( $n=0-4$ ) anions are actually more stable than  $\text{AlCl}_{4-n}\text{R}_n^-$  anions, where R=alkyl are the active anionic species in the solutions which were shown by Aurbach et al [23]. Their high stability provides good ion dissociation in solvents, which explains both the relatively high specific conductivity and enhanced properties for Mg deposition (low overpotentials and high cyclic efficiency close to 100%).

All chemical preparations and electrochemical measurements were executed under argon atmosphere in a glove box (M. Braun, Inc.) with traces of water and oxygen below 1 ppm. The preparation of APC electrolyte includes a reaction between  $\text{AlCl}_3$  (Aldrich, 99.99%) dissolved in THF (Aldrich, 99.9%, less than 20 ppm water) and PhMgCl (Aldrich, 2 M solution in THF). Different concentrations and molar ratios of components showed variations in properties of the solution; such as electrochemical stability window, overpotential for magnesium deposition, reversibility of magnesium deposition, ionic conductivity, etc. Figure 4 shows the cyclic voltammogram of 0,4M APC electrolyte with a platinum as working electrode. Mg foils were used for counter and reference electrode. This electrolyte is produced in situ via the reaction of one equivalent of aluminum trichloride with two equivalents of phenyl magnesium chloride. The stability against oxidation is 3.2 V versus Mg on a Pt working electrode and the Coulombic efficiency reaches practically 100% [11].



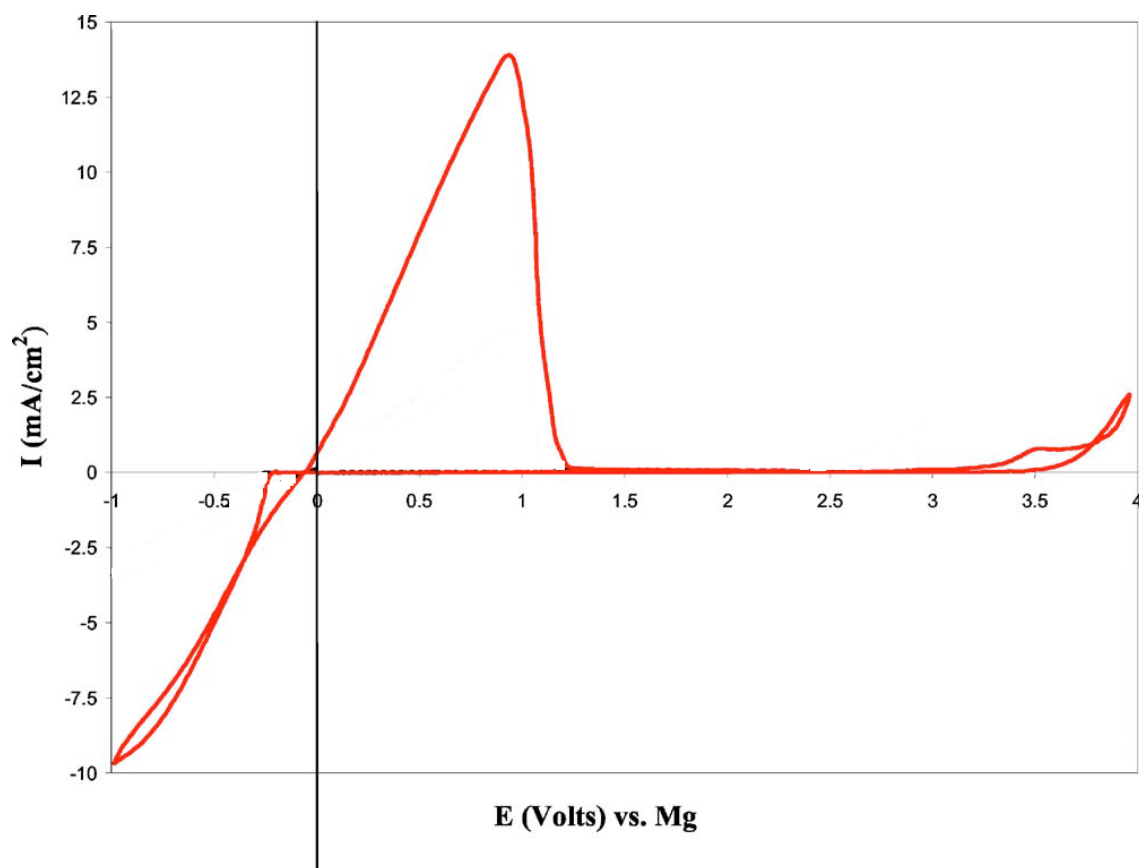


**Figure 4:** Steady-state cyclic voltammogram of 0,4M APC electrolyte measured with Pt electrode at 25 mV/s [11]

### 1.3.2 Magnesium hexamethyldisilazide (Mg-HMDS) Electrolyte

Kim et al. described the crystallization of the electrochemically active species formed from the reaction between hexamethyldisilazide magnesium chloride and aluminum trichloride which enables the synthesis of a non-nucleophilic electrolyte. This crystallization was important in the identification of the electroactive species,  $[\text{Mg}_2(\mu\text{-Cl})_3\cdot 6\text{THF}]^+$ , and critical to developments in the voltage stability and coulombic efficiency of the electrolyte [24]. The crystallized product had an anodic stability of 3.2 V vs magnesium on a platinum electrode Zhao-Krager et. al [25] also mentioned that the HMDS based electrolyte (both as prepared and crystallized) presented valuable electrochemical performance and had a high anodic stability (3.3 V vs Mg).

HMDSMgCl has been earlier described as being capable of reacting reversible magnesium deposition with similar current density like in Grignard reagents [26]. After the initial study

of Aurbach et al., the current density for the magnesium deposition was raised by a factor of seven by addition of  $\text{AlCl}_3$ . Unfortunately, the voltage stability did not increase and was equal to that of  $\text{HMDSMgCl}$ . For the purpose of examining the product of the reaction between  $\text{HMDSMgCl}$  and  $\text{AlCl}_3$ , crystals were acquired with the help of slow diffusion of hexane [24].

Unfortunately, it was found that the  $\text{MgCl}_2$  electrolytes are very corrosive; i.e., stability of stainless steel was lower than 1.8 V vs. Mg [27]. The  $\text{Mg}(\text{HMDS})_2:\text{AlCl}_3$  and  $\text{MgCl}_2:\text{AlCl}_3$  systems provide wide electrochemical window and good electrochemical properties without the requirement of supplementary crystallization progresses.

$\text{MgHMDS}$  electrolyte can be stored in a glovebox under Ar atmosphere for about one year without any loss in electrochemical efficiency [28](Figure 5).

In this thesis 0,2M  $\text{MgHMDS}$  and  $\text{AlCl}_3$  in THF solution were tested with different current collectors.

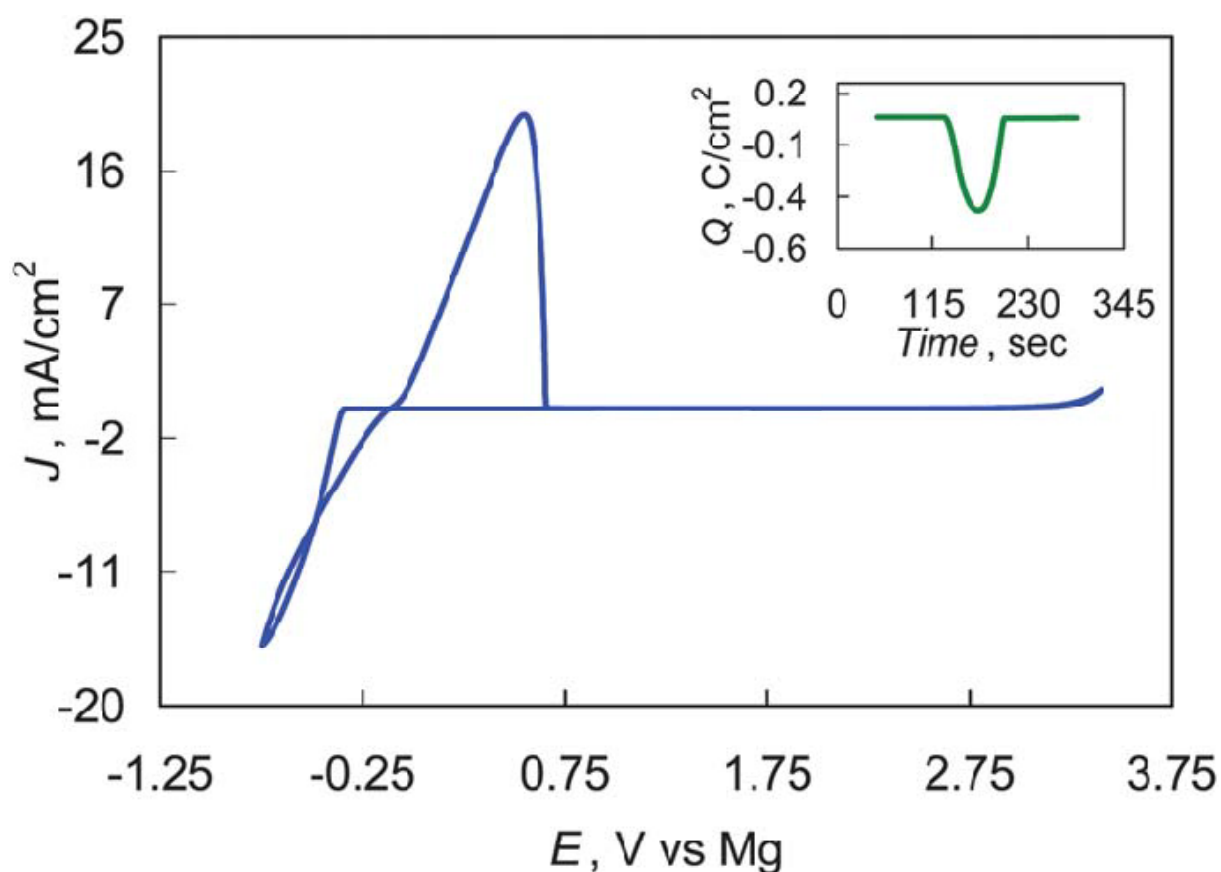


**Figure 5:** Electrochemical efficiency of 0.2M  $\text{MgHMDS}$  electrolyte ( $\text{Mg}_2(\mu\text{-Cl})_3 \cdot 6\text{THF}$ ) ( $\text{HMDS}_n\text{AlCl}_{4-n}$ ) ( $n= 1,2$ ) after one year of storage in Ar filled glovebox, by cyclic voltammetry on a Pt working electrode at a scan rate of 25 mV/s, with a Mg reference and counter electrode and 100% coulombic efficiency for deposition-dissolution of Mg [28].

### 1.3.3 Magnesium Aluminum Chloride Complex (MACC) Electrolyte

Aurbach et al. and Liu et al. improved an inorganic-based electrolyte (as described below), the magnesium aluminum chloride complex (MACC), which performs reversible Mg deposition with an anodic stability >3.0 V [29]. This system is promising because it can be joined with high voltage Mg cathodes.

The inorganic Magnesium Aluminum Chloride Complex (MACC) is formed by an acid–base reaction in a similar process to that stated for the transmetalation during the formation of the Grignard-based complexes. Expressed in a general formula one can write:



inorganic species exist which are similar to the organometallic species occurred in previous studies dealt with Grignard-based electrolytes (i.e., the active Mg cation is  $\text{MgCl}^+$  and  $\text{Mg}_2\text{Cl}_3^+$ ) [30].

The above reaction (1) is a simple and direct route to avoid organometallic compounds in the solutions; however it seems quite unreasonable that it will be put into practice because of the low solubility of  $\text{MgCl}_2$  in most solvents [31]. Furthermore  $\text{MgCl}_2$  is poorly dissociated in solutions based on aprotic organic solvents. Therefore a solution including only  $\text{MgCl}_2$  has very low-, even no measurable conductivity, and therefore allows no Mg deposition, dissolution or intercalation. In contrast to, Figure 6 reveals a typical cyclic voltammogram of a 0.03 M Mg salt solution depicted in equation (1) mixed with 1,2-dimethoxyethane (DME) measured with a Pt-working electrode. The reduction process in the range between 0 and -1 V vs. Mg is owing to the deposition of Mg metal. The oxidation peak with a current density maximum at about 0.6 V is ascribed to the subsequent electrochemical dissolution of the Mg metal. The electrochemical stability window acquired with this system is 3.25 V vs. Mg metal. It is obviously understandable from the cyclic voltammogram that the process of magnesium deposition and dissolution is reversible.

The MACC electrolyte in DME is synthesized with a 2:1 ratio  $\text{MgCl}_2 - \text{AlCl}_3$ . Figure 6 shows cyclic voltammetry of reversible Mg electrodeposition and dissolution containing 30mM of the MACC in DME on a Pt working electrode [31].

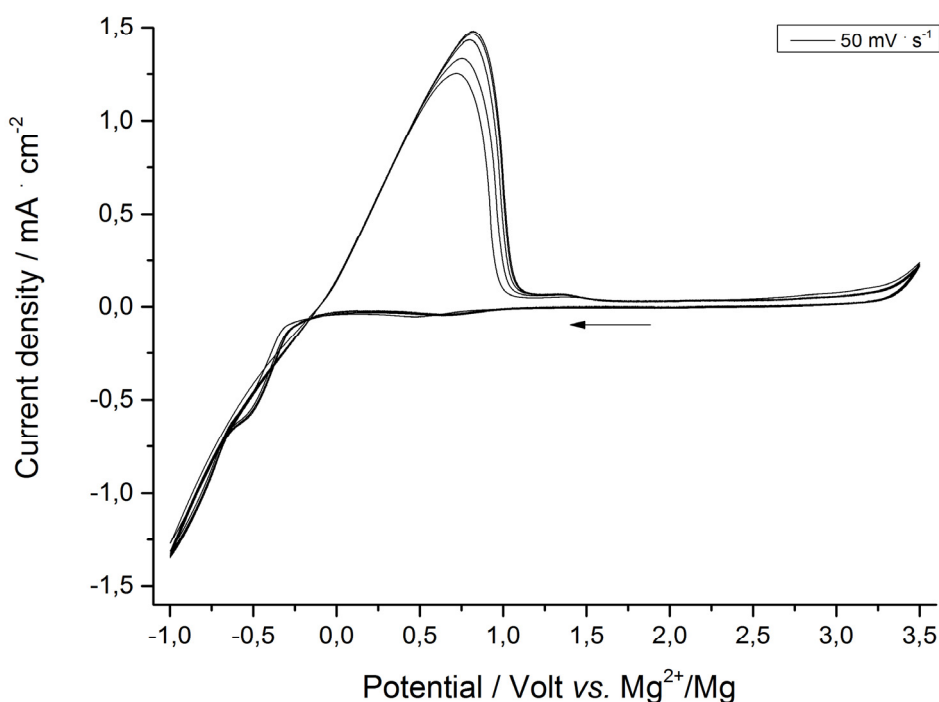


**Figure 6:** Cyclic voltammogram of 0.03 M MACC 2 : 1 solution in DME. The working electrode is Pt while the counter and reference electrodes are Mg metal. Measurements are obtained at 50mV/s and ambient conditions. [31]

## 1.4 Negative Electrodes

Mg metal has been viewed as an attractive battery anode (negative electrode) in the Mg ion battery. However, Mg shows undesirable reactivity with the electrolyte based on protic solvents. Interfaces formed on the Mg metal as a result of Mg - electrolyte interaction and this influences the electrochemical performance related to deposition and dissolution of the Mg, i.e., charge and discharge of the battery [22]. The formation of the blocking layer is unfavorable for reversible electrochemical dissolution and deposition because of an inhibition effect by blocking the diffusion or migration of the Mg ions. Before clarification of the nature of this blocking layer, it was described as “instability of the electrolytes with Mg metal”, or “electrolyte decomposition” [32]. The passivating nature of this layer on Mg are different compared to Li metal as the layer formed there, that allows Li ion- diffusion and prevents the further decomposition of the electrolyte during Li deposition [32]. This layer on

Li metal is called solid electrolyte interface (SEI). Figure 7 illustrates the different kind of layer formation on Mg and Li metal [33].

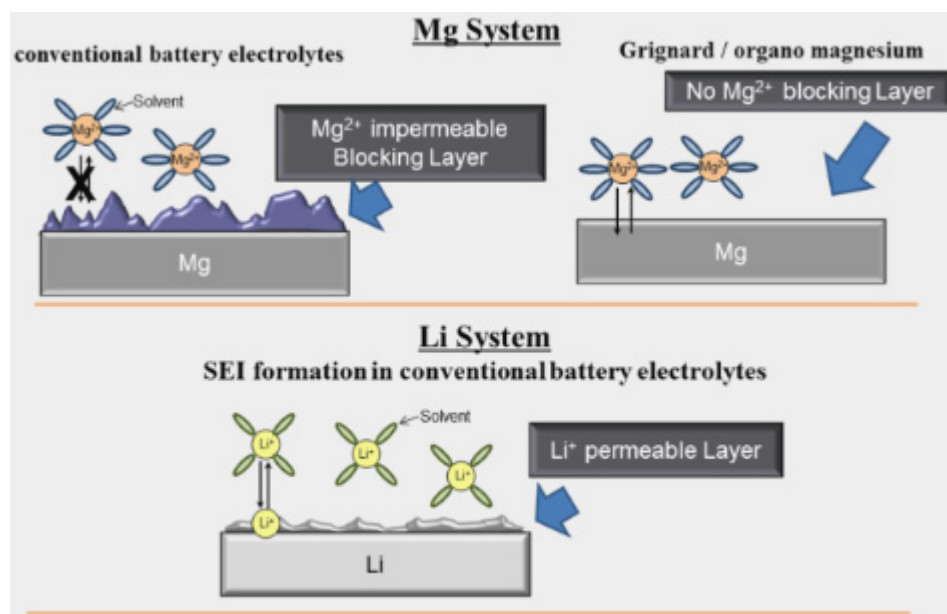


**Figure 7:** Schematic description of a simplified illustration of metal–electrolyte interfaces for Mg and Li metals. [33]

As it is also shown in Figure 7, Mg passivation layer does not exist in Grignard organo-magnesium electrolytes in contrast to simple ionic magnesium salts such as perchlorates, tetrafluoroborates or polar aprotic solvents carbonates and nitriles [34].

## 1.5 Positive Electrodes

The development of the positive electrode (cathode) material for the Mg battery is very difficult. This is related to the ability of material as it is difficult to accomplish reversible processes for Mg intercalation and deintercalation. Some cathode materials which have high reversible capacity and adequate operating voltage under appropriate power output conditions have been developed. Thus, typical examples of cathodes for such Mg batteries, which have been explained in the “Battery Handbook” so far were AgCl, CuCl, PdCl<sub>2</sub>, Cu<sub>2</sub>I<sub>2</sub>, CuSCN and MnO<sub>2</sub> [1]. Low reversible capacity and reduced power output occurs owing to the high valence of Mg<sup>2+</sup> ions. The kinetics of solid state diffusion of Mg<sup>2+</sup> ions through inorganic cathode materials is slow. Some research papers suggest that low Mg<sup>2+</sup> mobility is

determined by strong ionic interactions, in addition to redistribution of the divalently charged cations in the host material [35]. To deal with these problems, nanostructured and mesoporous materials which provide large surface area have been used as electrode materials in consideration of decreasing the diffusion length for  $Mg^{2+}$  ions into host cathode sites [36]. In spite of increasing current capabilities, materials with high divalent ion mobility have been used as cathode materials, these called Chevrel Phases (CPs)  $M_xMo_6T_8$  (M: metal T: S, Se) [37].

Nowadays, the reports involving cathode materials for Mg ion batteries are increasing as it is important to provide new concepts for future research.

In this thesis, after selection of the best suitable current collector, several cathode materials were tested, some of them were synthesized and some commercial materials were chosen. The best results were achieved with tunneled manganese oxides ( $\alpha MnO_2$ ). Tunneled  $\alpha MnO_2$  is a commercial material and it is also used for lithium batteries.

### **1.5.1 Tunneled Manganese Oxides ( $\alpha MnO_2$ )**

Manganese oxides are first used for Lithium ion battery and the spinel phase  $LiMn_2O_4$  is exploited commercially in lithium ion batteries, owing to its environmental benefits, rate capability, high energy density, ease of availability and low cost synthesis methods [38].

Manganese dioxides include a vast variety of oxides with a possible manganese valence of three or four and containing various cations and neutral molecules, like water in their structure [39].

Excellent supercapacitor performance of amorphous  $MnO_2 \cdot nH_2O$  was first expressed by Lee and Goodenough in 1999 [40]. Thereafter, they have attracted more attention from the scientific community. The miscellaneous crystal phases of manganese oxide have also been examined as cathode materials for magnesium ion batteries. The first investigations of electrochemical magnesium intercalation into manganese oxide such as  $Mn_2O_3$  and  $Mn_3O_4$  were demonstrated by using magnesium perchlorate/THF electrolytes [13].

$\alpha MnO_2$  has a  $2 \times 2$  tunneled structure that is called "hollandite". The size of the tunnels considerably affects their eventual electrochemical capacitive properties. A narrow tunnel size does not admit the insertion of electrolyte cations into the  $MnO_2$  microstructure as the

diameter of the electrolyte cations is larger than the size of the tunnel. The small capacity of these structures is only owing to surface adsorption. Conversely, a large tunnel structure is appropriate for the intercalation / deintercalation of Mg ions. Additionally, a large tunnel structure can gather a large amount of bivalent metal ions, which is necessary to maintain the capacity and stability of the electrode [41].

Zhang et al. illustrated that  $\alpha\text{MnO}_2$  is a promising cathode system where the divalent Mg ion can be intercalated electrochemically [42]. Figure 8 also shows that  $\alpha\text{MnO}_2$  provides a specific capacity  $\sim 280$  mAh/g during the 1st discharge cycle using Mg-HMDS electrolyte [43]. Significant capacity loss for hollandite  $\text{MnO}_2$  has also been observed with nearly 50% capacity lost between the first and second cycles.

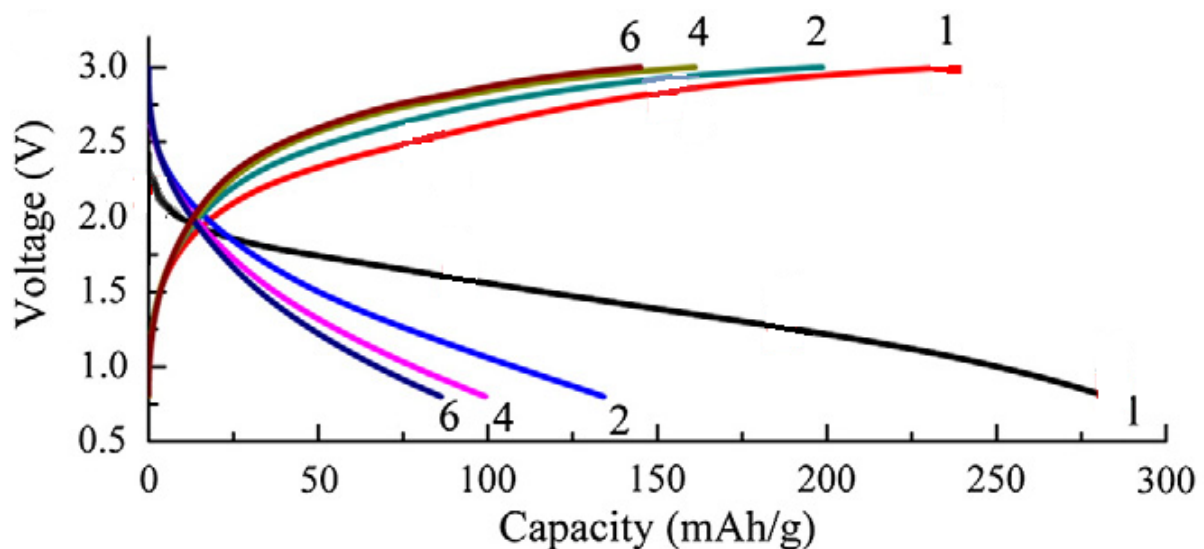


**Figure 8:** Charge-discharge test of  $\alpha\text{-MnO}_2$  at 0.015 C rate. [43] 1,2,4,6 are the number of the cycles of charge and discharge.

## 1.6 Current Collectors

The recent investigations show that the current collector material is also playing an extremely important role in the rechargeable Mg ion battery. It is well known that compatibility between current collectors and electrolyte, specifically the stability of current collectors, is a significant factor for designing a rechargeable battery with a long cycle life [38].

As it is mentioned above, the most studied Grignard reagent based electrolytes allow chemically reversible Mg deposition and dissolution. Nevertheless, the Grignard reagent based electrolytes are usually corrosive for non-noble metals [28]. For the foregoing reasons, it is very essential that stable and inexpensive materials should be implemented as current collectors for Mg rechargeable batteries for commercial applications. In the first part of the experimental section of this work, the anodic stability of several current collectors (Cu, Ni, stainless steel, Ti, glassy carbon, graphite, carbon papers and carbon textiles) have been investigated according to their stability in above described electrolyte systems.

### 1.6.1 Corrosion

Corrosion is defined as an electrochemical process with the specific qualifications of an anode, a cathode, a conducting electrolyte and a metallic path connecting the anode and cathode sites [44].

*Anode* is the electrode of an electrochemical cell, where oxidation is the major reaction leading to metal ions entering solution and the electrode where corrosion is mostly obtained.

*Cathode* is the electrode of an electrochemical cell, where reduction is the major reaction.

*Electrolyte* is an (in most cases aqueous) ionic conducting path where the anode and the cathode are submerged in.

Metallic path is the extrinsic circuit which binds the anode to the cathode and allows the flow of electrons from the anode to the cathode [44].

Figure 9 describes that generally corrosion cells are assembled when two different metals are attached together within an electrolyte (Figure 9a). The formation of a corrosion cell upon an isolated metal or alloy (Figure 9b) occurs as a result of several conditions like, differences in material microstructure, chemical heterogeneities in a matrix, heat treatment effects, imbalance of the distribution of the oxidizing agent over the metal surface, etc.



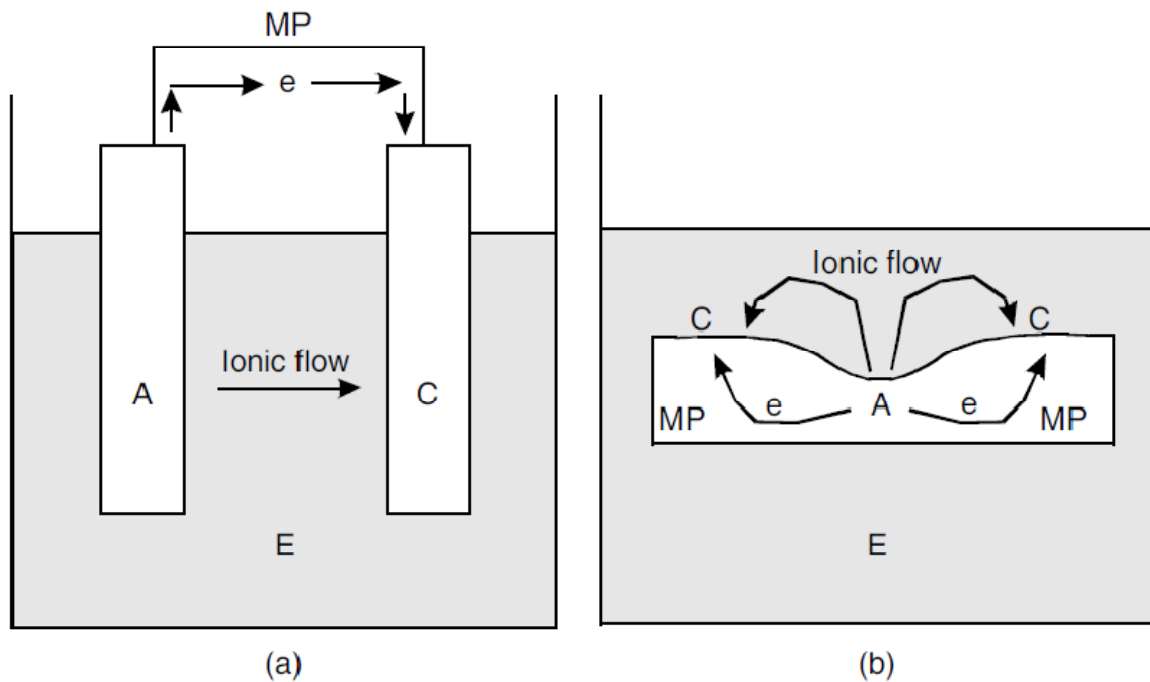
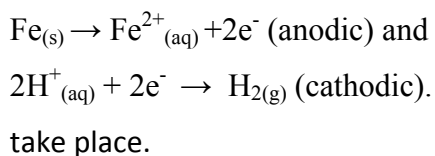
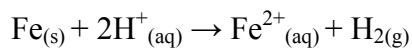


**Figure 9:** Illustration of corrosion cells (a) bimetallic system, A=anode (e.g., zinc), C=cathode (e.g., copper), E=electrolyte, MP=metallic path (e.g., wire) and (b) single metal system (e.g., pitting in stainless steel) [45]

A corrosion cell includes two half cell reactions, for instance in the case of steel immersed in an acidic solution, on the same surface the two half cell reactions:



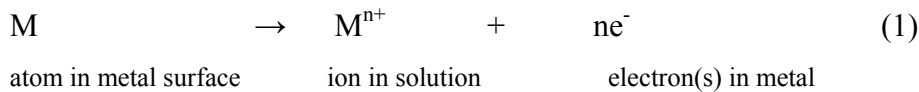
The overall reaction is:



The surfaces of all metals (except gold) in air are covered with oxide films. When such a metal is submerged in a, for example, aqueous solution, the oxide film starts to dissolve. With the acidic condition that oxide film may dissolve completely departing a nude metal surface, which is defined as in the active state. In neutral solutions, the solubility of the oxide will be much lower than in acid solution. If the near-neutral solution includes inhibiting anions, this dissolution of the oxide film may be restrained and the oxide film sustained to

produce a passivating oxide film that can efficiently prevent the corrosion of the metal, which is then in the passive state [46].

When the oxide-free surface of a metal is unprotected to the solution, positively charged metal ions are able to pass from the metal into the solution, departing electrons behind on the metal, i.e.



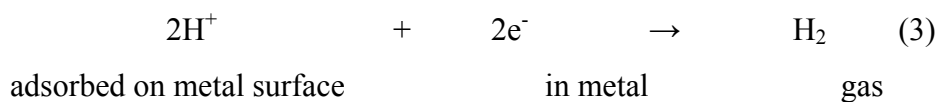
The aggregation of negative charge on the metal owing to the residual electrons provides an increase in the potential difference between the metal and the solution. This potential difference is called the electrode potential or, simply, the potential of the metal, which thus becomes more negative. This change in the potential decelerates the dissolution of metal ions but accelerates the deposition of dissolved metal ions from the solution onto the metal, i.e. the opposite direction of reaction (1). At equilibrium, the dissolution and deposition rate of metal ions is balanced and the metal is attaining a stable potential. This potential is termed the reversible potential  $E_r$  and its value relies on the concentration of dissolved metal ions and the standard reversible potential  $E^0$  for unit activity of dissolved metal ions,  $a_M^{n+}$ , i.e.



$$E_{r,Mn+ / M} = E_{Mn+/M}^0 + \frac{RT}{nF} \ln a_{Mn+} \quad \text{Eq. 1}$$

where R is the gas constant, T the absolute temperature, F the Faraday and n the number of electrons carried per ion. When the potential reaches the reversible potential, no more net dissolution of metal takes place. The net quantity of metal which dissolves during this process is generally very limited.

In acid solutions, electrons can react with hydrogen ions, adsorbed on the metal surface from the solution, to provide hydrogen gas [46].

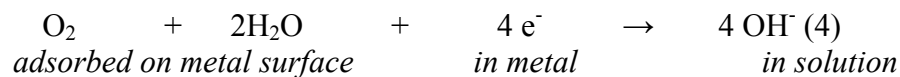


Because of the permanent consumption of electrons, reaction (3) allows the continuous-dissolution of an equivalent amount of metal ions by reaction (1). The hydrogen evolution reaction causes the corrosion of the metal. This type of corrosion is called hydrogen or acid corrosion. The reversible potential of reaction (3) is given by

$$E_{r,H^+/H_2} = E_{H^+/H_2}^0 - \frac{RT}{F} \ln \frac{p_{H_2}^{1/2}}{a_{H^+}} \quad \text{Eq. 2}$$

where  $P_{H_2}$  is the partial pressure of hydrogen gas. If the partial pressure of hydrogen is permitted to develop, then the hydrogen partial pressure would increase until the driving force, which is the difference between the reversible potential of reaction (1) and the reversible potential of reaction (3), becomes zero. Normally hydrogen gets away from the system, so that the potential stays more negative than the reversible potential and corrosion persists.

In neutral solutions, the concentration of hydrogen ions is too low to permit reaction (3) to advance at an important rate, but electrons in the metal can react with oxygen molecules, adsorbed on the metal surface from air dissolved in the solution, to provide hydroxyl ions



Again, the potential of the metal persists more negative than the reversible potential for reaction (4)

$$E_{r,O_2/OH^-} = E_{O_2/OH^-}^0 - \frac{RT}{4F} \ln \frac{a_{OH^-}^4}{p_{O_2}} \quad \text{Eq.3}$$

Hence corrosion can advance by the coupling of reactions (1) and (4). This type of corrosion is called oxygen corrosion.

Subsequently, the process of oxidation includes a loss of electrons by the reacting species, as exists in the metal dissolution reaction (1). Hence the area of a corroding metal where metal dissolution exists is an anode and metal dissolution is the anodic reaction of corrosion leaving electrons behind in the metal. The reduction that exists at the cathode, is consuming the electrons according to reactions (3) and (4). The reduction of hydrogen ions and oxygen are the cathodic reactions of corrosion [46].

However, dissolution of a metal can be also caused by applying an external current. If the dissolution is an unwanted reaction, this might be called corrosion. In corrosion science this type of corrosion of a metal is called stray current corrosion because the current is coming from an external circuit for other purposes, e.g. the stray current interaction between ac or dc power lines and buried pipes. In case of the battery, the oxidizing agent which dissolves the current collector could be the positive electrode itself or the external charging circuit which applies a relatively positive potential at the current collector. The electrode may facilitate the dissolution of the collector material by the formation of reaction products which dissolve or evaporate easily. Furthermore, hardly soluble reaction products may deposit at the surface and form a so called passive layer. On one hand this passive layer protects from further dissolution but on the other hand it may be insulating and block the current flow (see also the discussion of passivation and SEI formation in chapter 1.4). Pitting corrosion is a specific form of localized corrosion which is mainly observed on passivated surfaces. Defects in the passive layer leads strong dissolution restricted to a very small area and formation of little but deep holes [46].

## **1.7 Electrochemical Characterization Methods**

In this study, cyclic voltammetry is used for the selection of the best current collector and also to observe electrochemical performance of some cathode materials of Mg rechargeable battery. In a second step the galvanostatic cyclic voltammetry is also used for testing the cathode materials of the Mg battery.

### **1.7.1 Cyclic Voltammetry (CV)**

Voltammetry is one of the techniques, which is used to investigate electrochemical mechanisms. Potential step voltammetry, linear sweep voltammetry and cyclic voltammetry are the most preferred techniques. The cyclic voltammetry (CV) is the most extensively used method for obtaining qualitative information about electrochemical reactions. It provides a very quick estimation of redox potentials of the electroactive species. The method includes

linearly changing electrode potential between two potential limits at a specific rate while recording the current. Current indicates reaction rates of electrochemical reactions under situations where the electrode potential deviates from the equilibrium potential (the overpotential) anticipated by the Nernst equation [47]. Even though CV is the best at supporting qualitative information about electrode reaction mechanisms, several quantitative properties of the charge transfer reaction can also be concluded.

In CV a potential is applied to an electrode in an electrolyte solution (a voltage between the working electrode and a reference electrode), and the system reaction is recorded. In CV, three electrodes are used: the reference electrode – RE which electrochemical potential is usually steady and well known with respect to the standard hydrogen electrode, the working electrode – WE on which the half-cell reaction of interest takes place and the counter electrode – CE (sometimes called auxiliary electrode – AE) on which the counter reaction takes place providing the current for the WE. So the WE potential can be measured in terms of a voltage between WE and RE. The potential is applied to the working electrode by means of a potentiostat which controls the current between WE and CE in such a way that the desired potential of the WE against the RE is obtained. The nominal voltage is swept at a constant sweep rate and the resulting current is measured. CV can be executed to acquire analytical (e.g., concentration), thermodynamic (e.g., redox potentials and equilibrium constants), kinetic (e.g., rate constants for reactions including electrogenerated species) and mechanistic information about chemical systems in which redox chemistry plays a role [48].

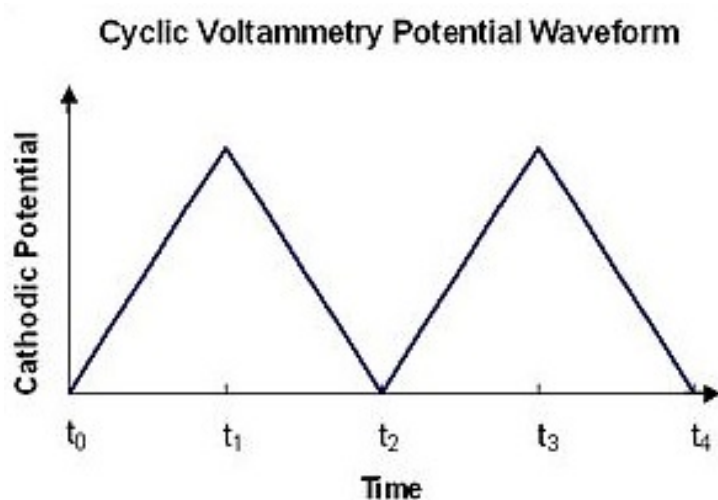


**Figure 10:** Potential against time program for cyclic voltammetry [49]

In a CV experiment the WE potential is ramped (as compared to RE) linearly versus time. The potential at  $t_0$  is the initial potential and the ramping is known as the experiment's scan rate (V/s). When the measurement reaches a set potential (Figure 10 potentials at  $t_1$  &  $t_3$ ), the WE potential ramp is reversed (Figure 10,  $t_1$  to  $t_2$  &  $t_3$  to  $t_4$ ) [49]. The voltammogram, in the scan from  $t_0$  to  $t_1$  (forward scan) and  $t_2$  to  $t_3$  (2<sup>nd</sup> cycle), is suitable to determine reduction or oxidation processes at or of the working electrode. The current between working electrode and counter electrode is plotted versus the applied voltage to obtain the cyclic voltammogram trace (Figure 11) [50].

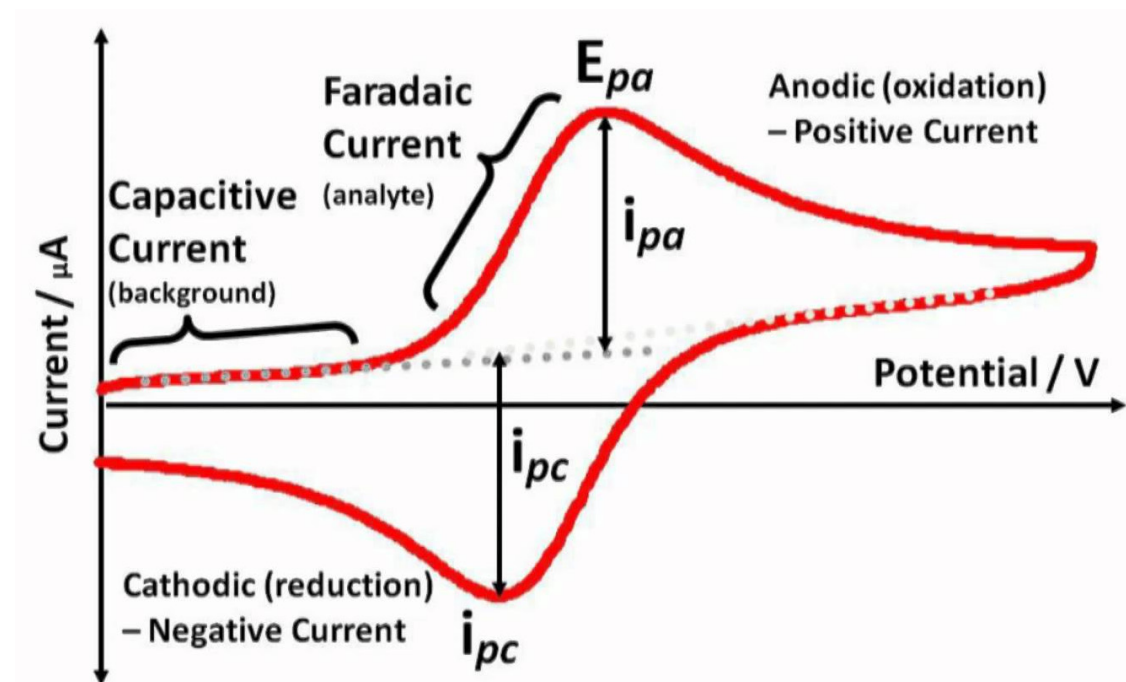


**Figure 11:** Cyclic voltammogram trace [50]

To comprehend the behavior of the cell under cyclic voltammetry, it is required to examine the impact of voltage scanning on the equilibrium existing at the electrode surface. If the rate of electron transfer is faster than the voltage sweep rate, the equilibrium is constituted at the electrode surface. Since the voltage is swept from initial potential to set potential, the equilibrium position moves from no transformation at initial potential to full transformation at set potential of the reactant at the electrode surface [51]. Nernst equation illustrates the situation very well. Because the voltage is changing initial (background) current is owing to the charging of the electro-double layer capacitance existing at the surface of the electrode. This capacitive current is constant (for constant scan rate) and proportional to the scan rate.

After that, current increases further since the voltage is swept additional from its initial value because the equilibrium position is moving to high potential side. This current is the faradaic current that is generated by the reduction or oxidation of some chemical substance at an electrode. The intensity and shape of the Faradaic current peak is determined by three phenomena: the kinetics of electron transfer, the rate at which the redox species advances to the surface and in case of full reversibility (no impediment of the faradaic reaction) by the amount of the active mass and the thermodynamic of the redox reaction. Fig. 11 shows a case in which the mass transport (diffusion) is the rate determining step in the Faradaic reaction. Since the potential is more increased, the current increases owing to the oxidation and a current peak ( $i_{pa}$ ) is acquired close to the reversible redox potential of the component. After this peak current decreases because the concentration of the analyte is decreased close to the electrode surface. Especially the peak exists, as the diffusion layer has grown adequately above the electrode so that the flux of reactant to the electrode is not fast enough to further increase the current. The peak current of  $i_{pc}$  is acquired at reduction potential. The reduction peak has usually a similar shape like the oxidation peak. Consequently, the information about the redox potential and electrochemical reaction rates of the compounds could be acquired [52]. Common properties of reversible diffusion controlled CV voltammograms are:

- The voltage range between the current peaks is characteristic of a system
- The locations of peak voltage do not change as a function of voltage scan rate
- The ratio of the peak currents is equal to one
- The peak currents are proportional to the square root of the scan rate [53]

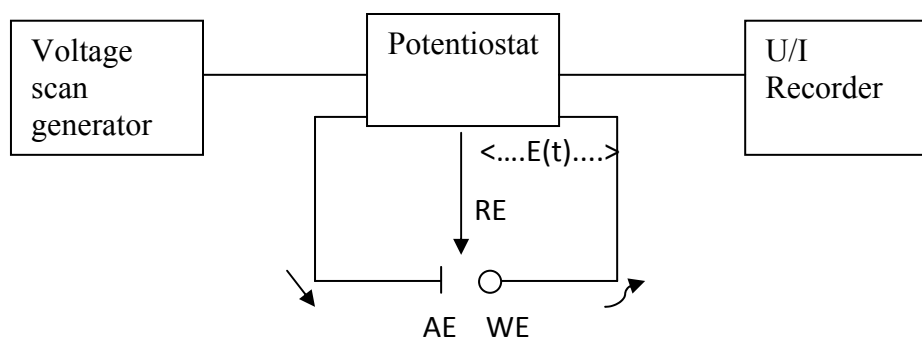


**Figure 12:** Schematic experimental setup for cyclic voltammetry; WE: working electrode, RE: reference electrode, AE: auxiliary electrode.

The figure 12 illustrates the schematic experimental setup for cyclic voltammetry. Besides potentiostats with the electrochemical cell adjustment, the common device for voltammetric experiments contains a voltage scan generator, which provides the suitable potential program, as well as recorder for voltage and current (i.e. an appropriate fast transient recorder) which records the current-voltage curve.

### 1.7.2 Evans diagrams

The Evans diagram is a kinetic diagram presenting the electrode potential in volts versus corrosion current density in amperes per unit area in a semilogarithmic plot. The Butler-Volmer equation describes the exponential relationship between the current and the electrode potential:

$$I = I_0 \left( e^{-\left(\frac{\alpha n F}{RT}\right)\eta} - e^{\left[\left(\frac{(1-\alpha)nF}{RT}\right)\eta\right]} \right)$$

The logarithm of the current density of an electrochemical reaction under charge transfer control displays a linear dependence at higher overpotential.

Anodic and cathodic linear regions in the Evans diagram are called Tafel-lines. An extrapolation of the portions of the two solid lines intersects at the corrosion potential ( $E_{\text{corr}}$ ) and corrosion current density ( $i_{\text{corr}}$ ) for the given system. Evans diagrams supply kinetic information, that is, the rate of a corrosion reaction, as a function of the applied potential [54].

### 1.7.3 Galvanostatic Cyclic voltammetry (GCV)

Galvanostatic cyclic voltammetry (Cyclic Charge-Discharge) is the common technique used to examine the performance and cycle-life of capacitors and batteries. A loop of charging and discharging until predefined cell voltages are reached is called a cycle. Galvanostatic testing executes a constant current to the electrochemical cell or capacitor utilizing a galvanostat and the consequent voltage change with time is measured. This results in charging of the cell up to a pre-set end-of-charge voltage. After that the electrochemical cell is discharged and the voltage decreases with time up to a pre-set end-of-discharge voltage [55].



For the galvanostatic cycling of batteries, the charge and discharge current are generally defined as a “C rate”, that is calculated from the battery capacity. The C-rate is a quantity of the rate at which a battery is charged or discharged approximately to its maximum capacity. For instance, a C-rate of 1 C means that the essential current is applied or drained from the battery to completely charge or discharge it in one hour. Generally, for the battery research, the mostly used is the C-rate of 0.1C (charge and discharge a battery in ten hours). The capacity is defined in Ampere per hour, where 1 Ah = 3600 coulombs.

If capacity falls by a set value (10 % or 20 % is customary), the actual number of cycles signifies the cycle-life of the battery.

The coulombic efficiency between charge and discharge is defined as

$$\eta = \frac{q_{discharge}}{q_{charge}} \times 100 \quad \text{Equation (5)}$$

An efficiency of 100% indicates that no side reactions occur, while  $\eta < 1$  involves a side reaction (in this case an oxidative side reaction). For the negative electrode the charge (is correctly treated negative) and  $-\eta > -1$  indicates that the side reaction is a reduction reaction. Generally, positive electrodes are subjected to oxidative side reactions and negative electrodes are subjected to reductive side reactions [56].

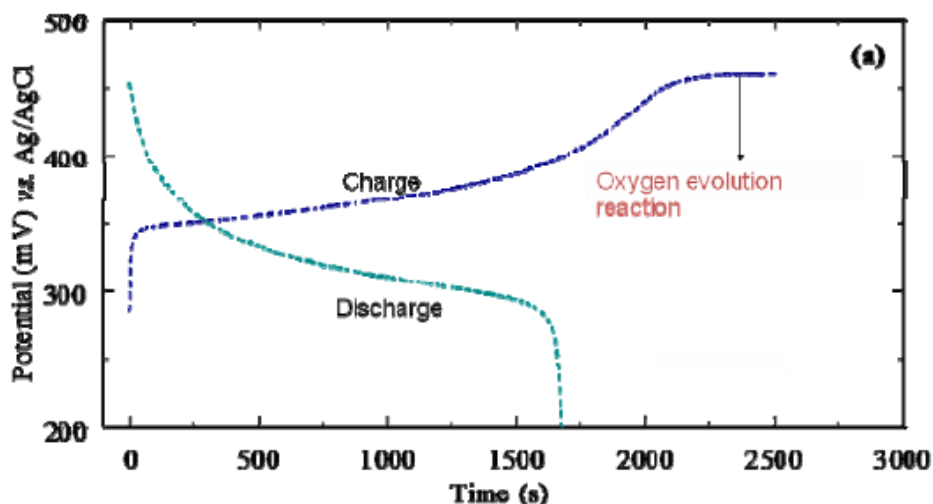


**Figure 13:** Typical (potential versus time) plot of galvanostatic cyclic voltammetry for a nickel electrode [57].

The Figure 13 illustrates the charge-discharge cycle of the nickel electrode under conditions for a nickel-metal hydride battery. While the electrode was charged for 2500 s, the discharge of the battery lasted only 1700 s. The capacity difference is the coulombs going toward the side reaction. A classic sign of a side reaction is an efficiency which is less than 100%. Charging the battery such that it does not reach the second plateau reduces the side reaction (oxygen evolution in this case) and therefore increases  $\eta$  [57].

### 1.7.4 Chronoamperometry (Stability test)

*Chronoamperometry* is a powerful electrochemical method in which the potential of the working electrode is held and the current is measured versus time. Most commonly it is investigated with a three electrode system. The measured current occurs from Faradaic processes at the electrode. The Faradaic current is owing to electron transfer activities and the current drops off with time according to the Cottrell equation because material must diffuse to the electrode surface in order to react.

$$\text{Cottrell equation: } |I| = \frac{nF\sqrt{D_0}c_0^\infty}{\sqrt{\pi t}}$$

For *diffusion controlled process*, it can be noticed that the current falls as  $t^{-1/2}$ . This feature is frequently used as a test for this type of process and from the slope of  $I$  vs.  $t^{-1/2}$  the diffusion coefficient  $D_0$  can be calculated [49].

Although the chronoamperometry is a comparatively simple technique, there are a number of difficulties, which are based on the interpretation of the current-transient curve. Hence, it is very essential to find the possibility of comparative analysis of the chronoamperometric results with the results of cyclic voltammetry or other techniques. This type of comparison will also help to understand the studied system more completely and with better precision. In part 2.1.2 the chronoamperometry technique was used for stability tests, so that the current drop was analyzed.

With Faradays law [59] and growth of passivating film equations [60]:

$$\text{Faradays law: } Q = \frac{m}{M/zF} \text{ where } Q: \text{ charge; } m: \text{ mass of material that reacts; } z: \text{ molar mass}$$

F:Faraday constant=96485 C/mol [59]

Growth of passivating film:  $\frac{dy}{dt} = \frac{k'}{y}$  where  $y$ : thickness of film and  $k'$ : parabolic rate constant [60]

Thickness of film “ $y$ ” is direct proportional to “ $m$ ” mass of material that reacts.

In measurements using modern electronic equipment, the charge  $Q = \int i(t)dt$  is determined by numerical integration of the current measured with a high sampling rate.

Therefore after integration of these equations,  $\int y dy = \int k' dt$

$Q(t) = \int i(t)dt = y = k''\sqrt{t}$  where  $k''$ : parabolic rate constant

the figures 25-28 c) are plotted  $\sqrt{t}$  versus  $Q(t)$ , where  $Q(t)$  is proportional to the film thickness.

## 2 EXPERIMENTAL SECTION

---

Target of this thesis includes these steps: The observation of corrosion processes in three different electrolytes with many current collectors, selection of the most stable current collector for the positive electrode, coating it with active material, assembling of a cell and electrochemical characterization of the materials.

In the first part, the electrochemical stabilities of current collectors in different electrolytes were investigated and in the second part the electrochemical characterization of the materials was performed.

### 2.1 Corrosion processes of current collectors

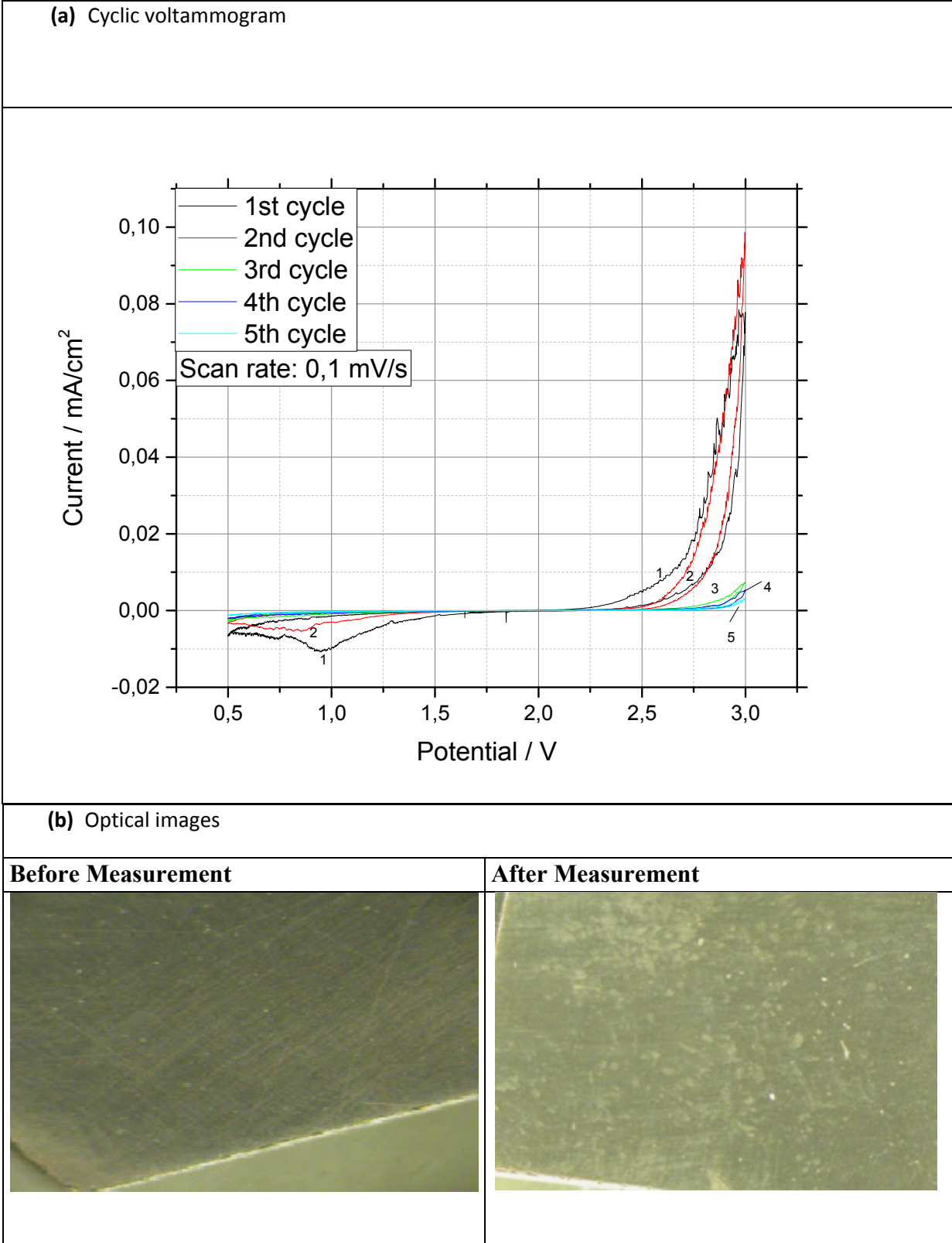
10 different materials are tested as a current collector. Glassy carbon is used as a reference system. The others are titanium, stainless steel, copper, nickel, graphite foil, carbon paper 1, carbon paper 2 (with Teflon), carbon textile 1, carbon textile 2 (Sorbent-C, Busofit-L).

At the beginning it was anticipated that, the most appropriate electrolyte is APC (All Phenyl Complex). Therefore all materials are tested with this electrolyte. Then the most stable materials are selected and these are also tested with other electrolytes; DME-MACC and Mg-HMDS.

The corrosion processes were investigated by cyclic voltammetry. Current collectors are washed and dried over night in a glass vacuum tube. The 3 electrode glass cells are assembled in a glovebox. Glass cells were chosen for the experiments in order to observe corrosion reactions better because of excess of electrolyte. Current collectors are used as a working electrode and magnesium as a counter and reference electrode. The glass cell is very tightly closed with teflonised caps and also parafilm to prevent any reaction with air. The aim of the project of AIT is to develop materials for the 3V range Mg-ion battery. Therefore the voltage range of the corrosion test is between 0.5V to 3V. The scan rate of the measurements is 0.1mV/s and 5 cycles are performed. Evans diagrams are also calculated and drawn from the CV data, in order to compare the corrosion rates for different current collectors.

## 2.1.1 Corrosion test with APC electrolyte

### 2.1.1.1 Glassy carbon with APC electrolyte



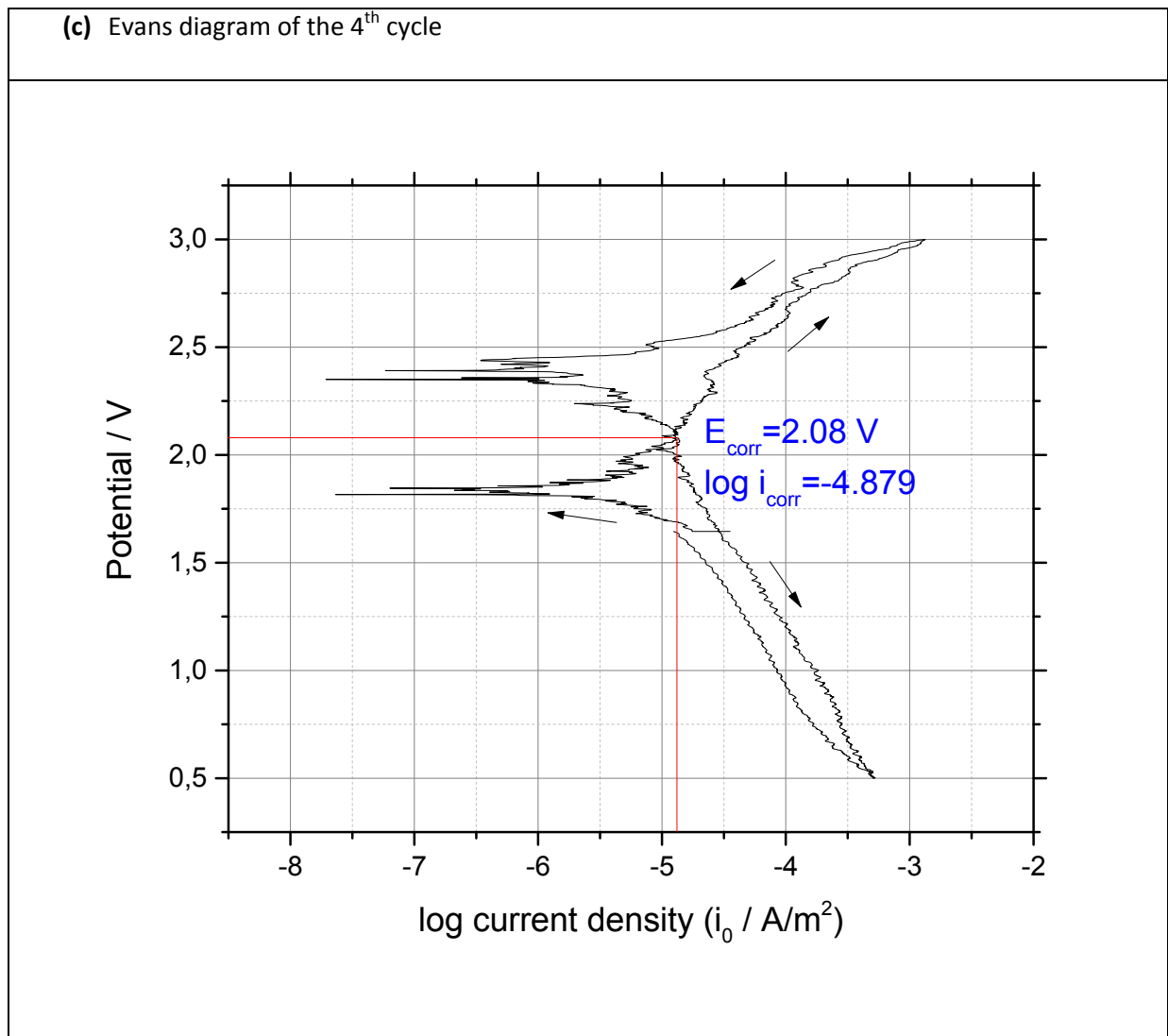
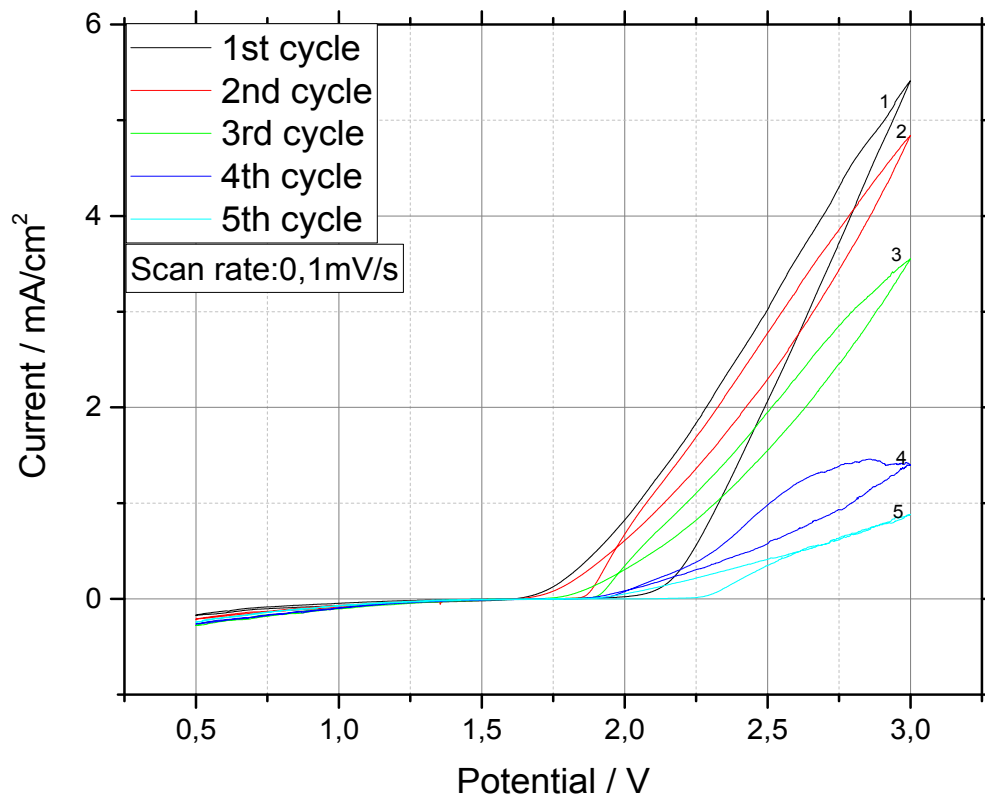


**Figure 14:** (a) Cyclic voltammogram, (b) optical microscope images and (c) Evans diagram of **glassy carbon** with APC electrolyte

Figure 14 illustrates (a) cyclic voltammetry measurement with glassy carbon in APC electrolyte, (b) optical images of glassy carbon before and after measurement and (c) the Evans diagram of the 4<sup>th</sup> cycle. From the Evans diagram a corrosion potential of 2.08V and  $\lg(\text{corrosion current density}/ \text{A/m}^2)$  of -4.879 are obtained. Glassy carbon is the reference material for the current collector (in the search for a non-reacting electrode material). It has been found inert to magnesium organohaloaluminates and it is ideal for high voltage oxidative stability tests. After some initial anodic dissolution in the first two cycles, the glassy carbon shows stability till about 2.8V. The surface morphology of glassy carbon was unchanged but it can not be used as a current collector for a commercial Mg battery as it is not flexible and breakable.

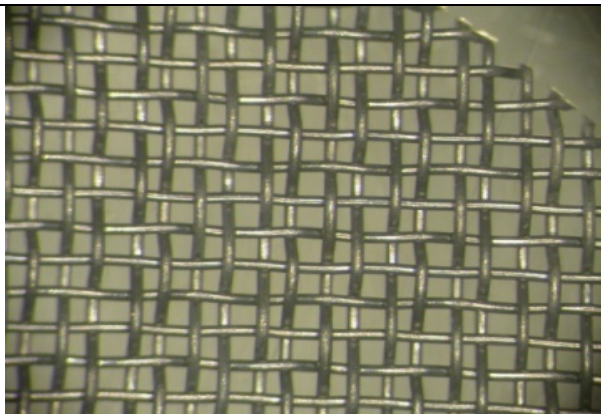
### 2.1.1.2 Titanium with APC electrolyte

(a) Cyclic voltammogram

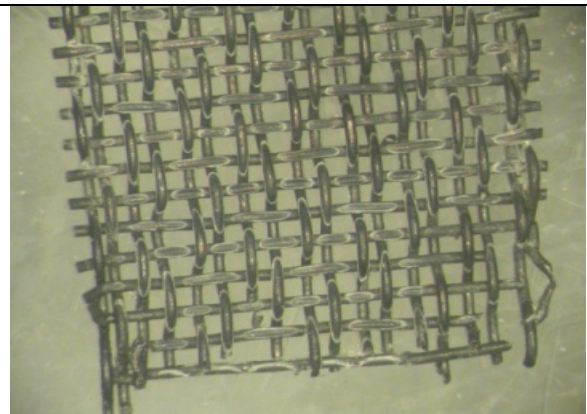


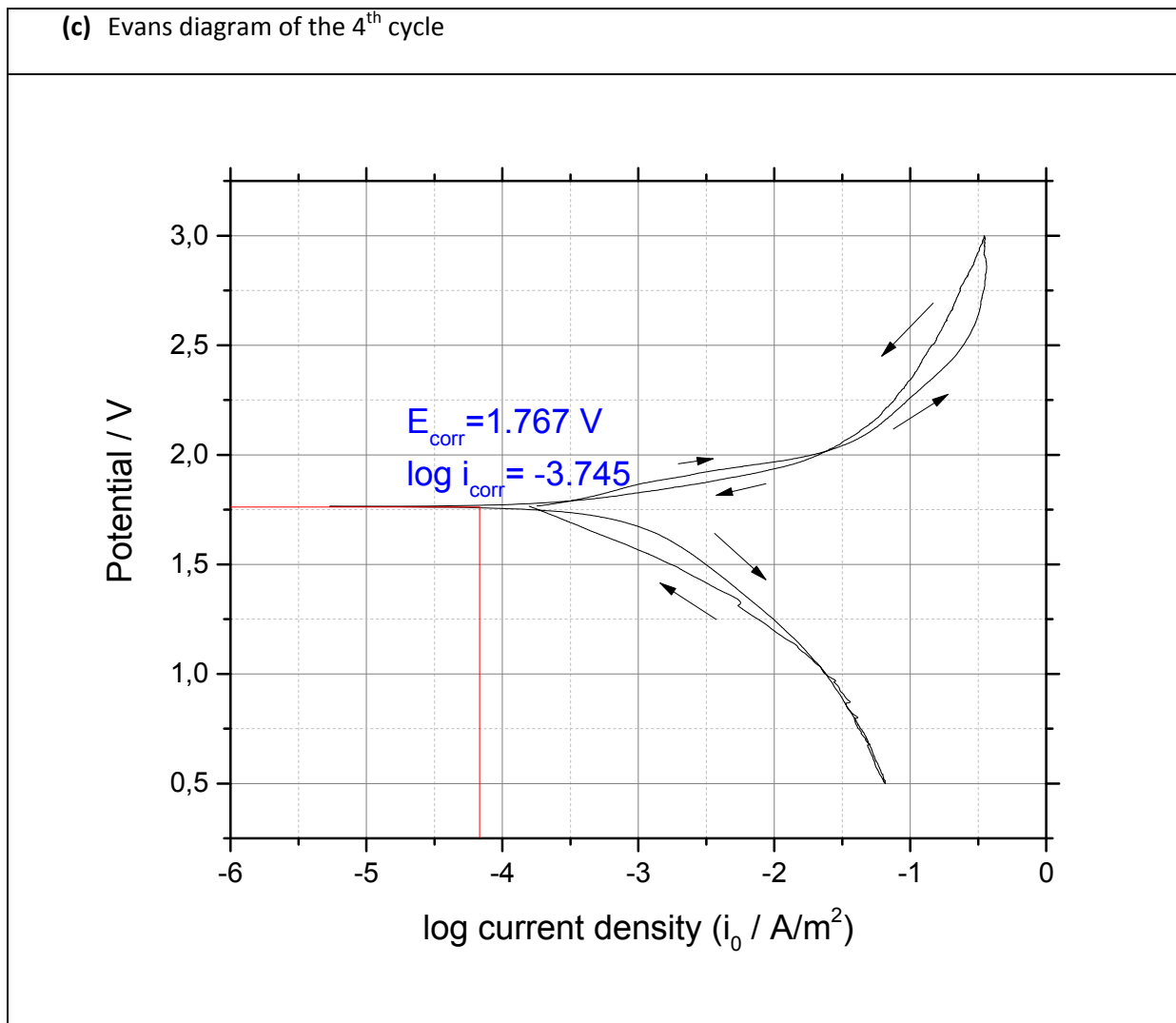
(b) Optical images

Before Measurement



After Measurement





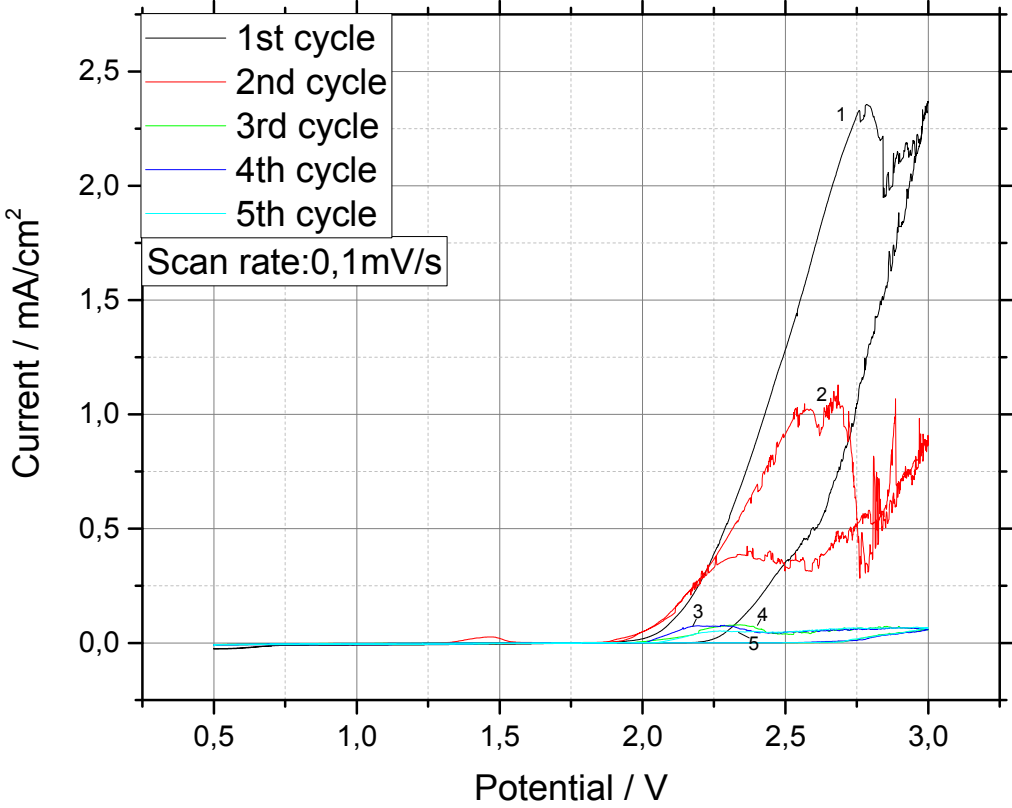
**Figure 15:** (a) Cyclic voltammogram, (b) optical microscope images and (c) Evans diagram of **Titanium** with APC electrolyte

Figure 15 depicts (a) cyclic voltammetry measurement with Titanium mesh (99.8% pure), 0.33 mm thick, in APC electrolyte (b) optical images of Titanium before and after measurement and (c) the Evans diagram of the 4<sup>th</sup> cycle. The corrosion potential is 1.767V and the  $\lg(\text{corrosion current density} / \text{A/m}^2)$  is -3.745. Titanium is the least stable material compared with the others. The increase in the current density, which is started at about 1.7V, is due to the increase in the effective surface area by the pitting formation and electrode dissolution. At the fifth cycle, the anodic stability of titanium is about 2V. Furthermore, the color of the APC electrolyte was changed, some Ti particles were dissolved in the electrolyte, Mg counter and reference electrodes turned into black. These visual observations indicate the obvious side-reactions happened with titanium.



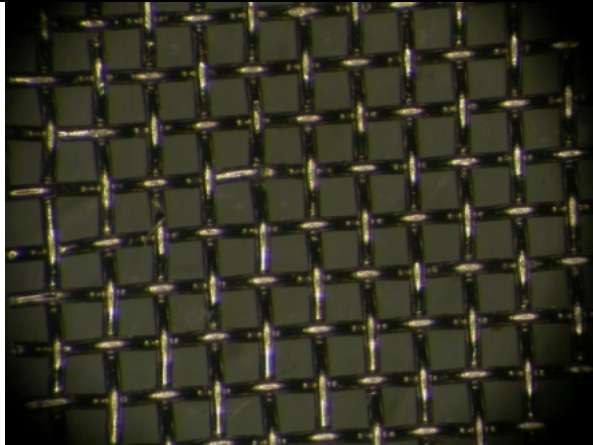
2.1.1.3 Stainless steel with APC electrolyte

(a) Cyclic voltammogram

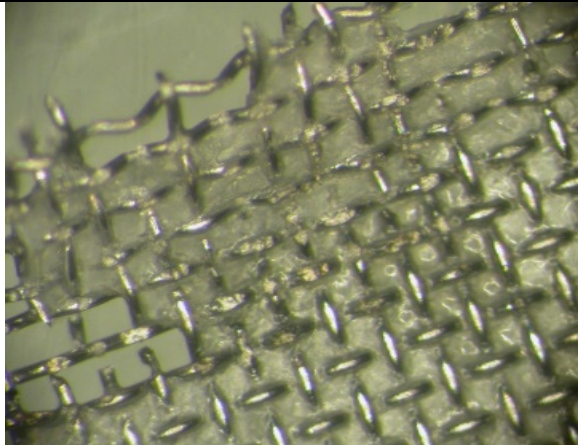


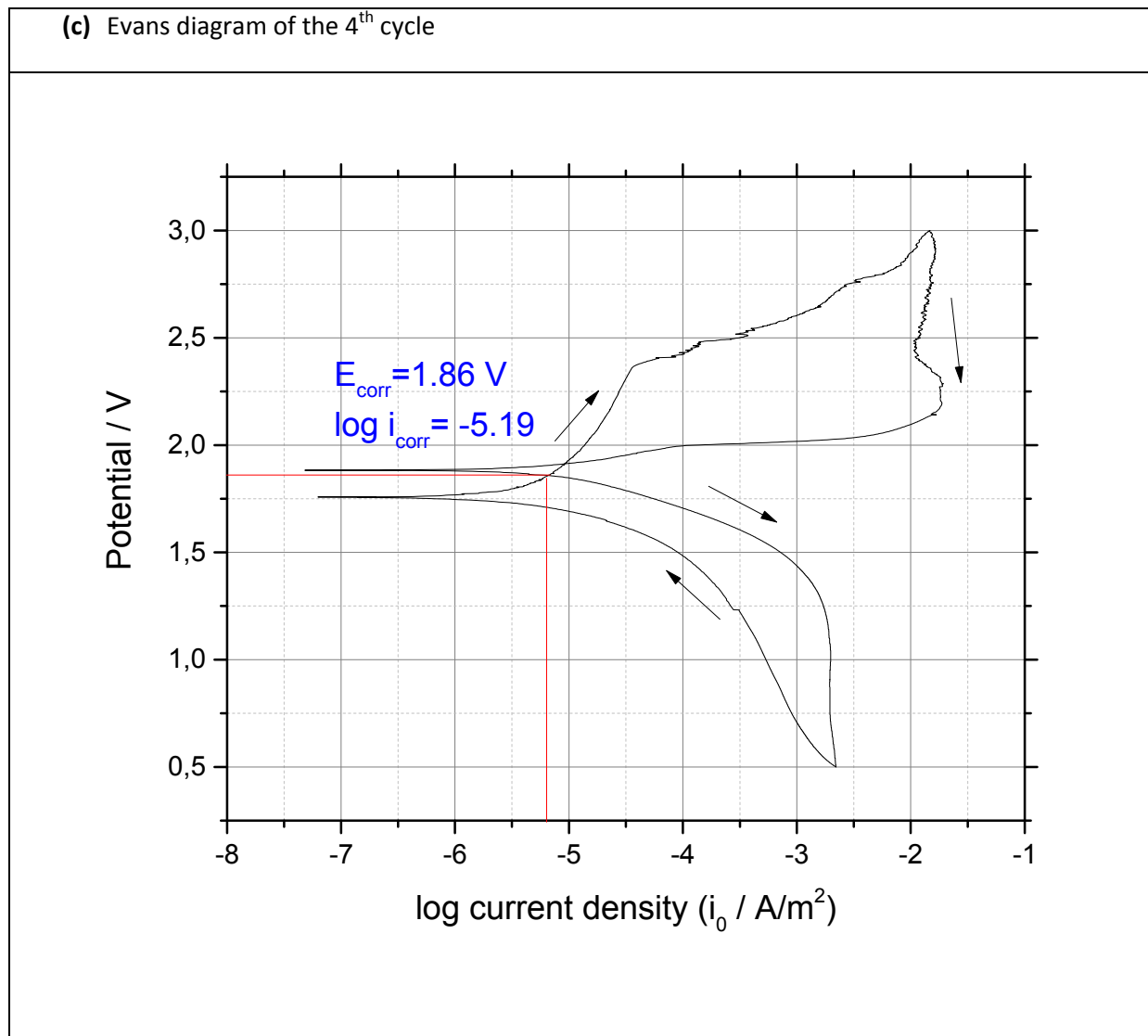
(b) Optical images

Before Measurement



After Measurement





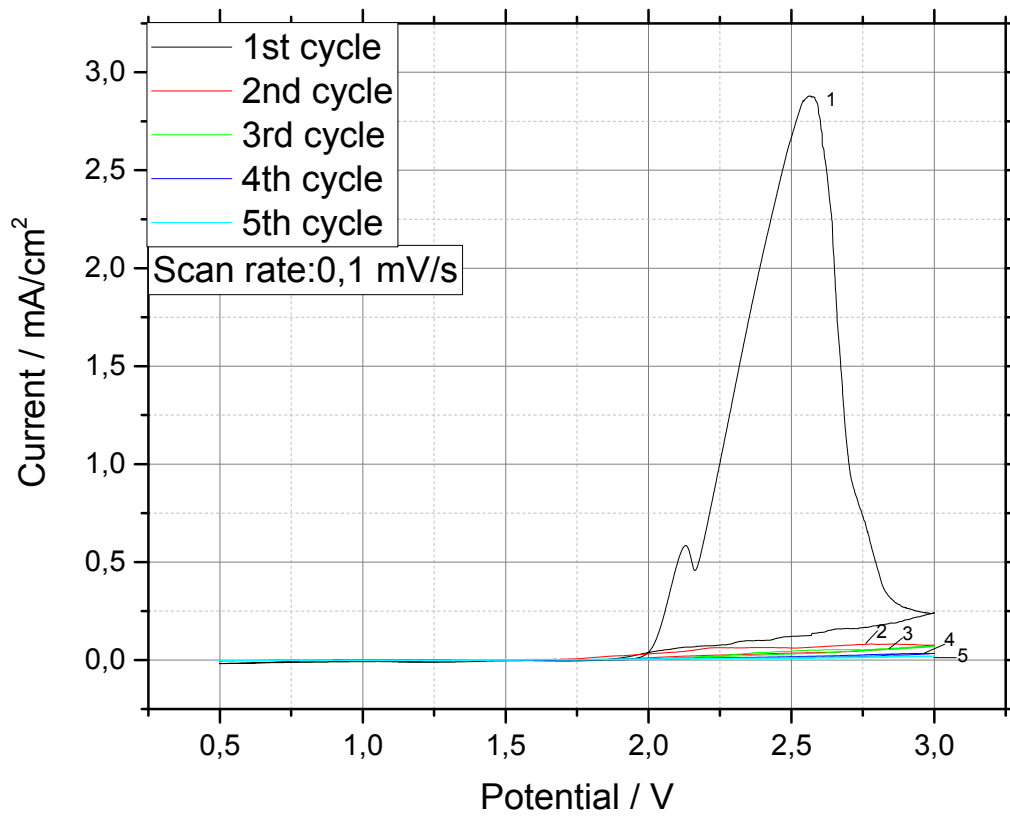
**Figure 16:** (a) Cyclic voltammogram, (b) optical microscope images and (c) Evans diagram of **stainless steel** with APC electrolyte

Figure 16 represents (a) cyclic voltammetry measurement with stainless steel mesh, 0.15 mm thick, in APC electrolyte, (b) optical images of stainless steel before and after measurement and (c) the Evans diagram of the 4<sup>th</sup> cycle. The corrosion potential is 1.86V and the  $\lg(\text{corrosion current density/ A/m}^2)$  is -5.19. Stainless steel is also very susceptible to corrosion. Corrosion damages can be also observed from the light microscope images and together with the shape of the voltammograms. It indicates pitting corrosion in the voltage range 1.8V -3V, as shown in figure 16(a). The anodic current begins to increase at about 1.8V, and an obvious oxidation peak was observed at 2.7 V.

Moreover, some stainless steel particles were dissolved in the electrolyte, the color of the APC electrolyte was changed and Mg counter and reference electrodes turned into black.

### 2.1.1.4 Copper with APC electrolyte

(a) Cyclic voltammogram

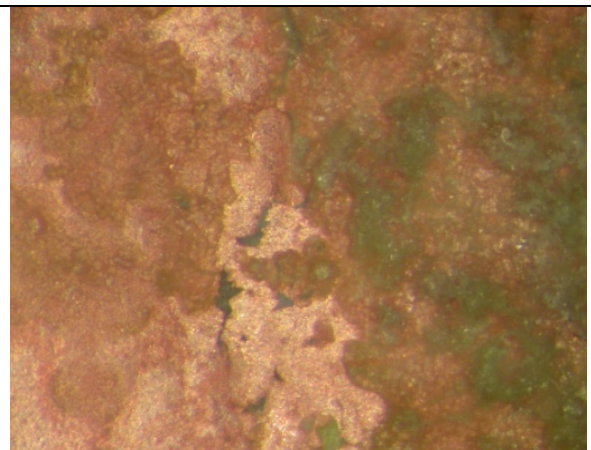


(b) Optical images

**Before Measurement**



**After Measurement**



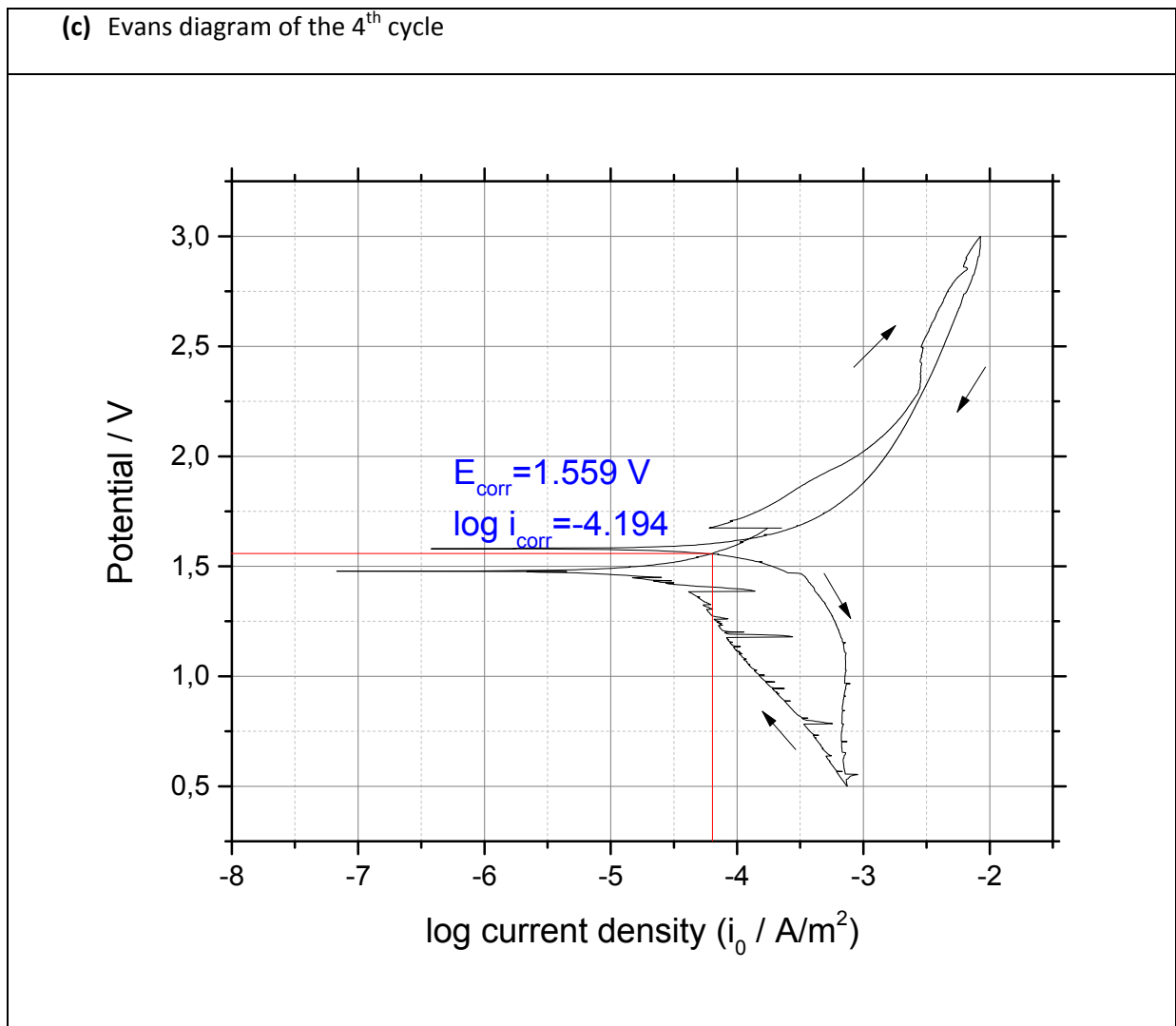
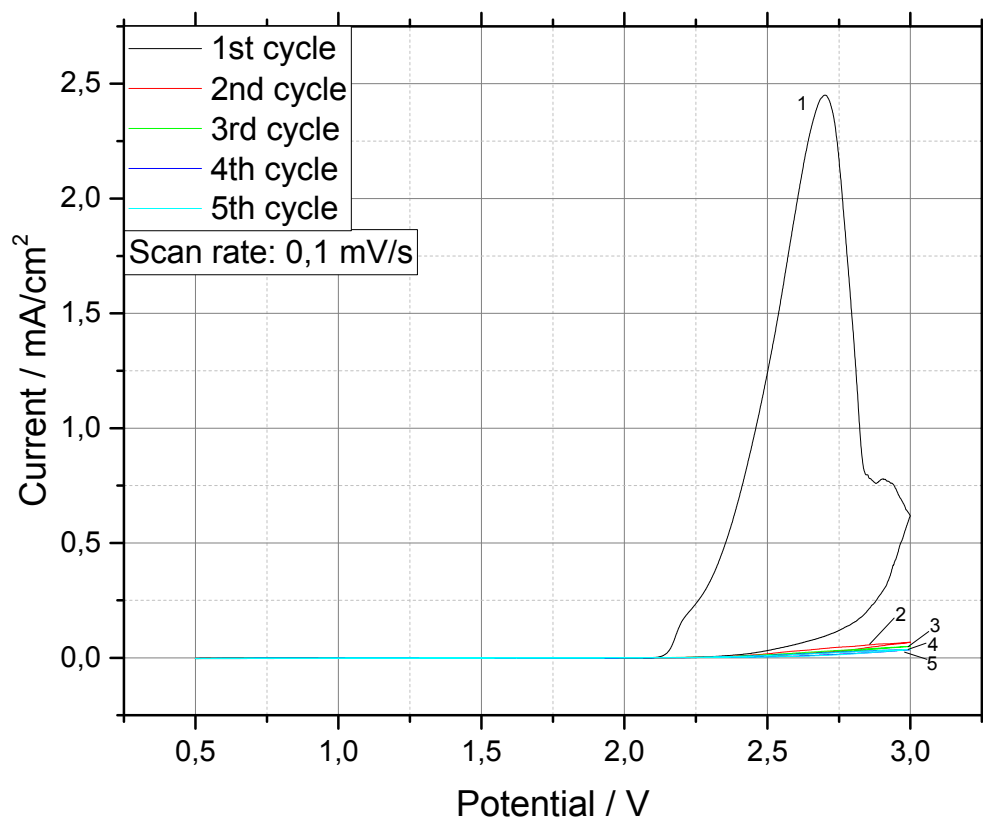


**Figure 17:** (a) Cyclic voltammogram, (b) optical microscope images and (c) Evans diagram of **copper** with APC electrolyte

Copper was found to behave better than Ti and stainless steel electrodes and did not dissolve below +1.7V vs. Mg. Figure 17 reveals that significant electrochemical corrosion was observed in the voltage range 1.8V-2.5V. The anodic current starts to increase at about 1.8 V and a prominent oxidation peak was observed at about 2.05V in the first scan. This indicates the formation of some insoluble oxidation products which remain at the surface after the cathodic scan and reduces oxidation in the following anodic scan. Anyhow, the CV measurement (a) and optical images (b) indicate unacceptable electrochemical corrosion respectively dissolution of copper. From the Evans diagram, the corrosion potential is 1.559V and the  $\lg(\text{corrosion current density}/ \text{A}/\text{m}^2)$  is -4.194. Because of reversible oxidation and reduction of Cu around 1.8V, copper is not a suitable current collector material with APC electrolyte.

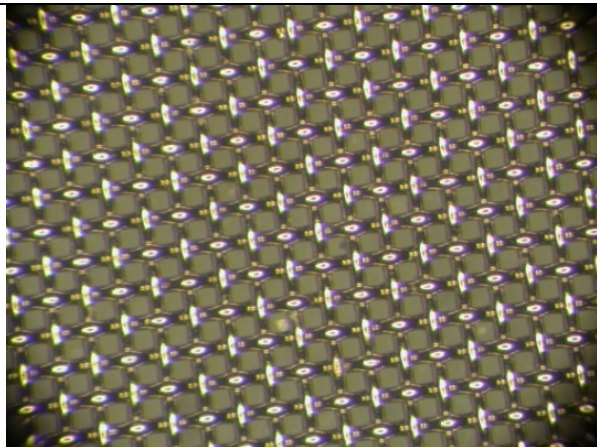
### 2.1.1.5 Nickel with APC electrolyte

(a) Cyclic voltammogram

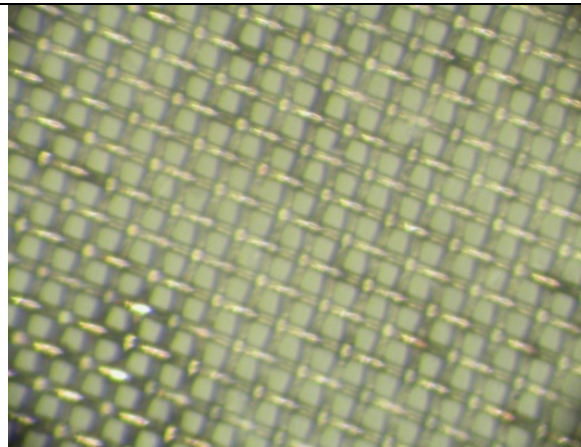


(b) Optical images

Before Measurement



After Measurement



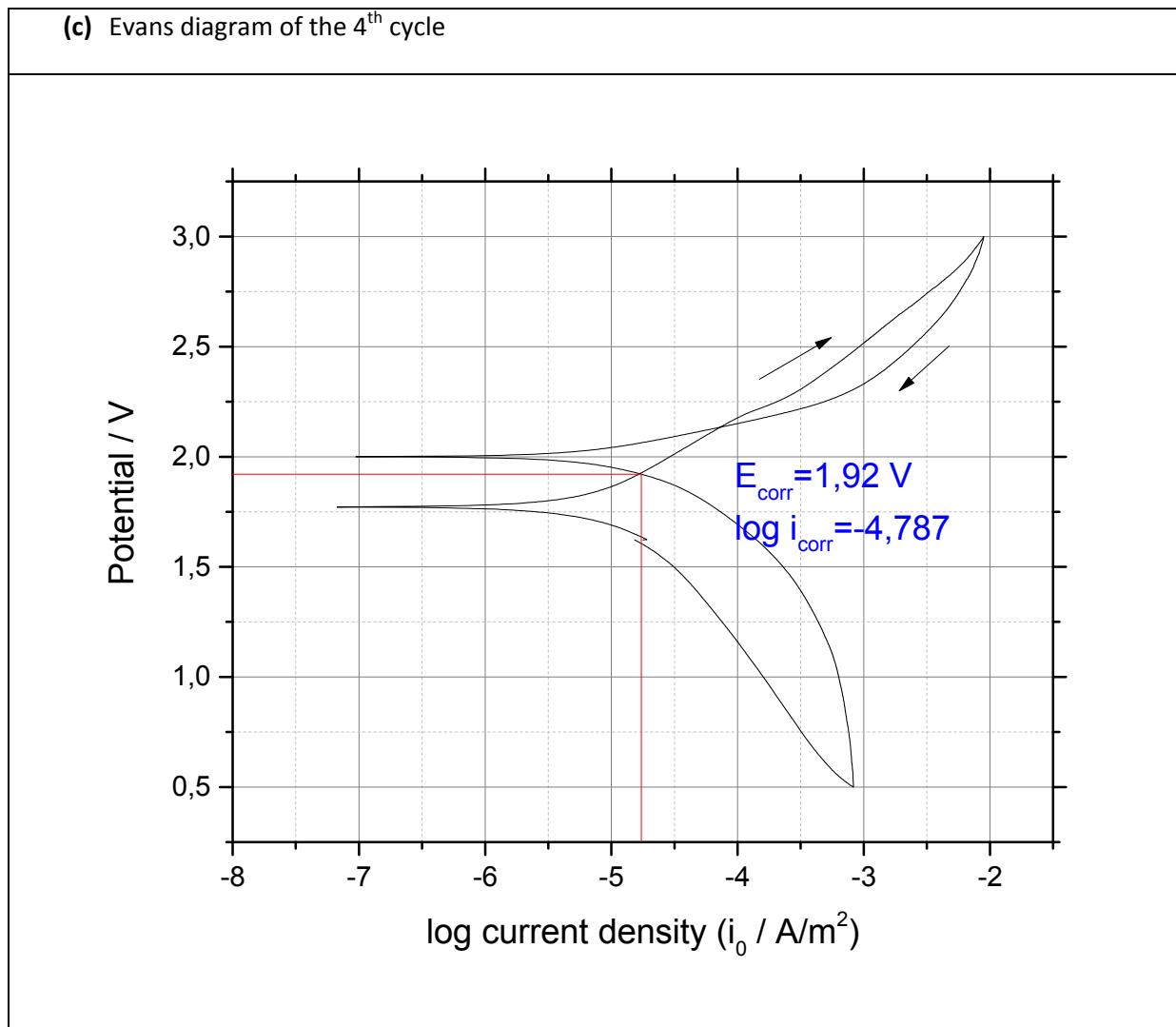
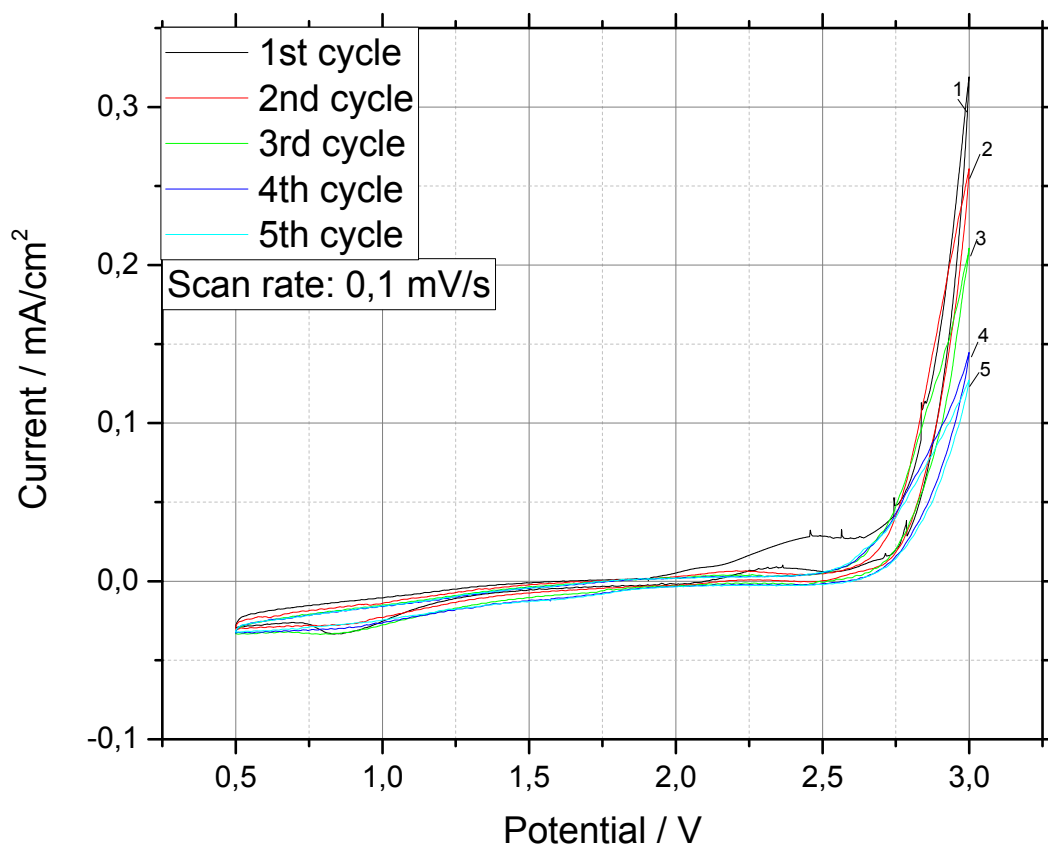


**Figure 18:** (a) Cyclic voltammogram, (b) optical microscope images and (c) Evans diagram of **nickel** with APC electrolyte

Figure 18(a) shows the oxidation peak of Ni at about 2.2V in the first cycle. The following cycles shows the formation of a passive layer. It occurs at high potentials (2.1V - 2.6V) followed by some minor Ni dissolution into the electrolyte. Optical images (b) also illustrate less corrosive attack on Ni than for other metals as there were only some color changes after CV measurement whereas Ti, Cu and stainless steel are broken into pieces and the particles were found in the electrolyte. The color of the electrolyte after measurement was clearer than the others. Mg counter electrode has some black points and reference electrode did not turn into black. The Evans diagram (c) of Nickel exhibits that, the corrosion potential is 1.92V and the  $\lg(\text{corrosion current density}/ \text{A/m}^2)$  is -4.787.

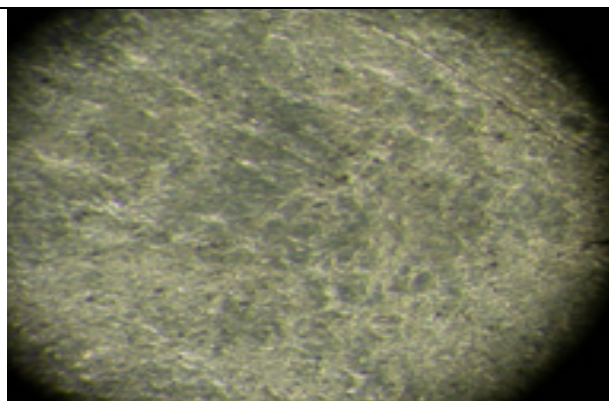
### 2.1.1.6 Graphite foil with APC electrolyte

(a) Cyclic voltammogram

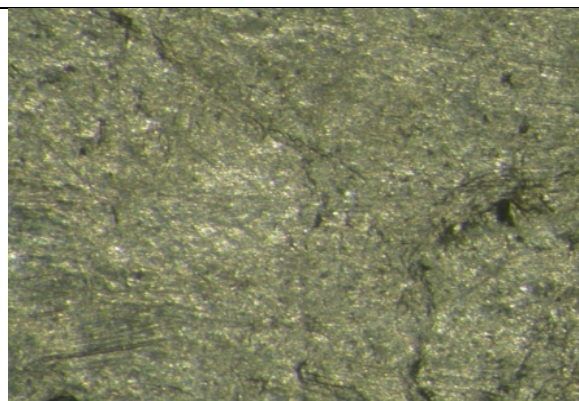


(b) Optical images

Before Measurement



After Measurement



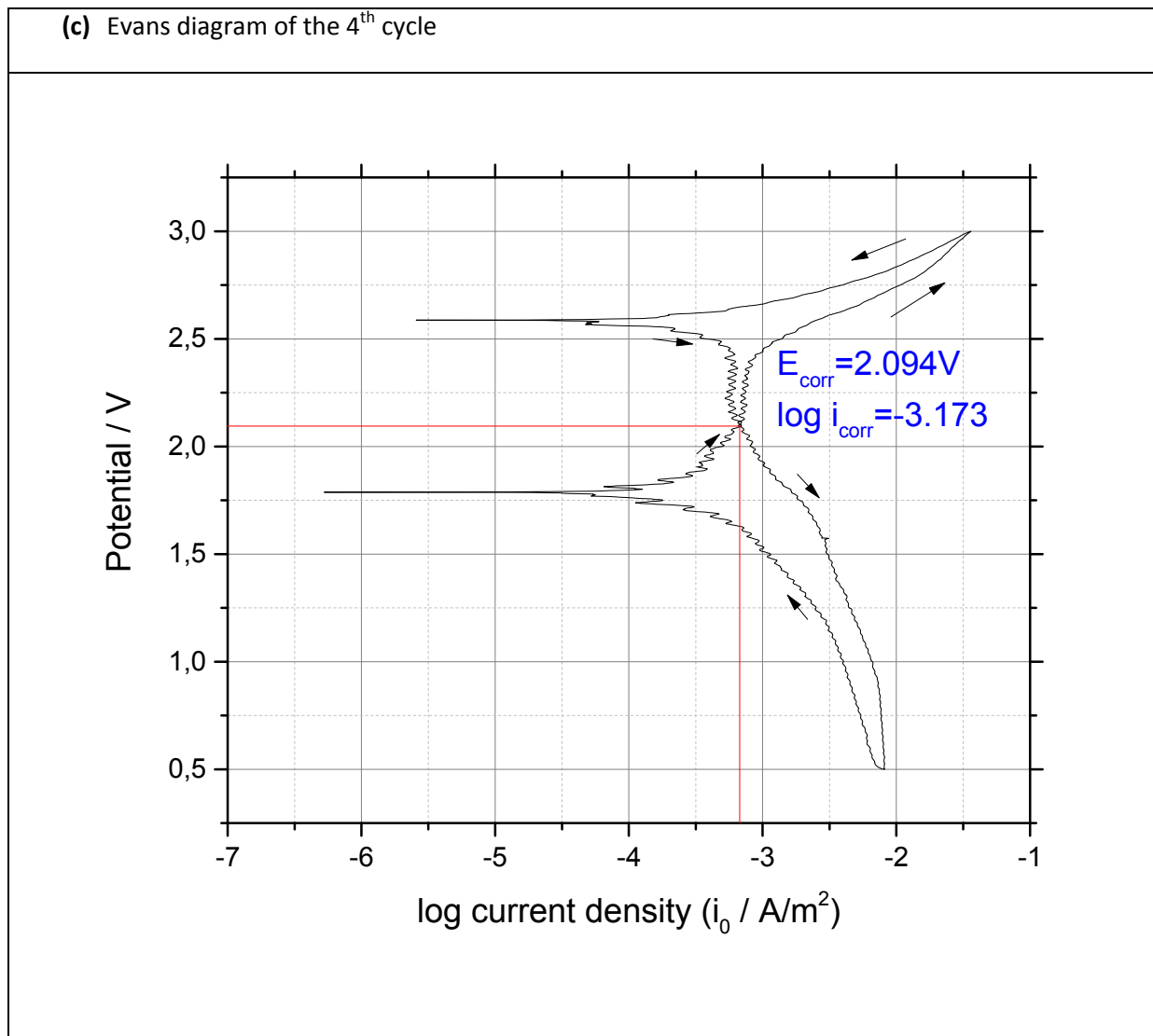


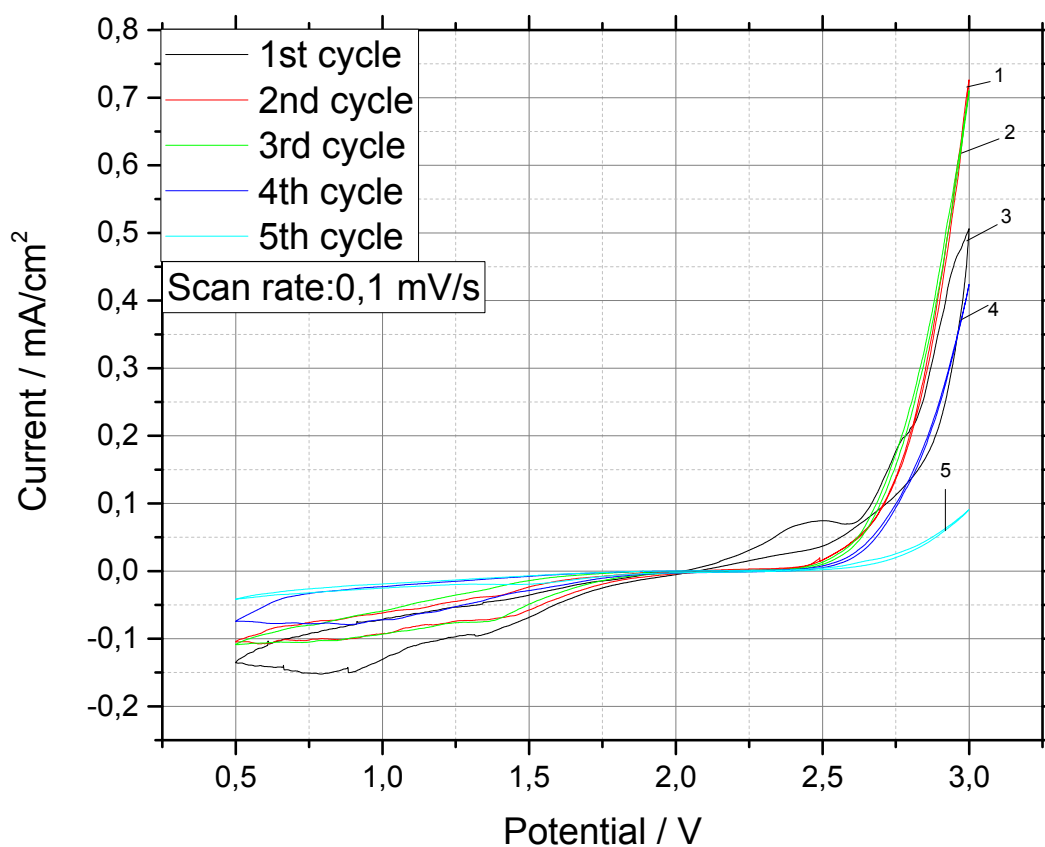
**Figure 19:** (a) Cyclic voltammogram, (b) optical microscope images and (c) Evans diagram of **graphite** with APC electrolyte

Graphite foil has a higher anodic stability than metals but it is brittle and the preparation of the electrode is more difficult than with metals. Figure 19 illustrates that graphite foil is not corroding like metals. From CV data, only the peaks of electrolyte decomposition are observed. Optical images (b) show that, there is no big difference before and after measurement. Although, the Evans diagram of graphite claims that the corrosion potential is 2.094V and the  $\log(\text{corrosion current density}/ \text{A/m}^2)$  is -3.173.



### 2.1.1.7 Carbon paper 1 with APC electrolyte

(a) Cyclic voltammogram

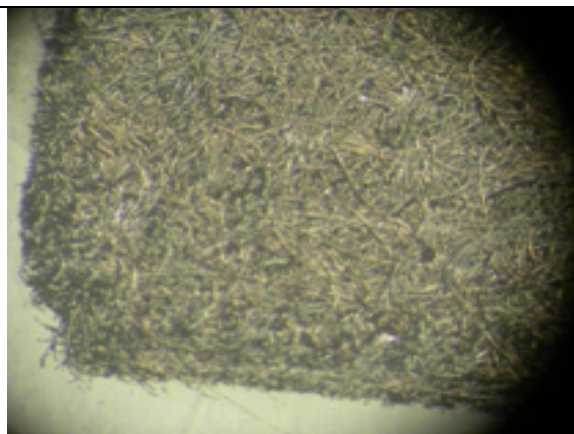


(b) Optical images

Before Measurement



After Measurement



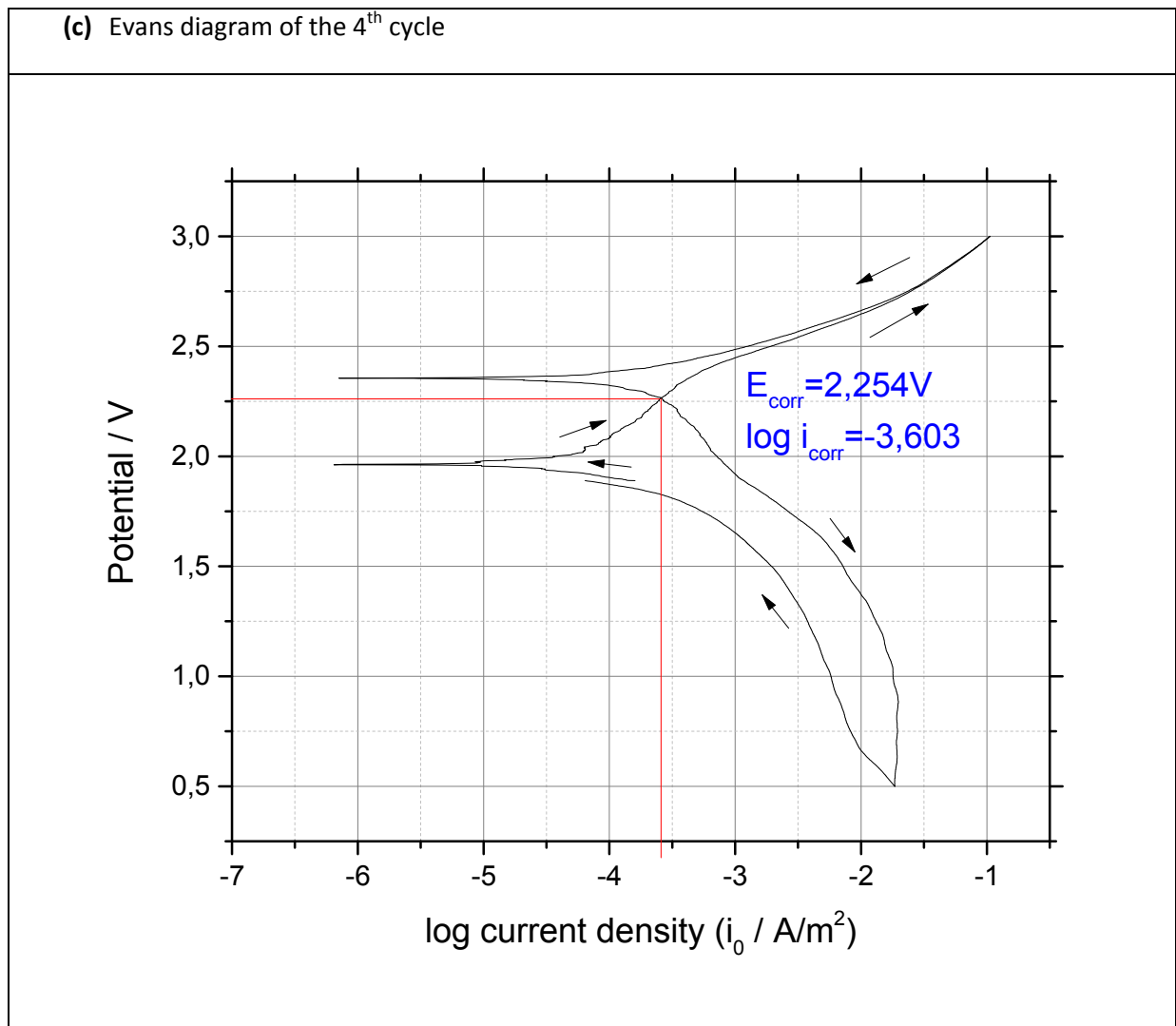
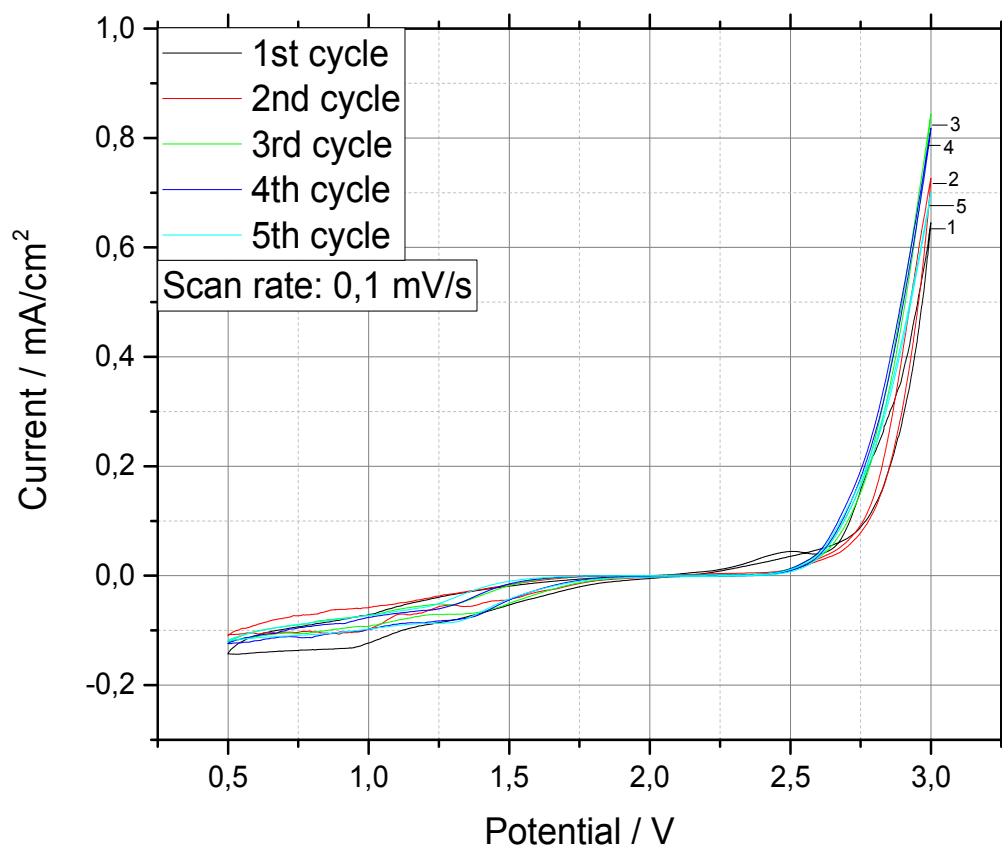


**Figure 20:** (a) Cyclic voltammogram, (b) optical microscope images and (c) Evans diagram of **carbon paper 1** with APC electrolyte

Carbon papers (like graphite foil) had also higher anodic stability than metals. They were both stable and behaved similar to glassy carbon in terms of anodic stability, and no appreciable anodic current corresponding to electrode dissolution or cathodic current corresponding to deposition of dissolved ions (if any) in the potential range of 0–3 V was observed. However, the carbon paper 1 is not very suitable for a current collector as the optical images figure 20(b) illustrates that the corners of the electrode are dissolved in the electrolyte. The corrosion potential of carbon paper 1 in the 5<sup>th</sup> cycle is calculated as 2.263V and the  $\lg(\text{corrosion current density}/ \text{A}/\text{m}^2)$  is calculated as -3.603 from the Evans diagram Figure 20(c).

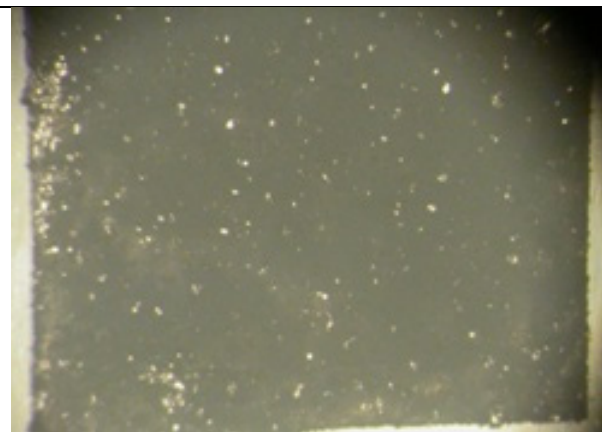
### 2.1.1.8 Carbon paper 2 with APC electrolyte

(a) Cyclic voltammogram

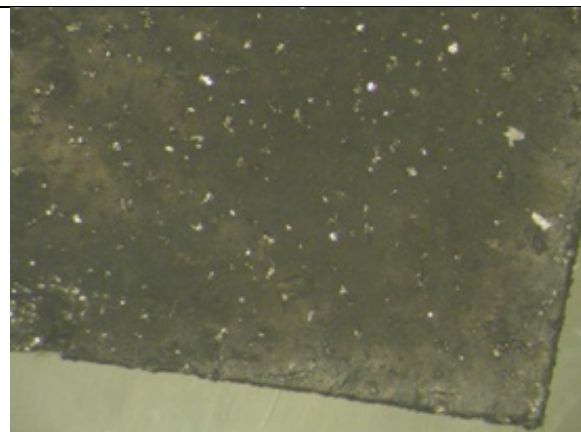


(b) Optical images

Before Measurement



After Measurement



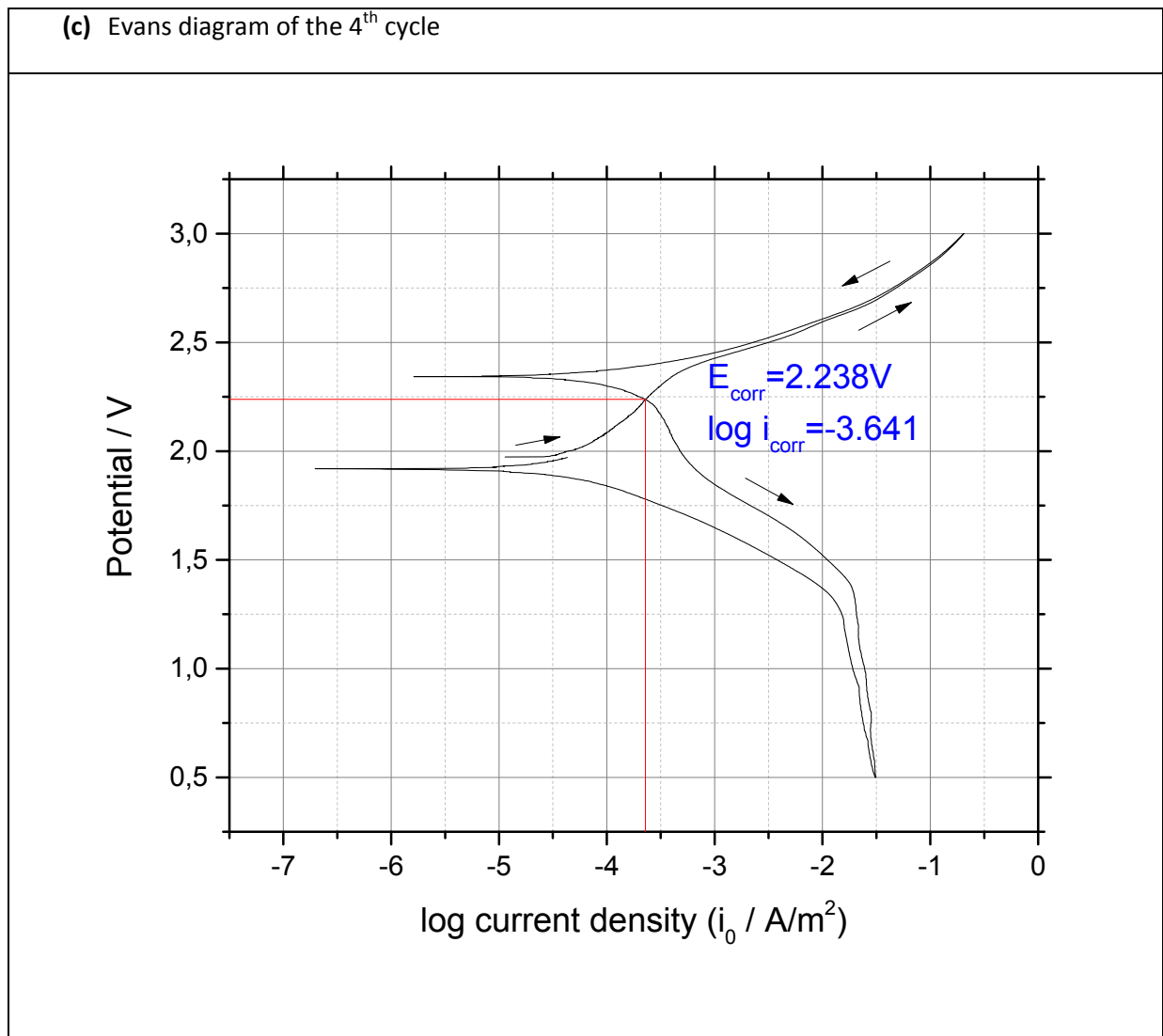
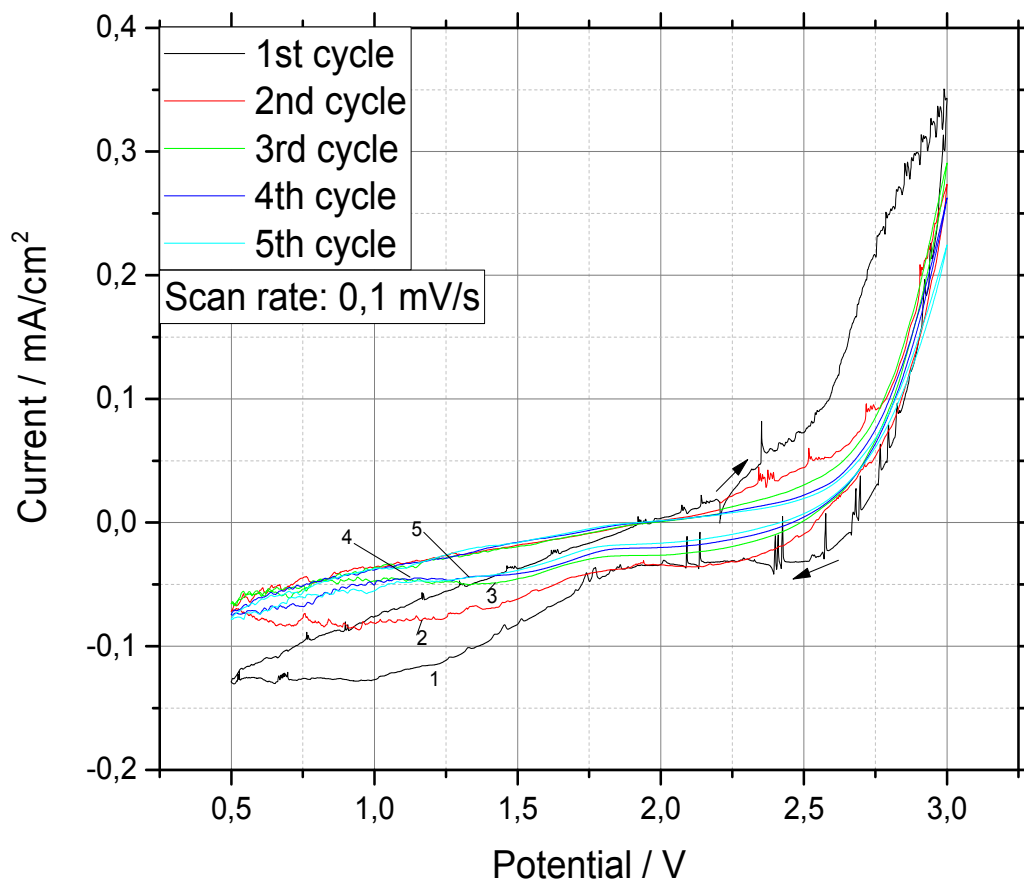


**Figure 21:** (a) Cyclic voltammogram, (b) optical microscope images and (c) Evans diagram of **carbon paper 2 (teflon)** with APC electrolyte

Figure 21 represents that carbon paper 2 with Teflon is almost like carbon paper 1 and has high anodic stability. The optical images (b) claim that, there is no big difference before and after measurement and it performs better than carbon paper 1. The Evans diagram illustrates that, the corrosion potential is 2.238V and the log(corrosion current density/  $A/m^2$ ) is -3.641.

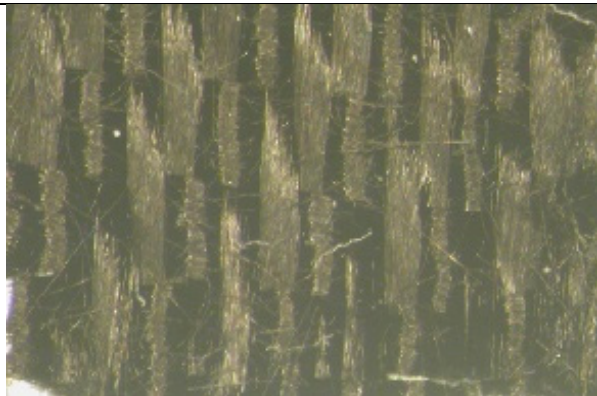
### 2.1.1.9 Carbon textile 1 with APC electrolyte

(a) Cyclic voltammogram



(b) Optical images

Before Measurement



After Measurement



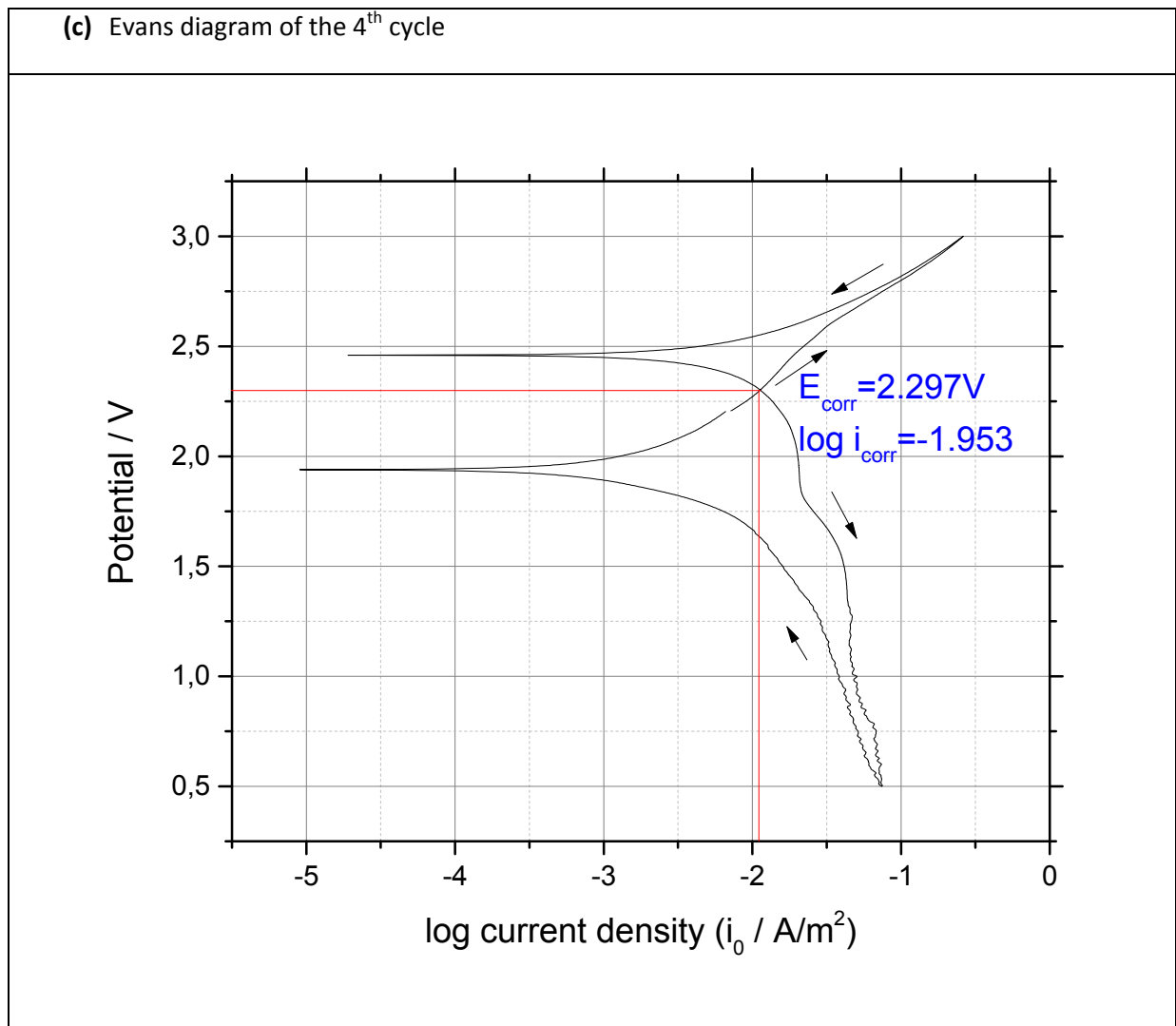
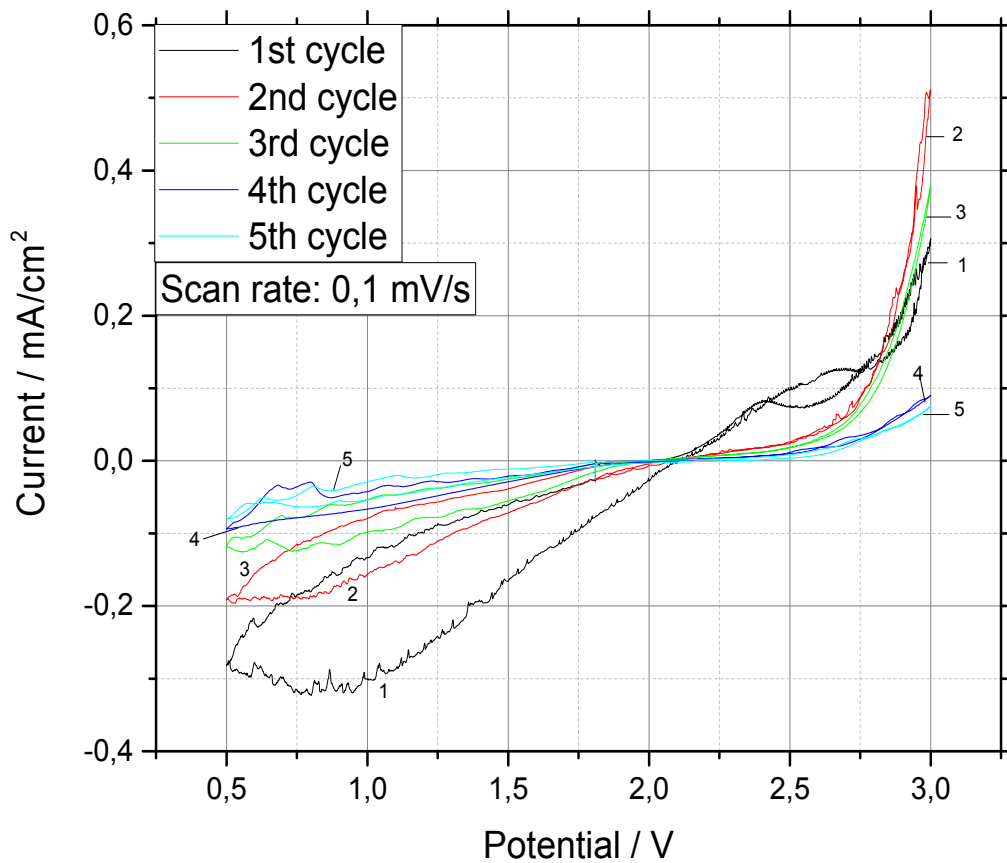


**Figure 22:** (a) Cyclic voltammogram, (b) optical microscope images and (c) Evans diagram of **carbon textile 1** with APC electrolyte

Carbon textiles are not very suitable for commercial magnesium battery as cutting and coating processes are more difficult than for metals and carbon papers. Nevertheless, Figure 22 (a) CV measurement illustrates that it has good anodic stability. However, optical images (b) reveal that the fiber textures are expanded after measurement. The corrosion potential of carbon textile 1 in the 5<sup>th</sup> cycle is calculated as 2.297V and the log(corrosion current density/  $A/m^2$ ) is calculated as -1.953 from the Evans diagram Figure 22(c).

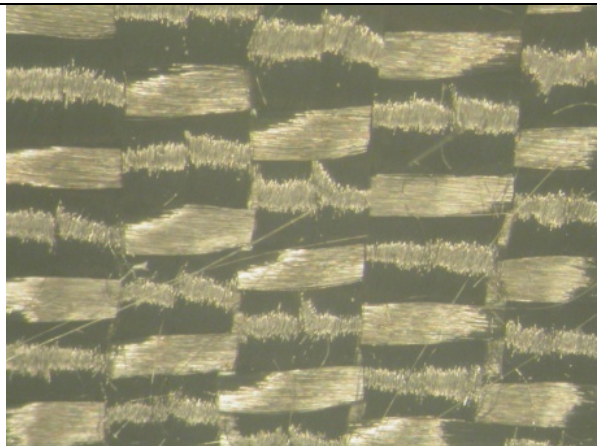
### 2.1.1.10 Carbon textile 2 (Sorbent) with APC electrolyte

(a) Cyclic voltammogram



(b) Optical images

Before Measurement



After Measurement



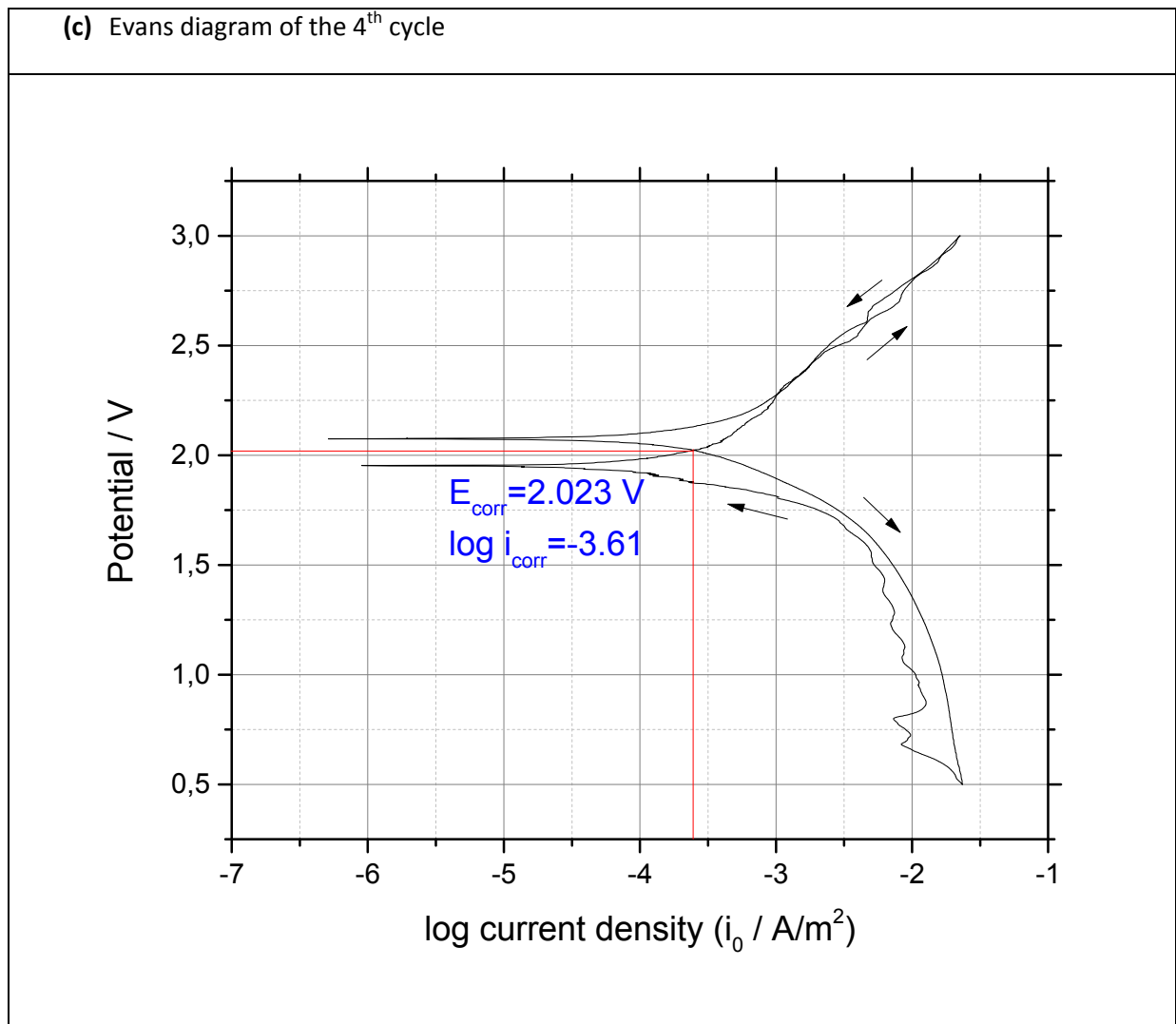


**Figure 23:** (a) Cyclic voltammogram, (b) optical microscope images and (c) Evans diagram of **carbon textile 2 (sorbent)** with APC electrolyte

Figure 23 illustrates that carbon textile 2 Sorbent is almost like carbon textile 1 and has a bit higher anodic stability than carbon textile 1. The optical images (b) show that the meshes of the textile fibers are expanded after measurement. The Evans diagram (c) represents that the corrosion potential is 2.023V and the  $\lg(\text{corrosion current density}/ \text{A/m}^2)$  is -3.61.



### 2.1.2 Comparison of current collectors with APC electrolyte

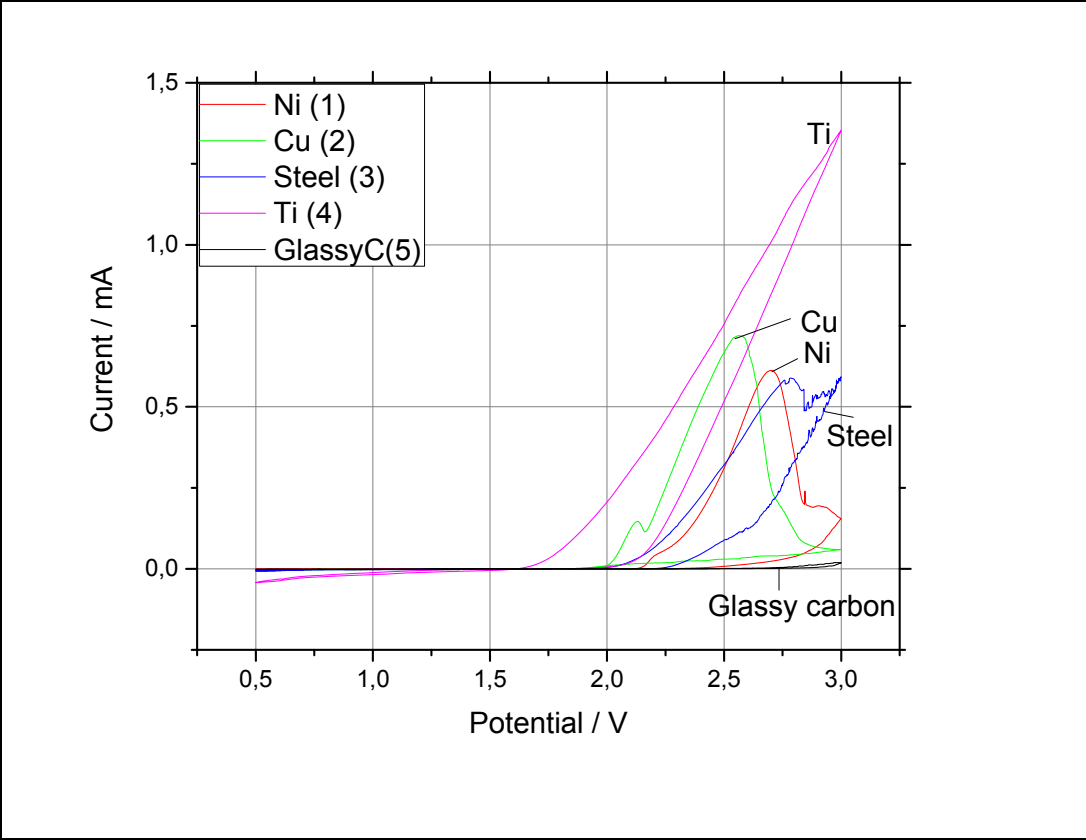


Figure 24: Comparison of metal current collectors with APC electrolyte at 1<sup>st</sup> cycle

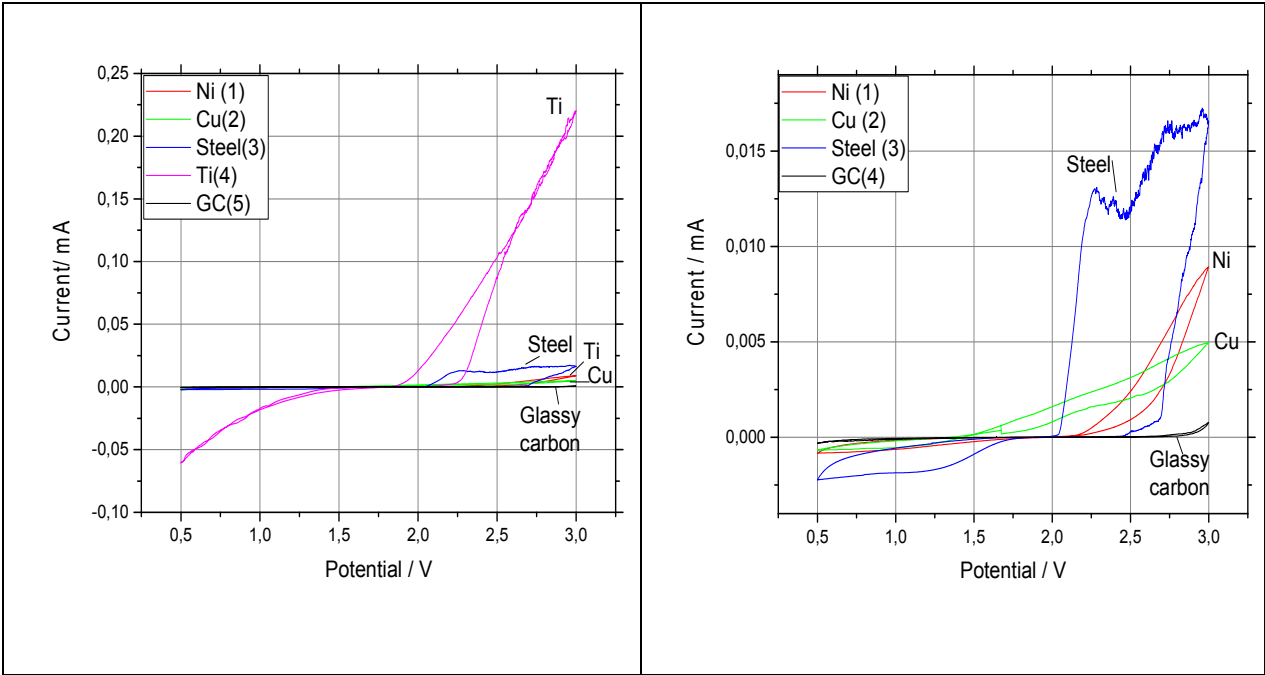
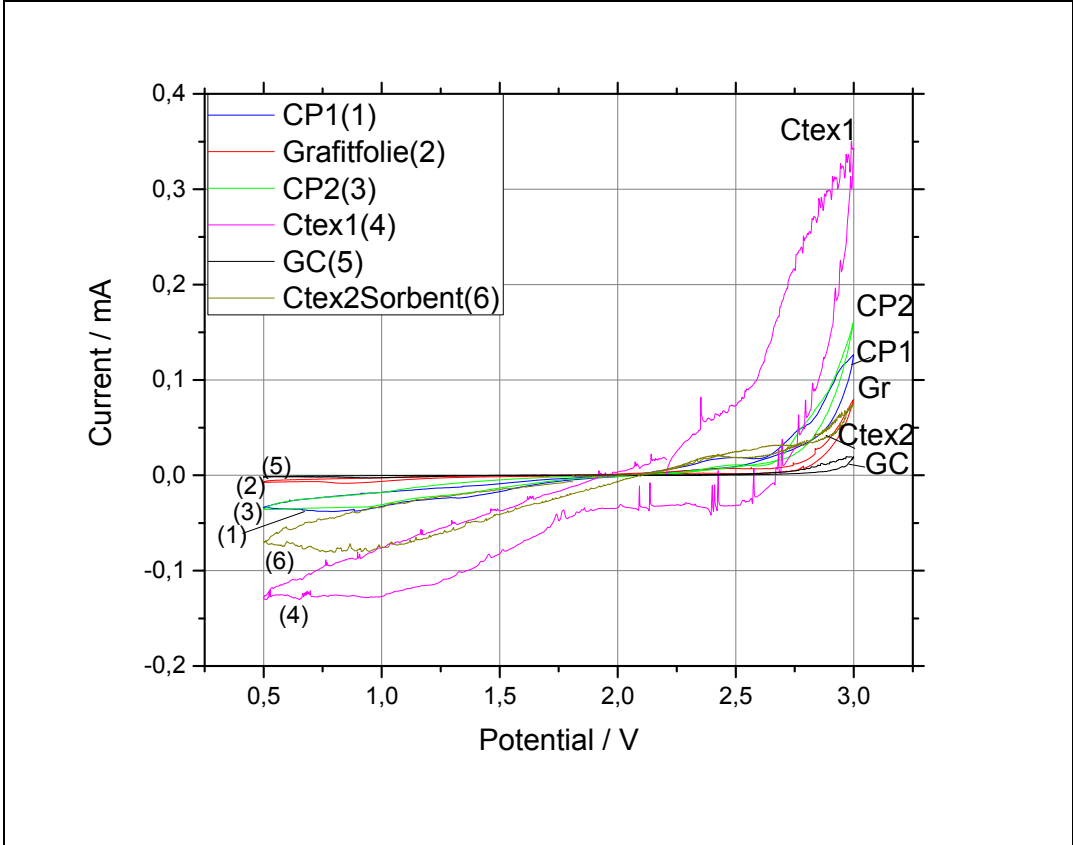


Figure 25: Comparison of metal current collectors with APC electrolyte at 5<sup>th</sup> cycle with and without Titanium. Current scale in the right diagram enlarged.

In a chloride-rich environment (as chloride is found in both the cation and anion components of the APC electrolyte), the predominant corrosion mechanism for metals is through the reactions with chloride anions [28]. The order of stability limits of different metal current collectors is like Ni > Cu > Steel > Ti. As by Figure 24 and Figure 25 represented, nickel has higher corrosion resistance with APC electrolyte than the other metal current collectors. It is stable till about 2.2 V. In the next step, the stability tests are performed.



**Figure 26:** Comparison of carbon based current collectors with APC electrolyte at 1<sup>st</sup> cycle

Figure 26 and Figure 27 illustrates that the most stable current collectors with APC electrolyte are graphite and carbon textile 2 with sorbent. The stability tests were executed also for glassy carbon, graphite foil and carbon textile 2.

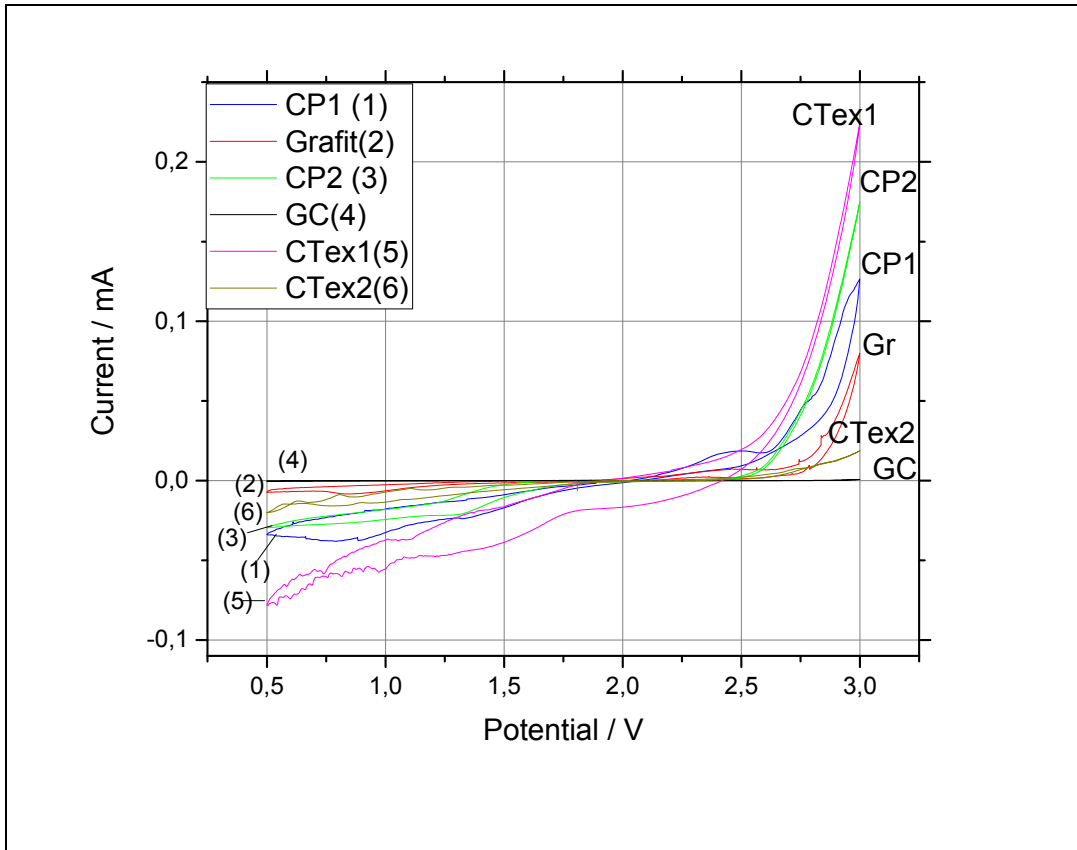
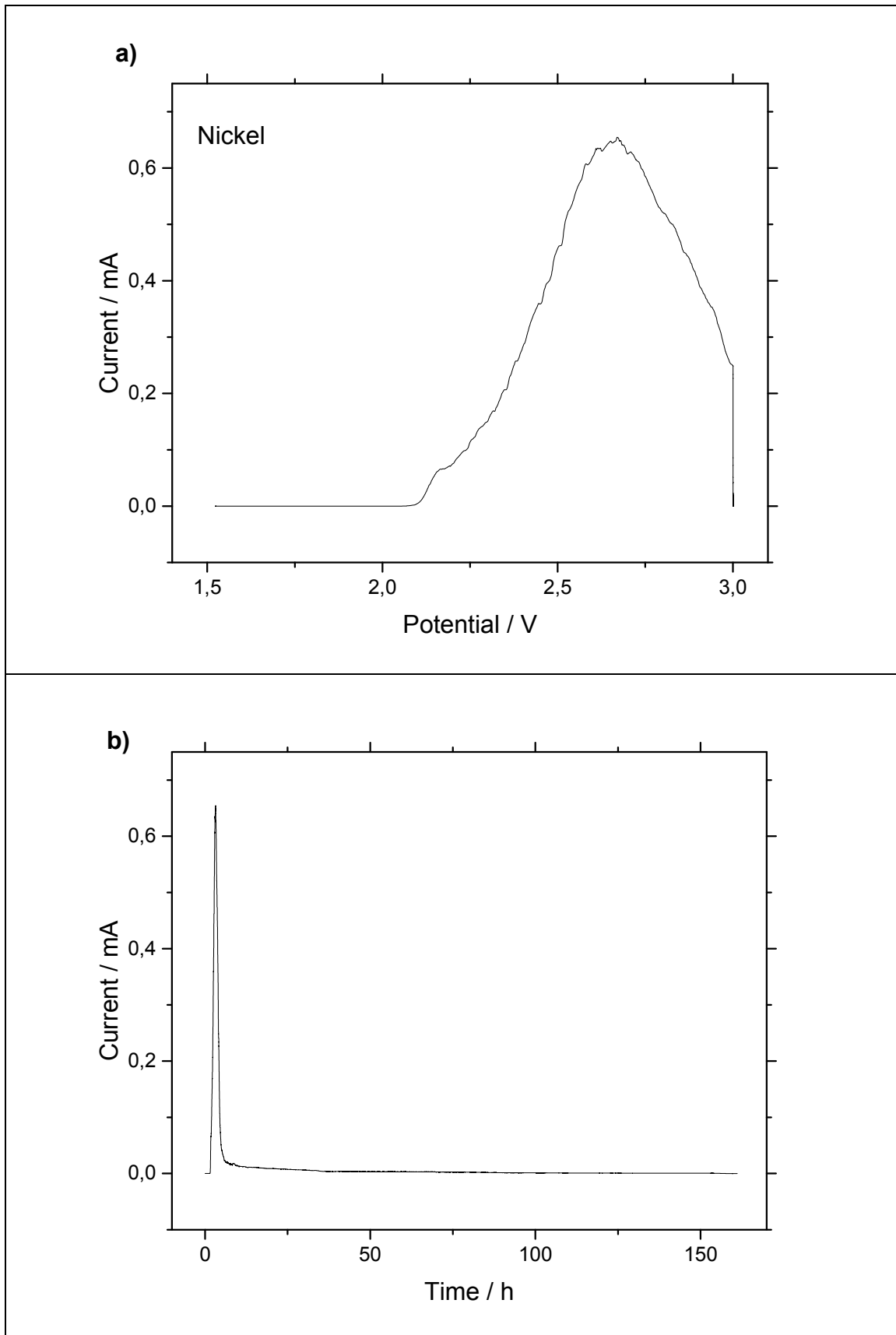


**Figure 27:** Comparison of carbon based current collectors with APC electrolyte at 5<sup>th</sup> cycle

### 2.1.3 Stability test of current collectors with APC electrolyte

After a linear scan from OCV to 3V with a scan rate of  $0.1 \text{ mVs}^{-1}$ , this potential was kept and the current for a longer period of time up to almost 160h was recorded. Figure 28-31 b) represent linear plots of the current at this final holding potential of 3V over the total stability testing time of about 50 to 160 hours. The stability test was performed for nickel, glassy carbon, graphite foil and carbon textile 2. Figures 28-31 illustrate the progress of corrosion current versus potential in a) and versus time in b). From Faraday laws and growth of films due to Wagner theory of oxidation (described in part 1.7.4), in figure 28-31 c)  $\int i(t)dt$  is plotted versus  $\sqrt{t}$ .

### 2.1.3.1 Nickel



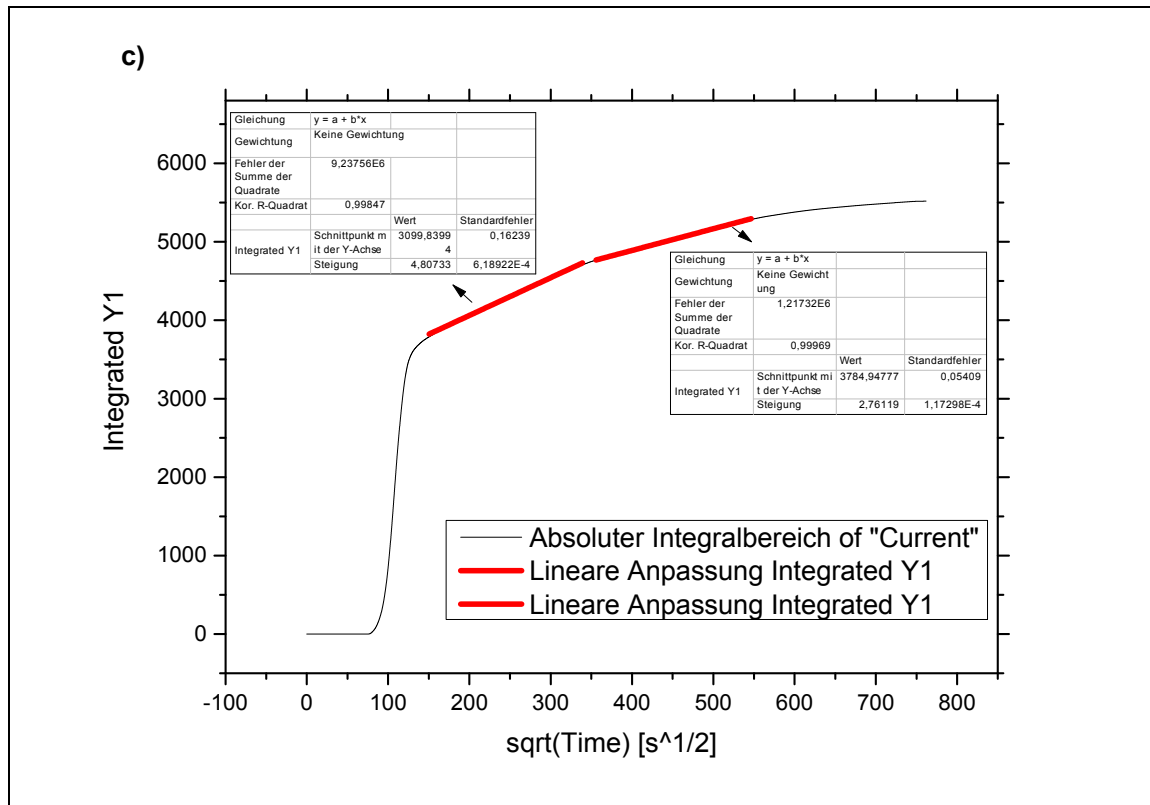
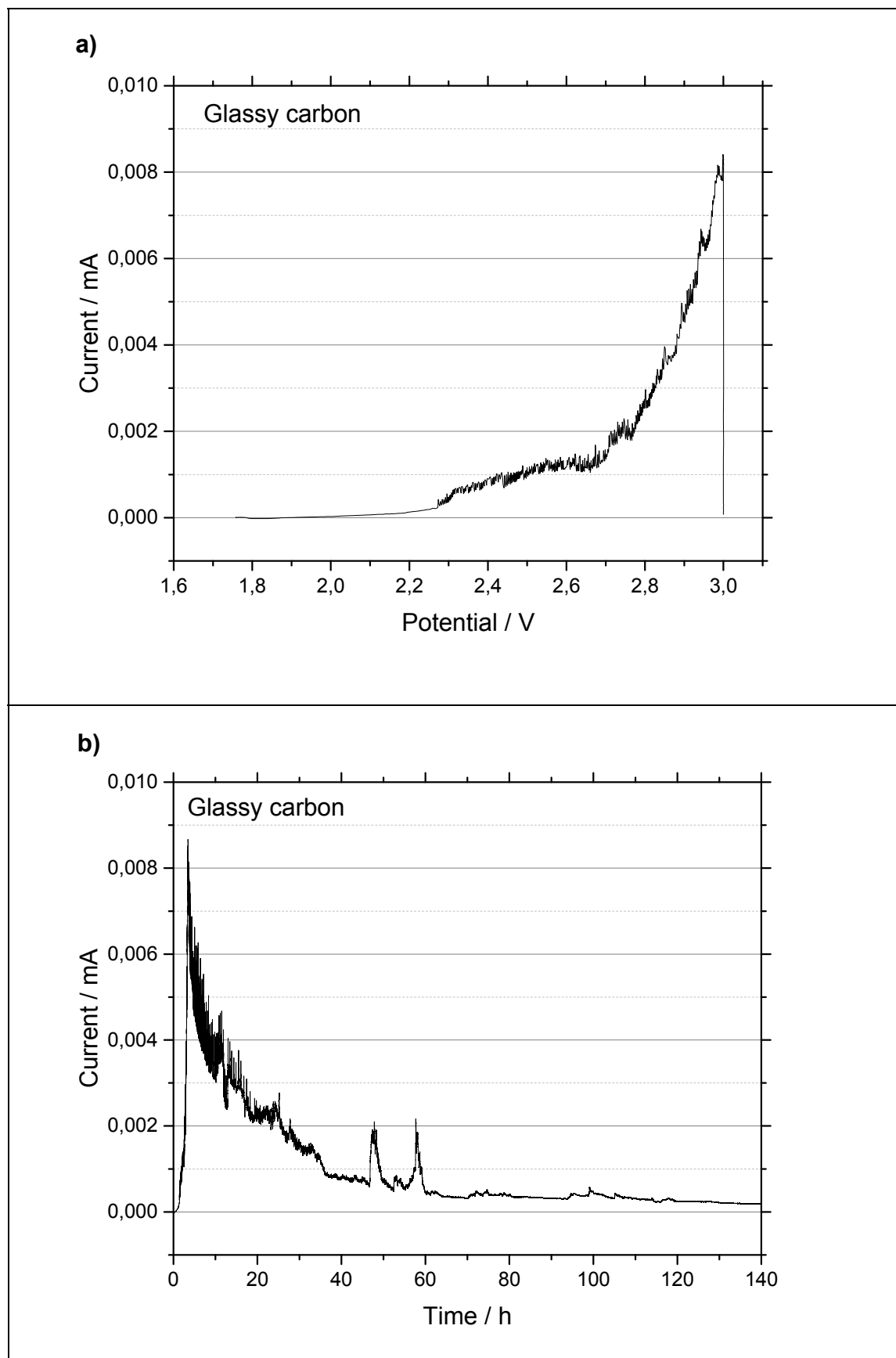
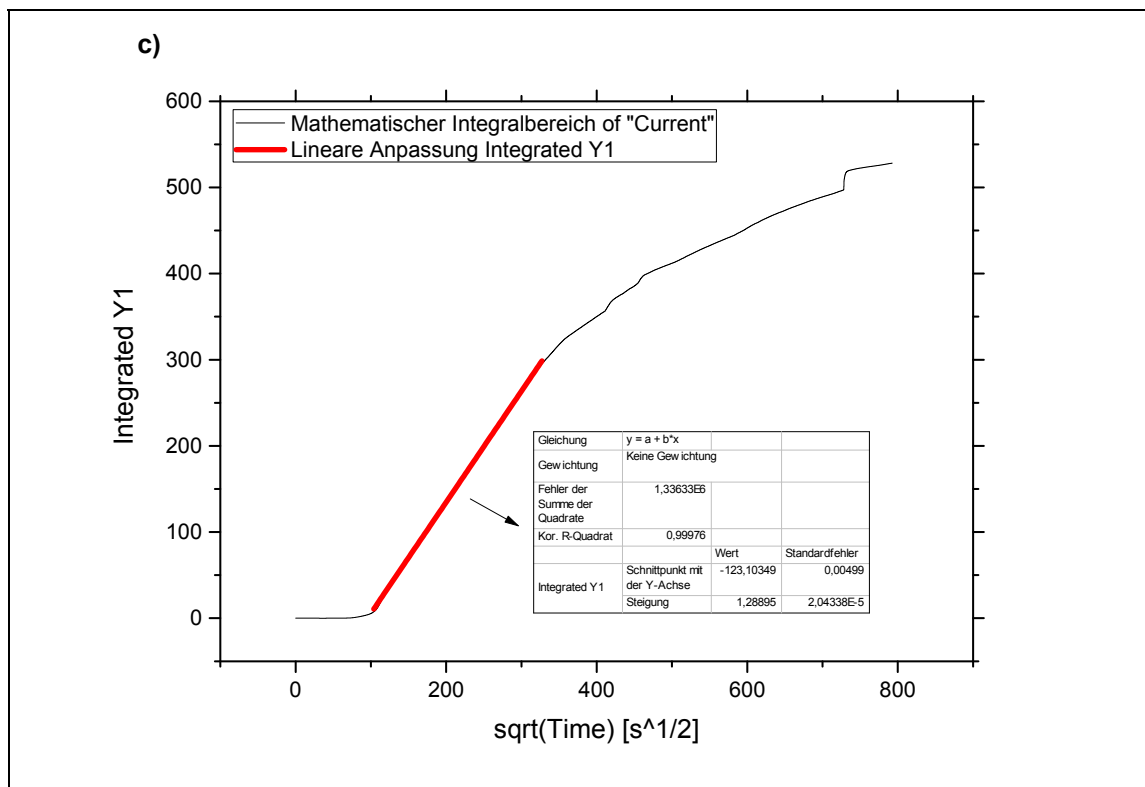


Figure 28: Stability test of Ni with APC electrolyte

Figure 28 a) illustrates the decrease of current density by holding potential at 3V and figure 28 b) shows that in 80 hours the current density was very low (almost 0). The low current densities (0-1  $\mu\text{A cm}^{-2}$ ) indicate that the electrolyte solution is stable in contact with the Nickel up to 3.0 V. The decrease of the current density suggests the formation of a passive film on the electrode surface. In general, the corrosion resistivity of a material depends on scales consisting of the reaction products formed on its surface as well as the stability of the products [60]. As in chapter 1.7.4 explained, the linear dependence of the charge versus  $\sqrt{t}$  in Fig. 28 c) might indicate the formation of a stable passivation layer on Ni surface in APC electrolyte.

### 2.1.3.2 Glassy carbon

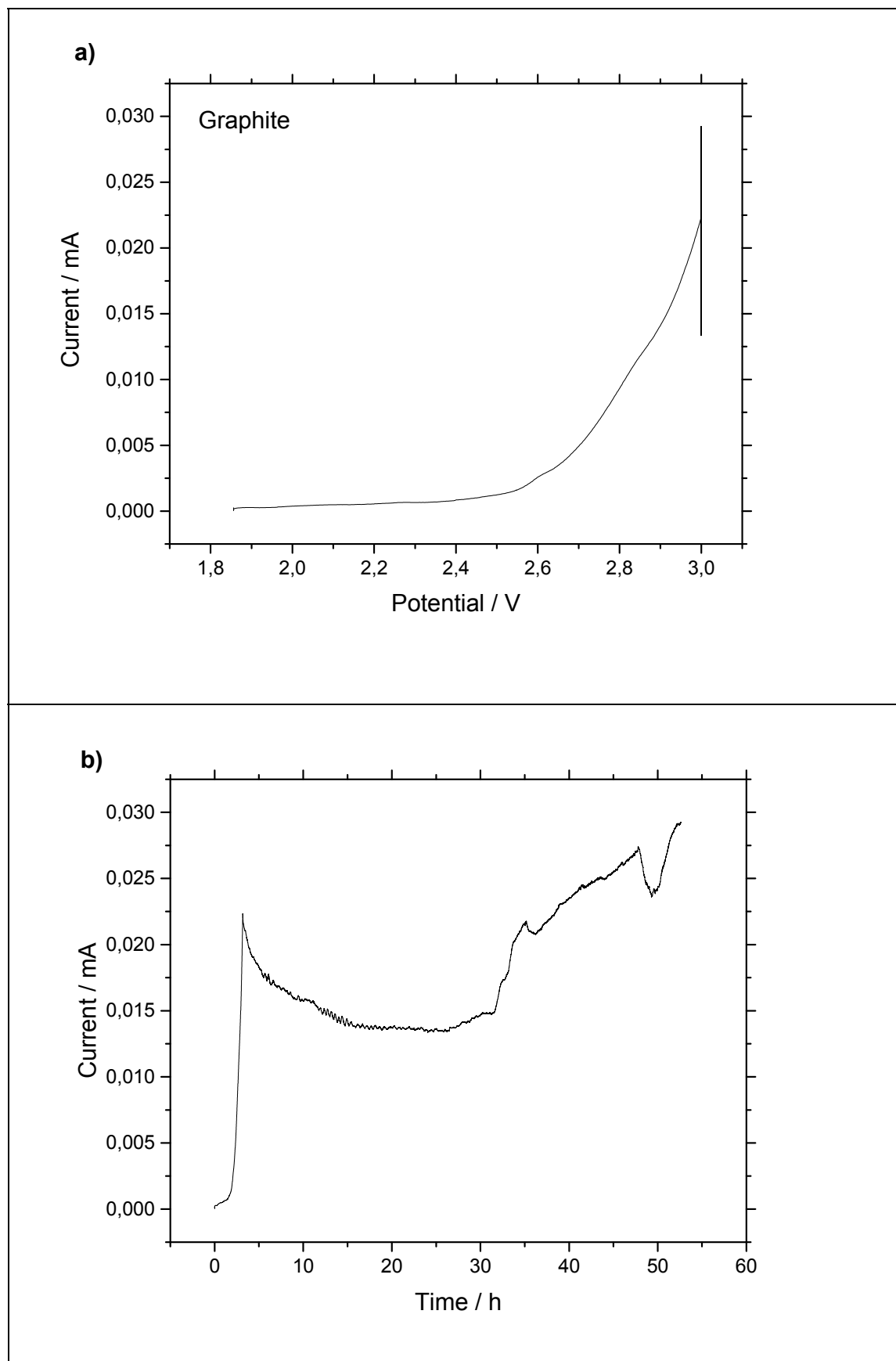




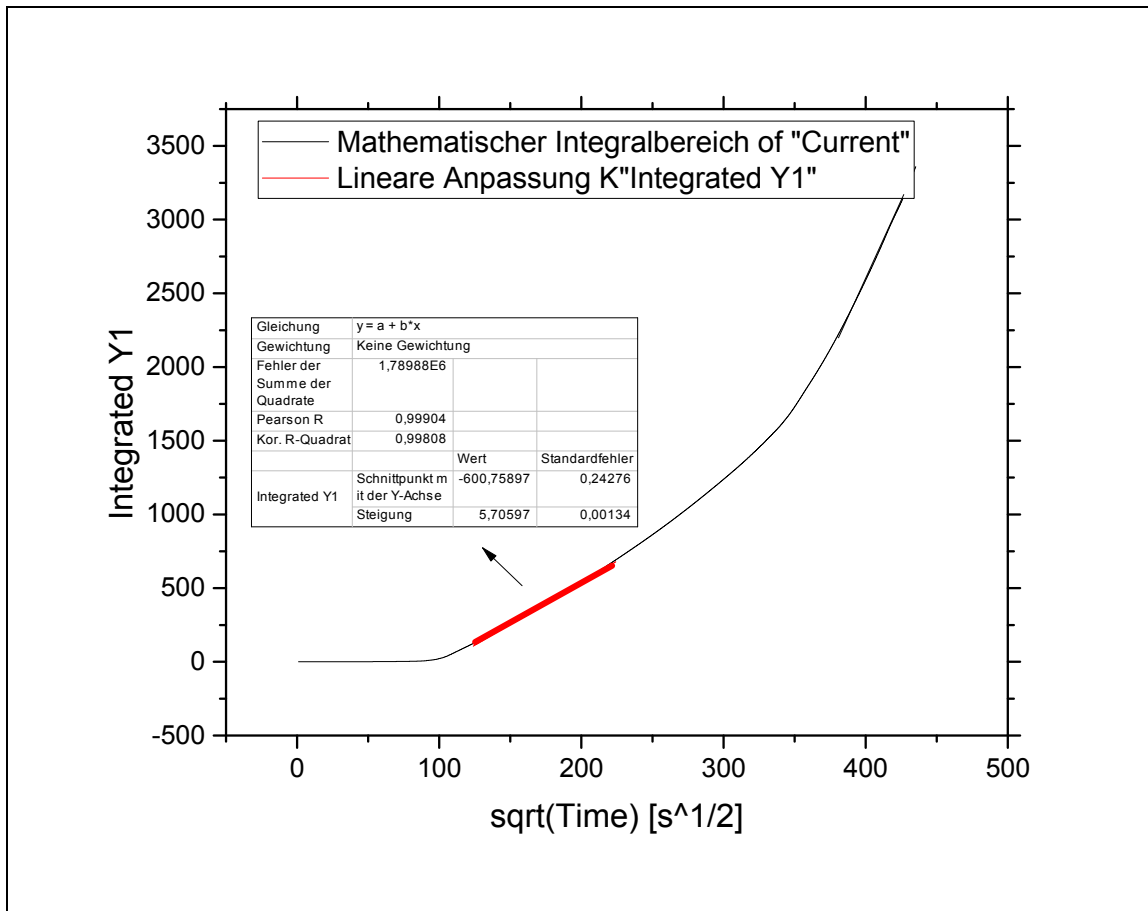
**Figure 29:** Stability test of glassy carbon with APC electrolyte

Figure 29 a) shows the decrease of current density by holding potential at 3V and as seen in figure 29 b) the current density declined to almost 0 in 140 hours. 28 c) illustrates that some reaction products on the glassy carbon surface caused the decrease of the current density. Due to the lowest current density, glassy carbon is the most stable material with APC electrolyte.

### 2.1.3.3 Graphite



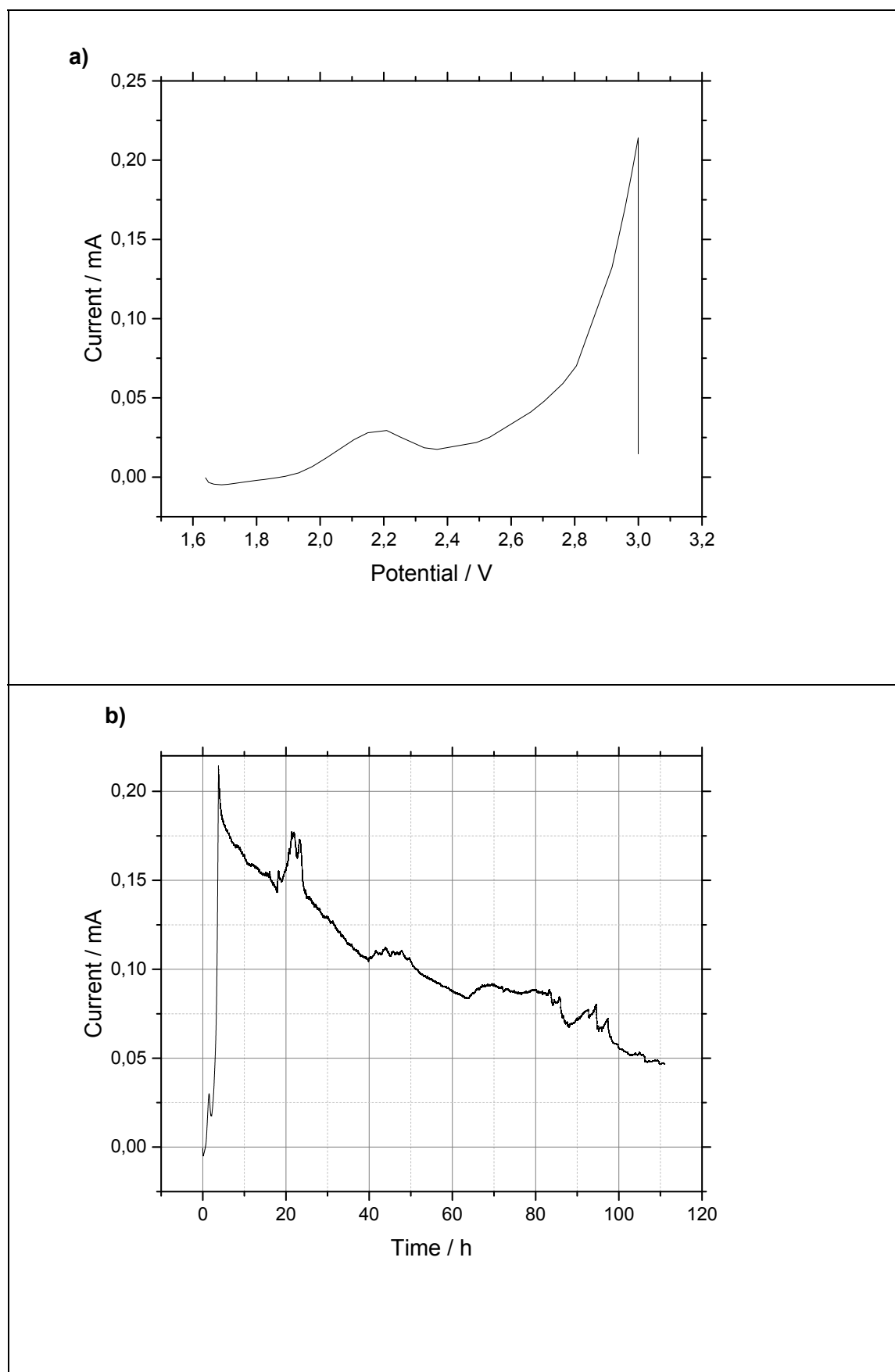


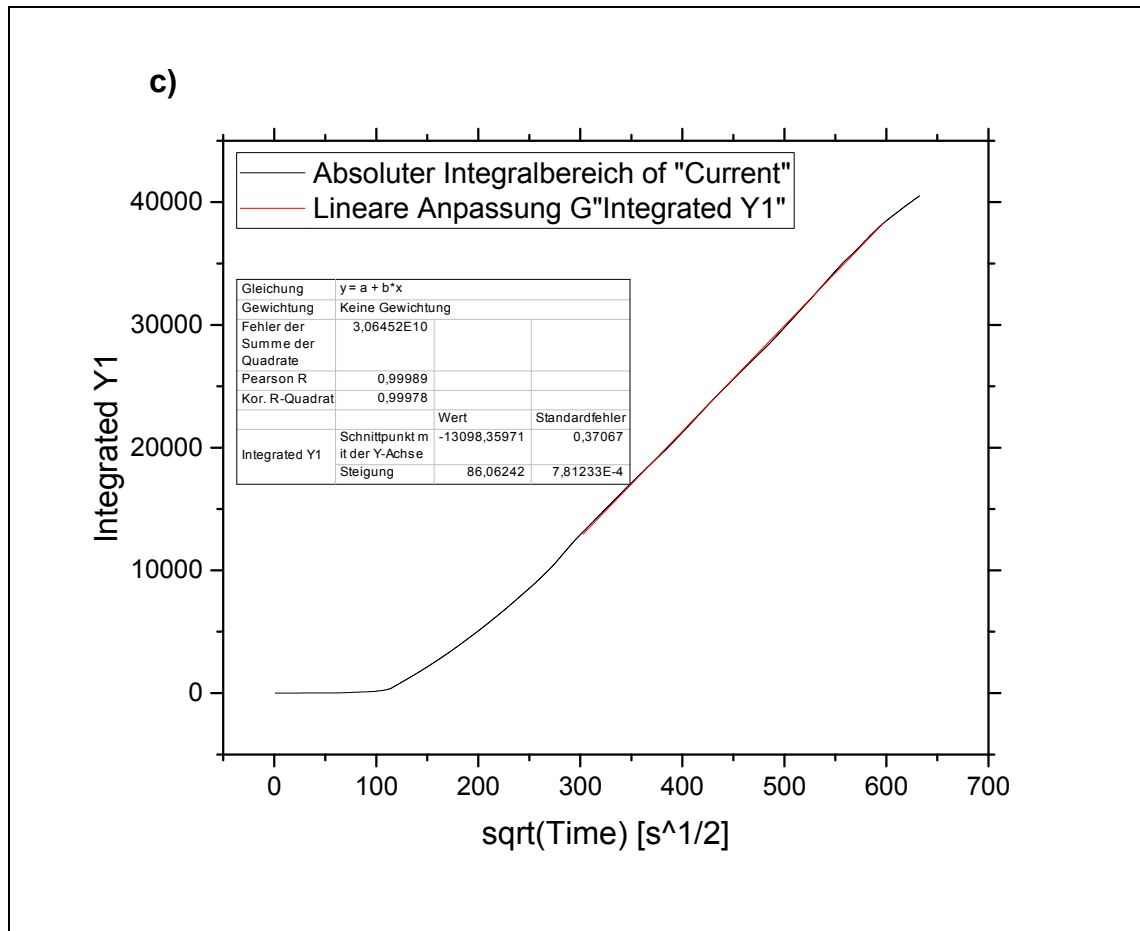


**Figure 30:** Stability test of graphite with APC electrolyte

Figure 30 a) illustrates that at the beginning the current density decreased and then increased by holding potential at 3V. Figure 30 b) shows that in 25 hours the current density decreased to 0.012 mA and then increased to 0.025mA. During chronoamperometry at a potential of 3V versus  $Mg/Mg^{2+}$  no increase of the current density was measured during the first 25 h, confirming a good initial stability of the graphite current collector in the electrolyte. However, after 25h the rise of the current density revealed deterioration of the passivation film. This might be related to intercalation of anions like chloride into the graphite layers [61] after long polarization time.

### 2.1.3.4 Carbon textile 2 (with sorbent)



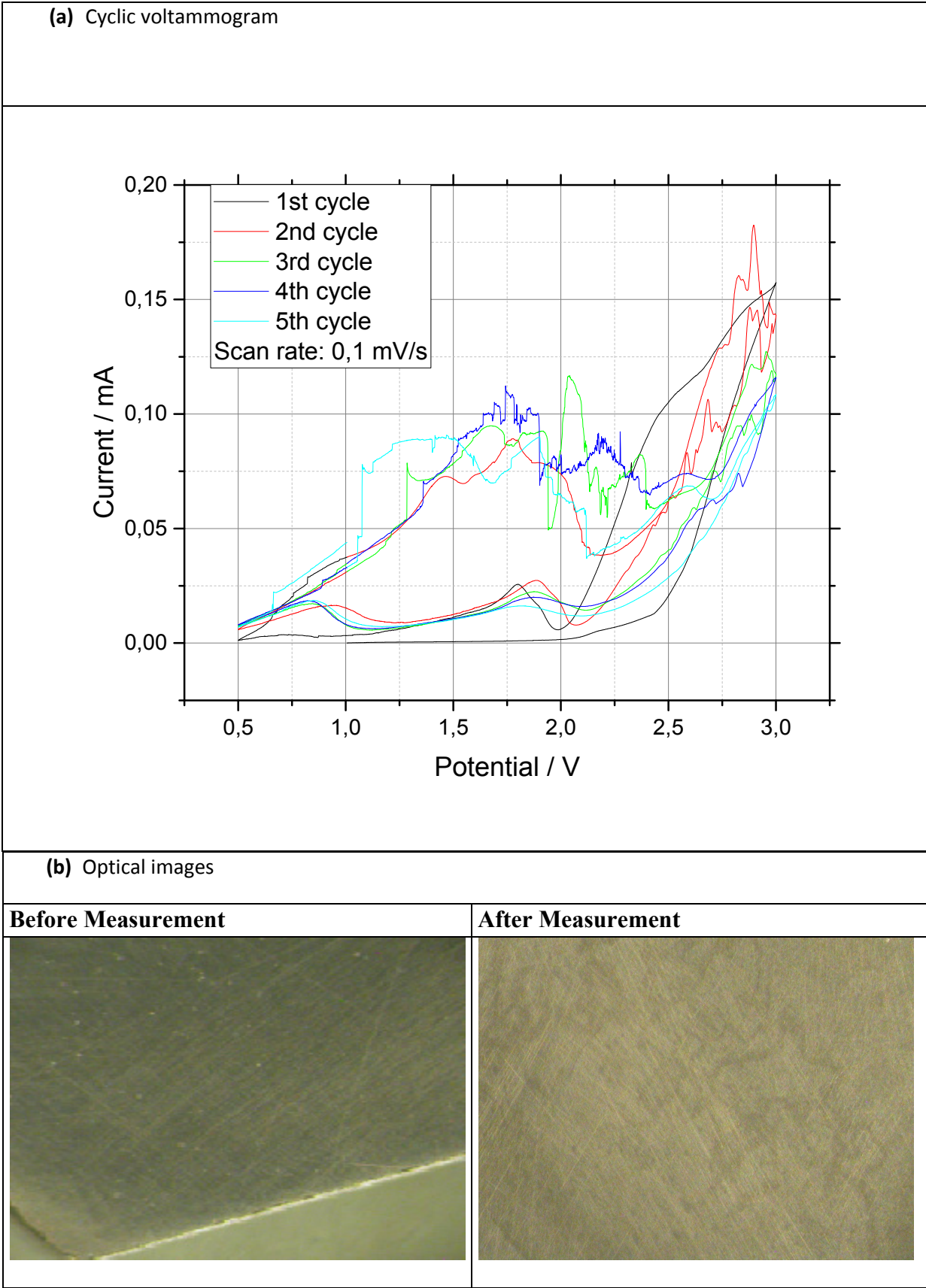


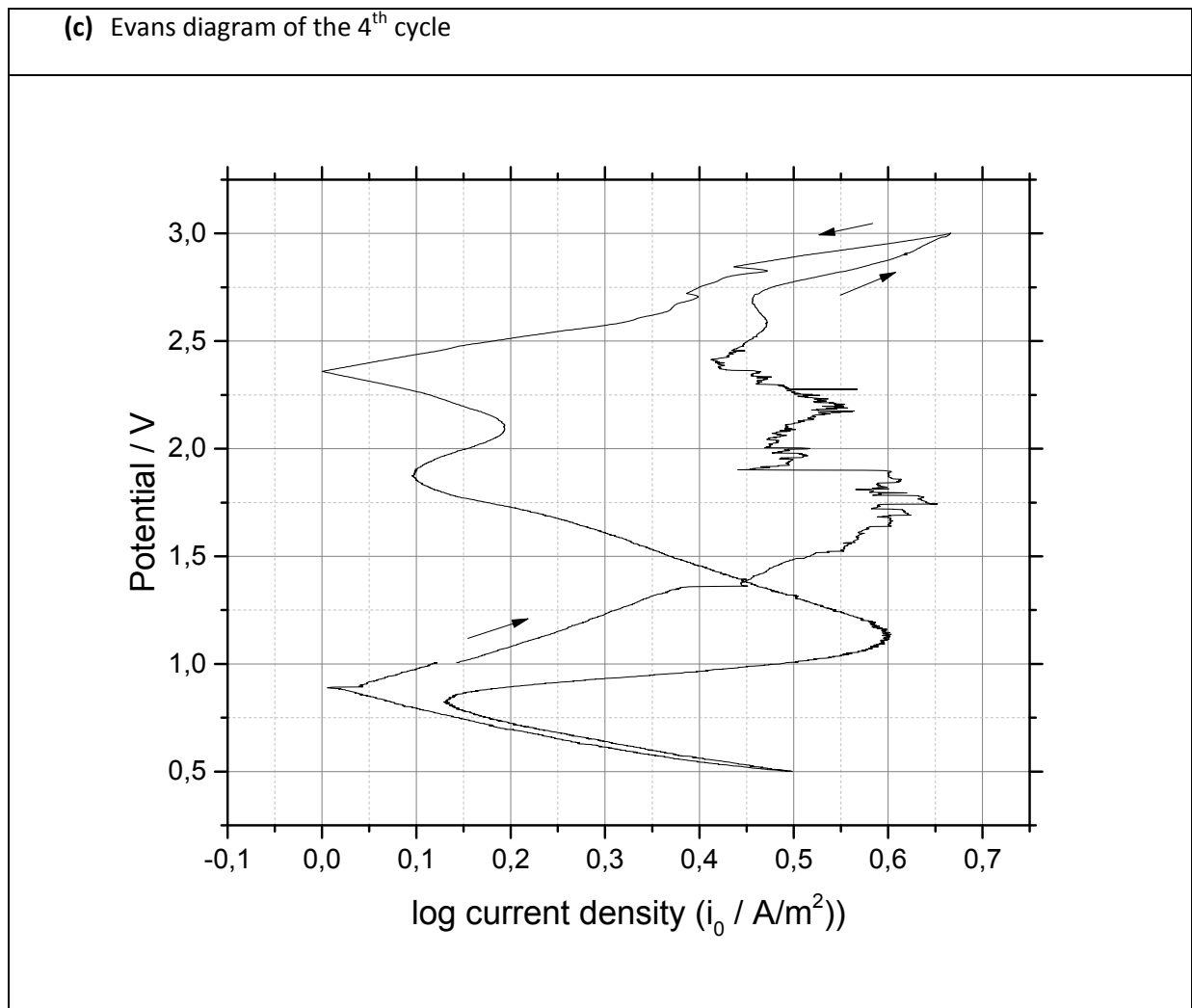
**Figure 31:** Stability test of carbon textile 2 with sorbent with APC electrolyte

Figure 31 shows chronoamperogram measured with carbon textile2. Fig.31 a) illustrates the current density decreased by holding potential at 3V. Figure 31 b) shows that in 110 hours the current density decreased to 0.005 mA. Fig.31 c) illustrates the linear plot that it was confirming the good stability of the carbon textile (2) current collector in the APC electrolyte.

## 2.1.4 Corrosion test with Mg-HMDS electrolyte

### 2.1.4.1 Glassy carbon with Mg-HMDS electrolyte



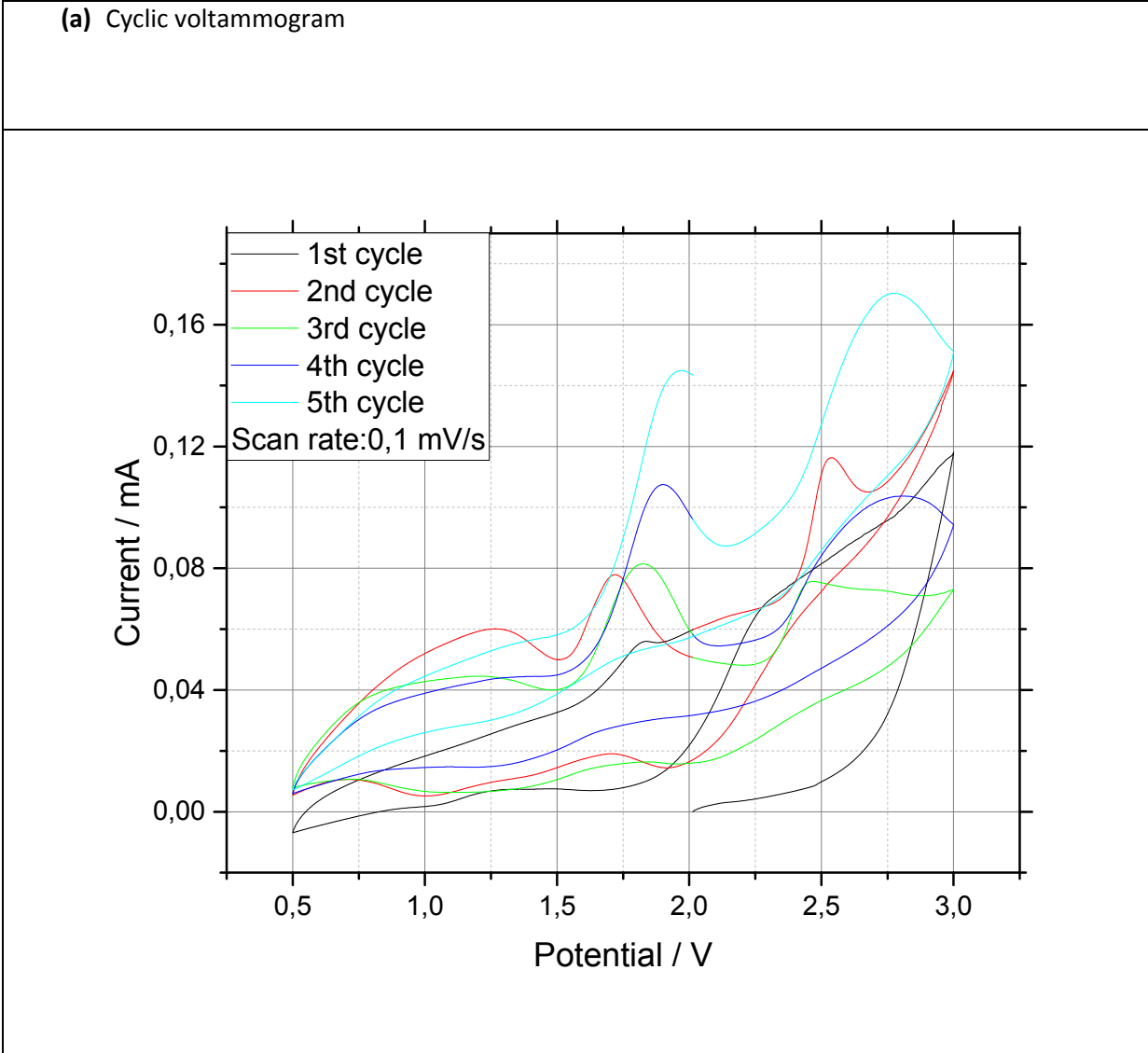


**Figure 32:** (a) Cyclic voltammogram, (b) optical microscope images and (c) Evans diagram of **glassy carbon** with Mg-HMDS electrolyte

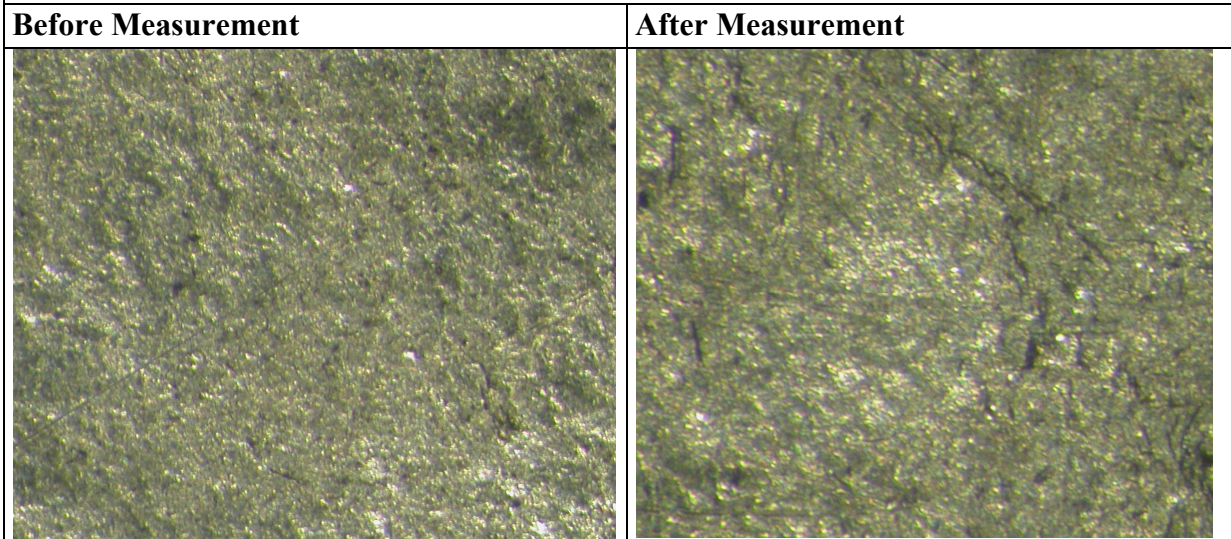
As it is mentioned above, the most stable current collectors with APC electrolyte were glassy carbon, graphite and nickel. They were also tested with Mg-HMDS electrolyte.

Figure 32 shows the cyclic voltammogram of glassy carbon which has the anodic current peak at 1.75V and the electrolyte decomposition starts at about 2.5V. The voltammogram (in the Figure 32 a)) illustrates the current was only positive so that there was corrosion current at all potentials. As a result, glassy carbon is acceptably stable with Mg-HMDS electrolyte.

2.1.4.2 Graphite foil with Mg-HMDS electrolyte



(b) Optical images



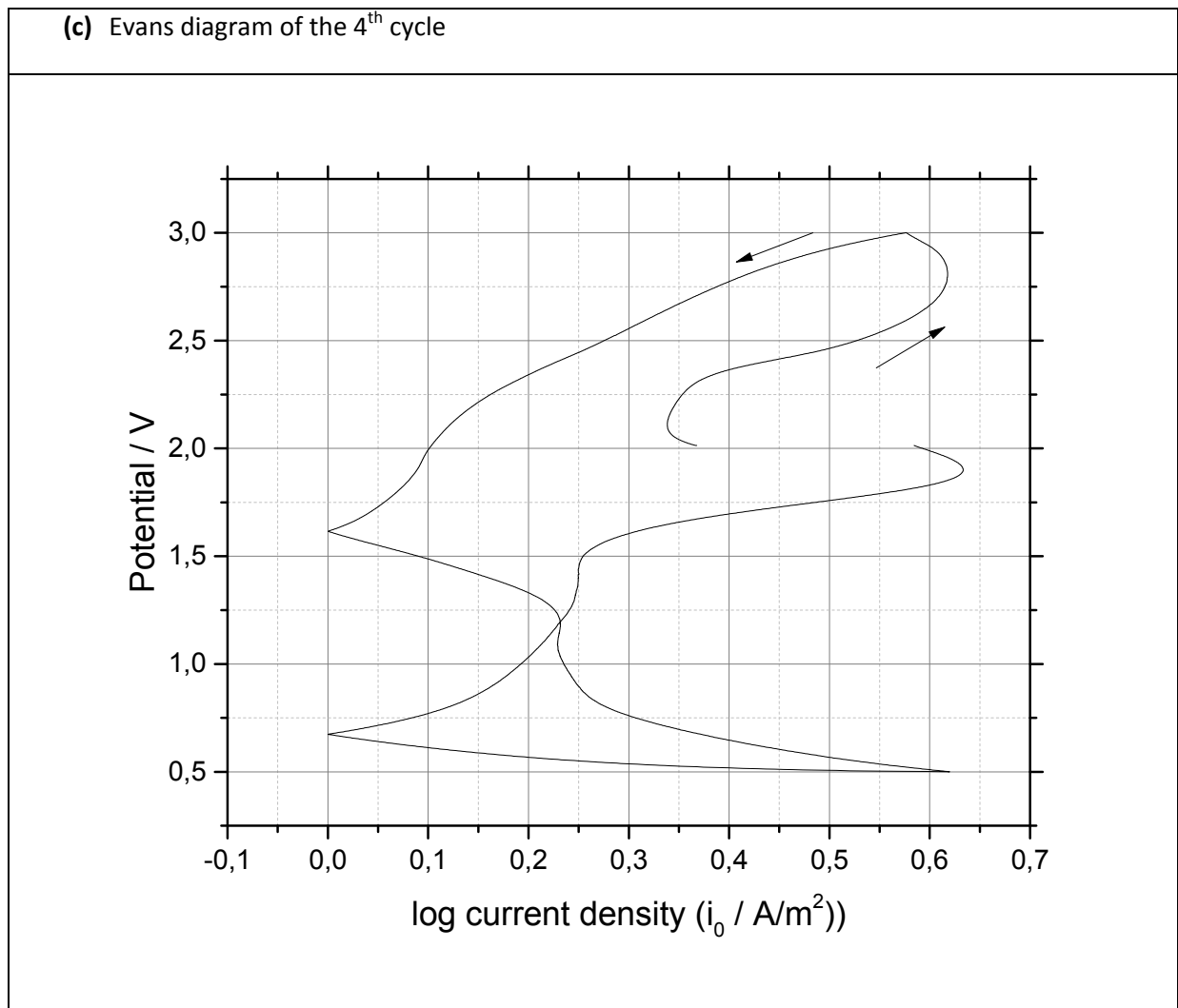
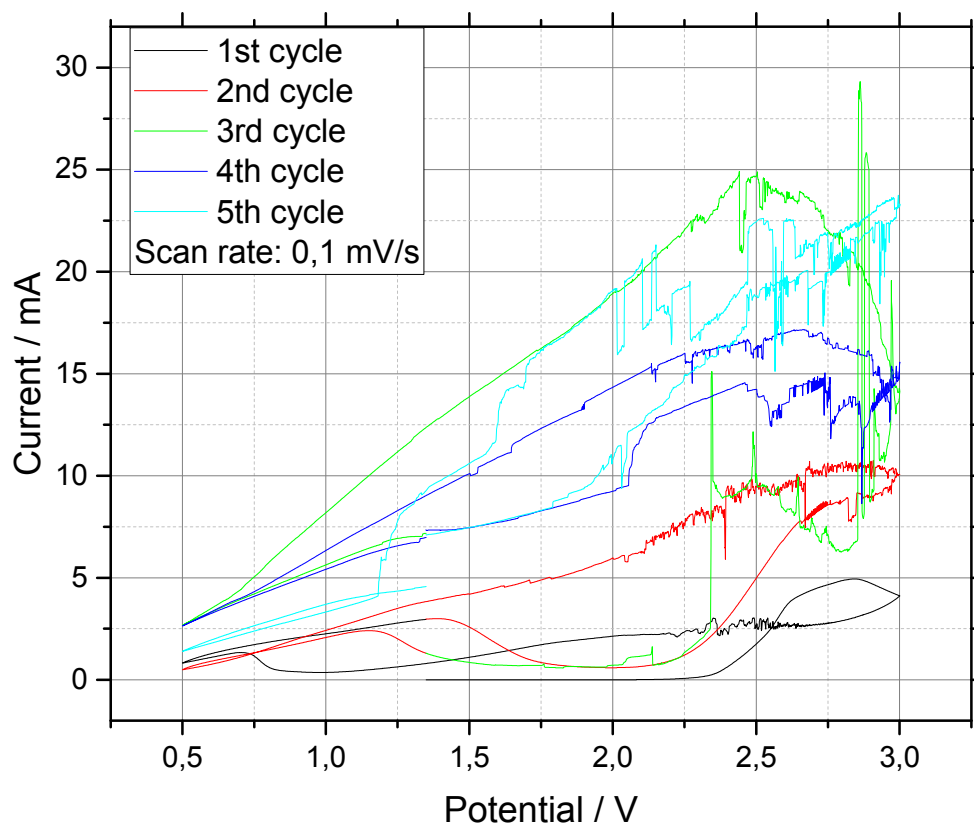


**Figure 33:** (a) Cyclic voltammogram, (b) optical microscope images and (c) Evans diagram of **graphite foil** with Mg-HMDS electrolyte

Figure 33 illustrates the cyclic voltammogram of graphite foil which behaves like glassy carbon. It has at about 1.80V the anodic current peak and the electrolyte decomposition starts at about 2.5V. The optical images of graphite foil in figure 33 b) before and after measurement shows also acceptably stability of graphite foil with this electrolyte. Cyclic voltammetry measurement (in the Figure 33 a)) presents the current was only positive and corrosion current was observed in the whole potential range. As a result, the graphite foil is equally stable with Mg-HMDS electrolyte than the glassy carbon.

### 2.1.4.3 Nickel foil with Mg-HMDS electrolyte

(a) Cyclic voltammogram



(b) Optical images

Before Measurement



After Measurement





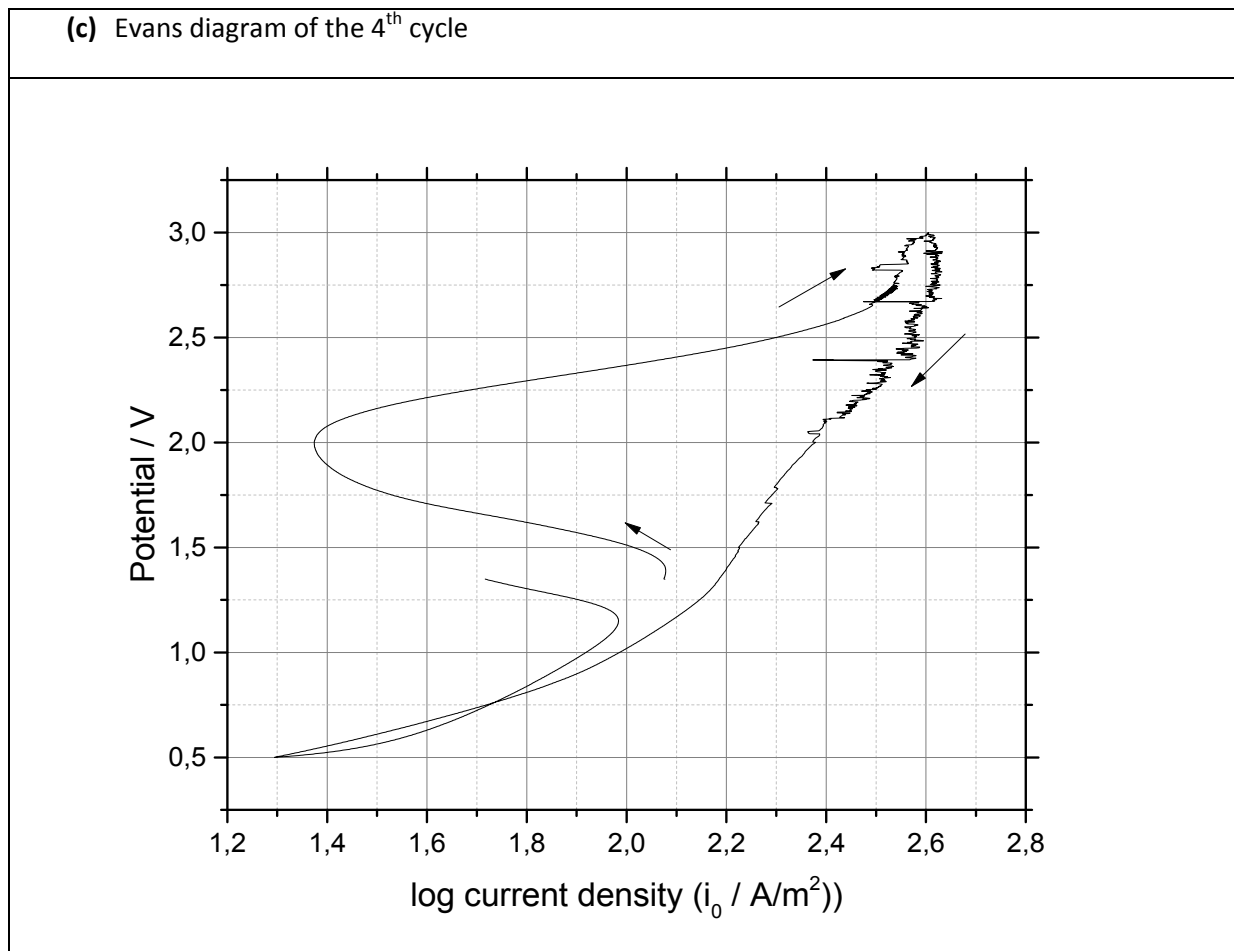


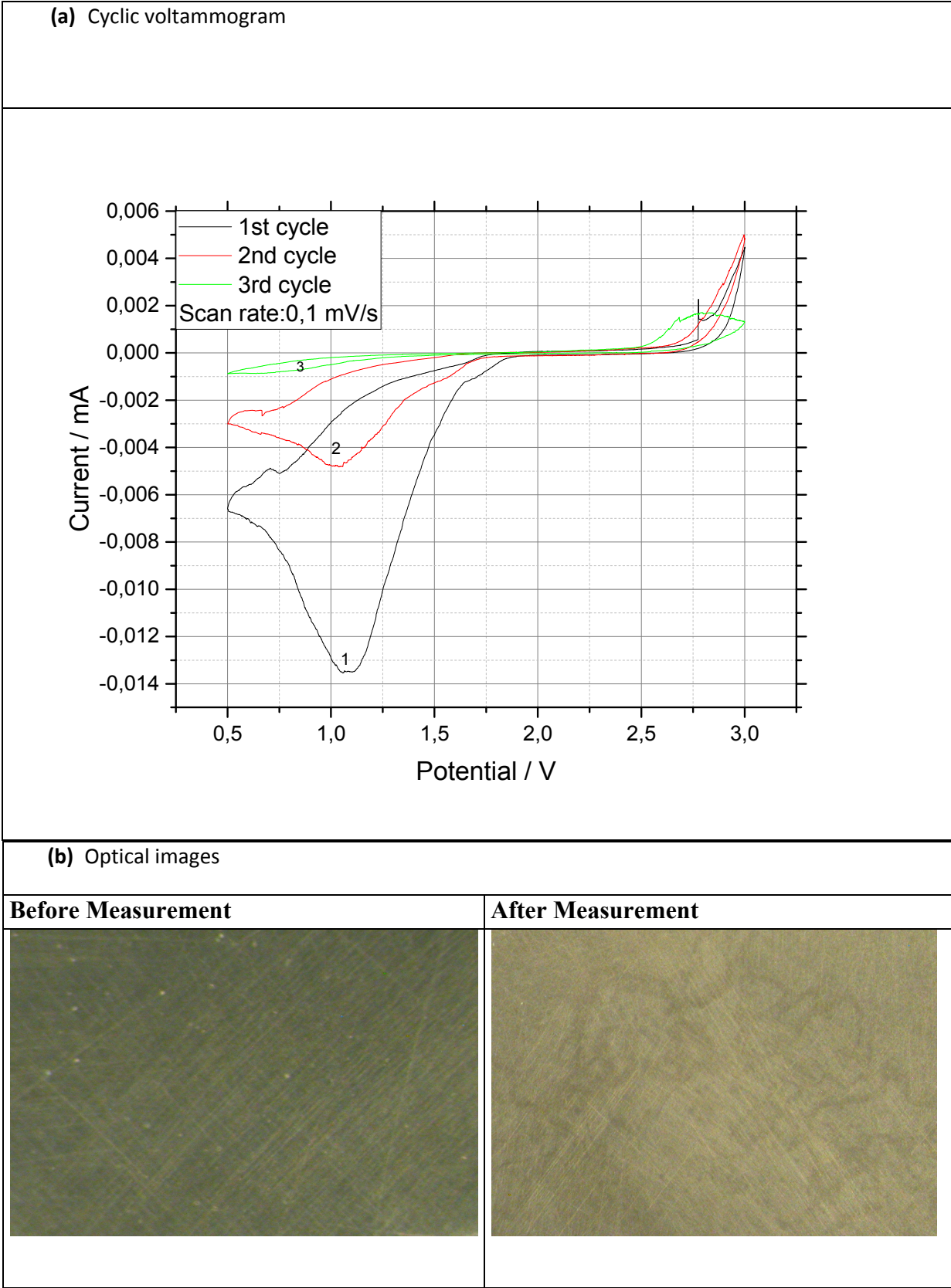
**Figure 34:** (a) Cyclic voltammogram, (b) optical microscope images and (c) Evans diagram of **nickel foil** with Mg-HMDS electrolyte

The cyclic voltammogram of nickel foil in figure 34a) shows the increase of current density due to the electrolyte decomposition and the current was only positive so that the nickel foil did not form a passivation layer on its surface. The electrodes were active and only the dissolution of the electrode was observed. As a result, the nickel foil is not stable with Mg-HMDS electrolyte.

According to the results of corrosion test with nickel foil, Ni is not a suitable current collector with Mg-HMDS electrolyte. Ni was also tested with active material coated, but there is no useful result as it has very corrosive behavior with this electrolyte. On the other hand, graphite foil is a bit more stable than glassy carbon current collector. As a result of the experiments, the best choice between these current collectors is the graphite foil with Mg-HMDS electrolyte. This electrolyte is in literature mostly used with graphite rods. At the end of these corrosion tests, the graphite foil was coated with manganese oxides as a cathode material and electrochemically examined.

## 2.1.5 Corrosion test with MACC electrolyte

### 2.1.5.1 Glassy carbon with MACC electrolyte



(c) Evans diagram of the 3<sup>rd</sup> cycle

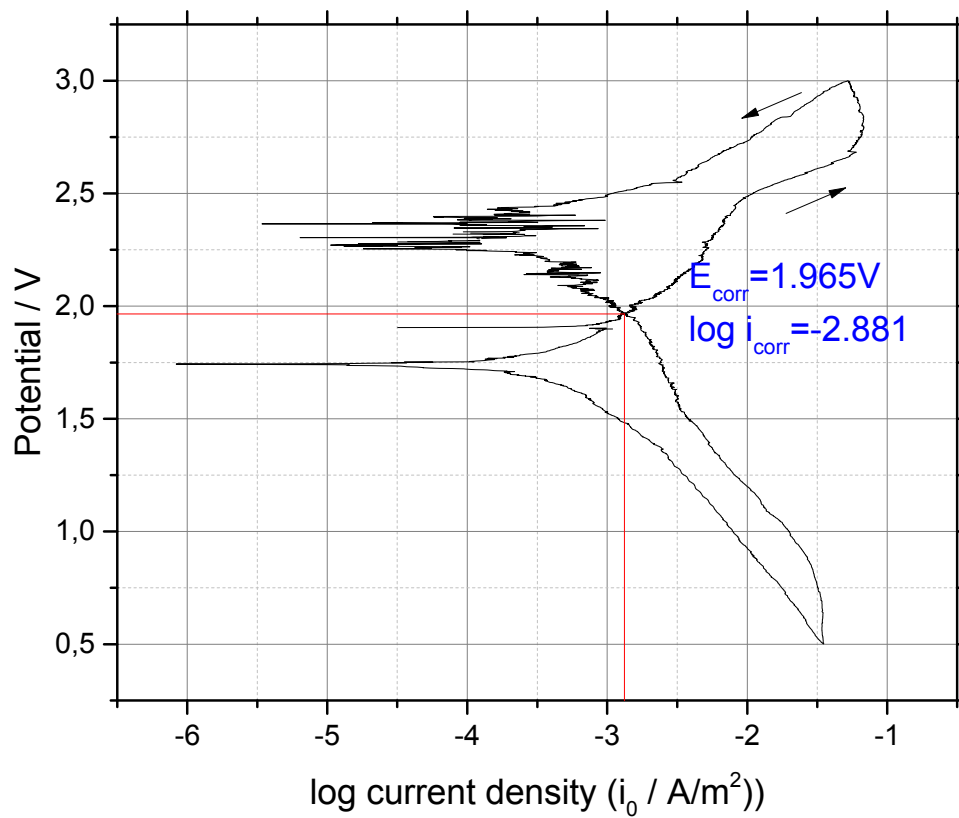


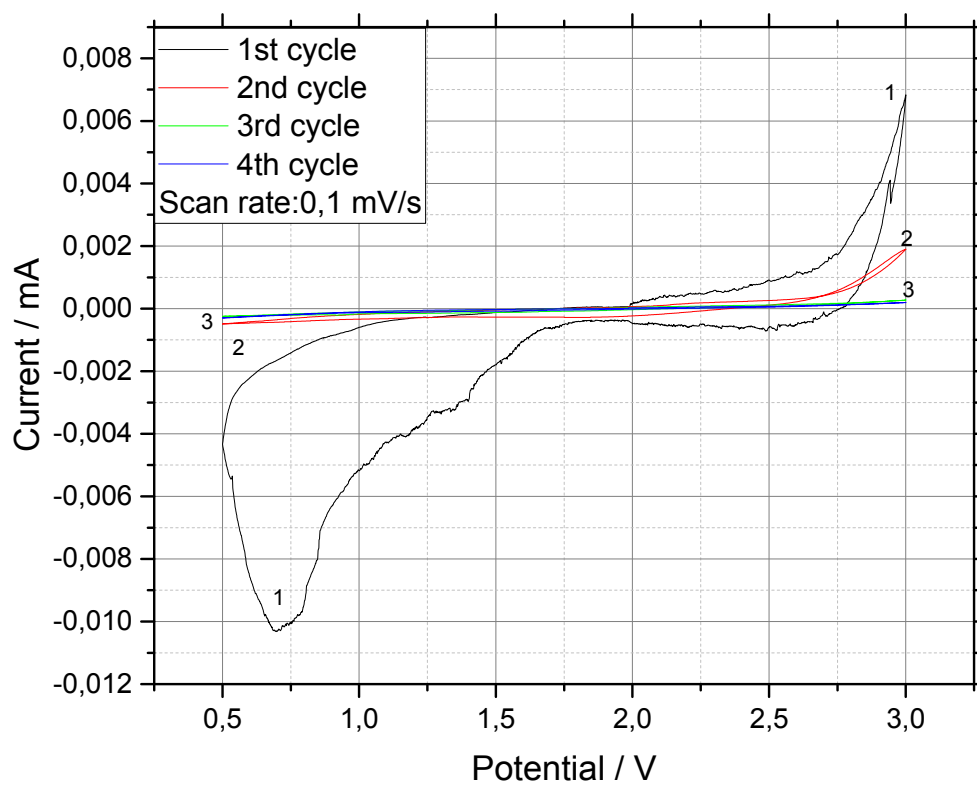
**Figure 35:** (a) Cyclic voltammogram, (b) optical microscope images and (c) Evans diagram of **glassy carbon** with MACC electrolyte

Glassy carbon, nickel and graphite were also measured in MACC electrolyte.

Figure 35 a) shows cyclic voltammogram of a 30 mM 1:2 DME-MACC electrolyte on a glassy carbon working electrode. As a result, the glassy carbon is stable up to 3V with this electrolyte as a current collector. Figure 35 c) Evans diagram exhibits that, the corrosion potential is 1.965V and the  $\lg(\text{corrosion current density}/ \text{A/m}^2)$  is -2.881.

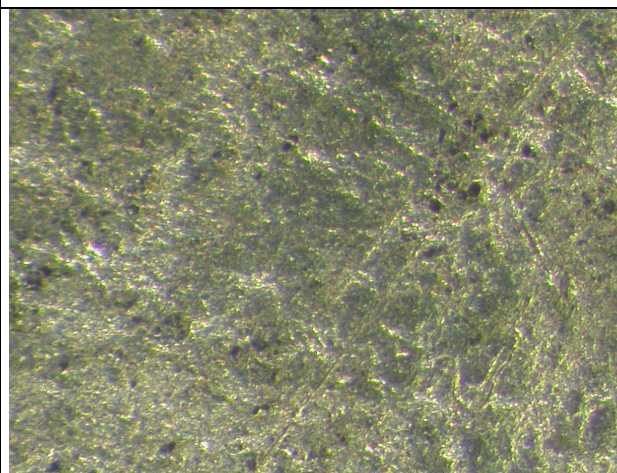
### 2.1.5.2 Graphite foil with MACC electrolyte

(a) Cyclic voltammogram

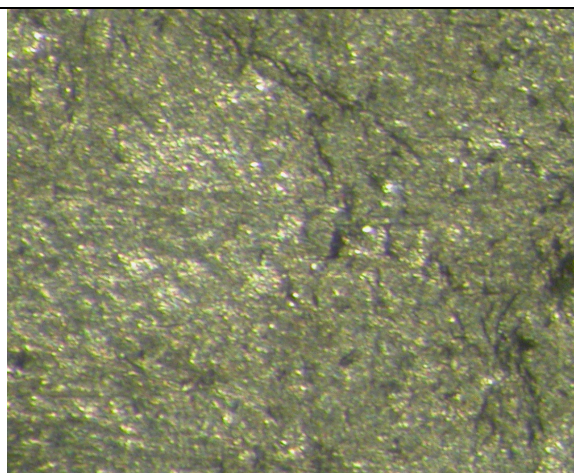


(b) Optical images

Before Measurement



After Measurement



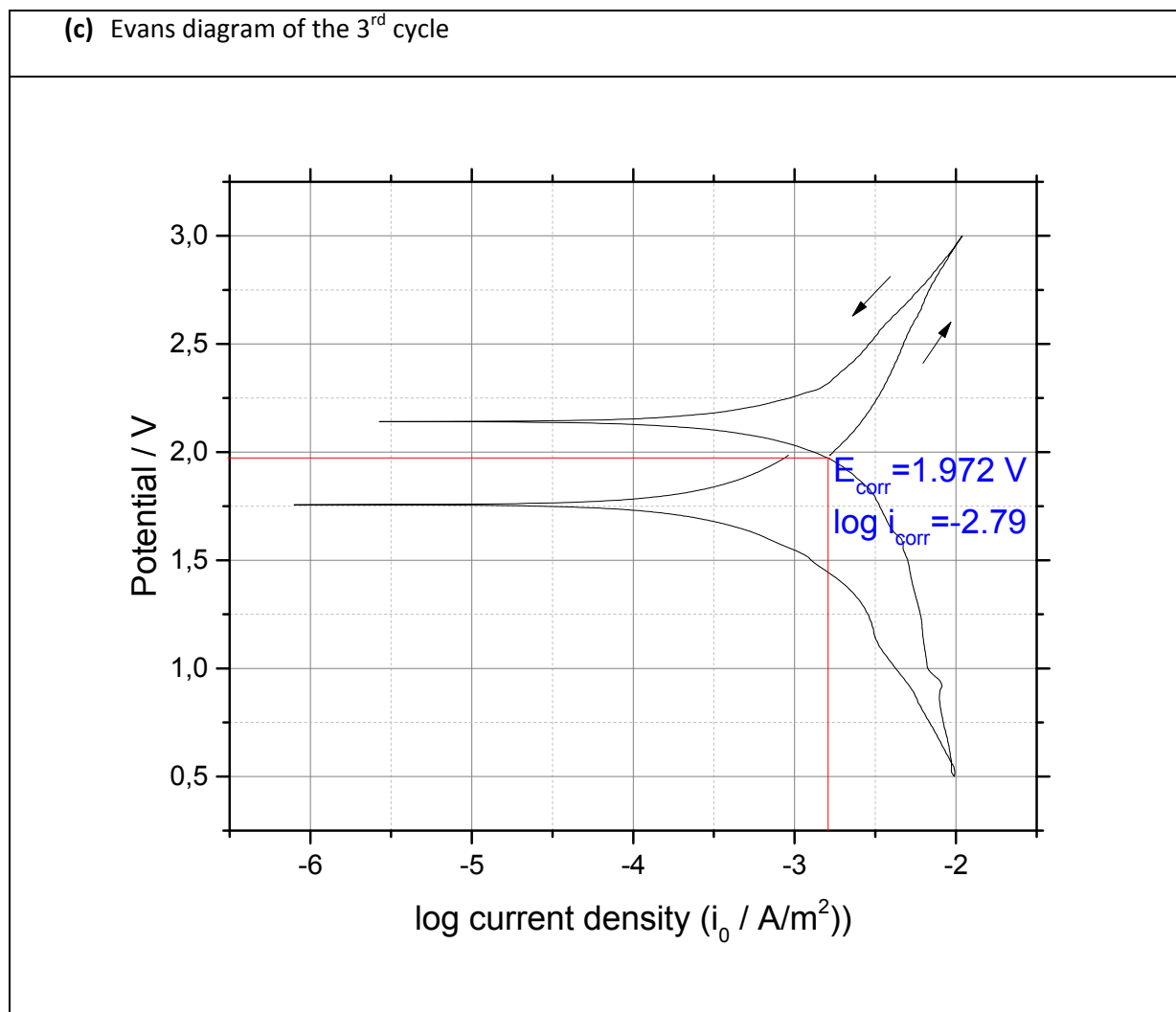
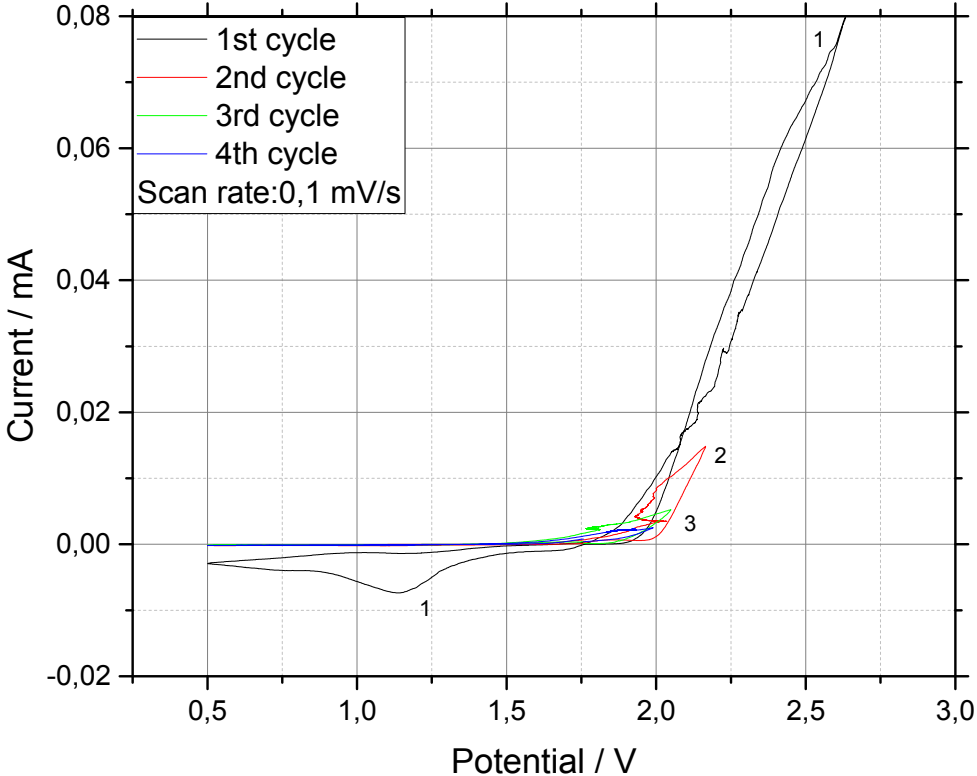


**Figure 36:** (a) Cyclic voltammogram, (b) optical microscope images and (c) Evans diagram of **graphite foil** with MACC electrolyte

Figure 36 a) illustrates cyclic voltammograms of a 30 mM 1:2 DME-MACC electrolyte on a graphite foil working electrode. The graphite foil shows (like glassy carbon) high stability up to 3V with this electrolyte as a current collector. Figure 36 c) Evans diagram shows that, the corrosion potential is 1.97V and the  $\lg(\text{corrosion current density}/ \text{A/m}^2)$  is -2.79.

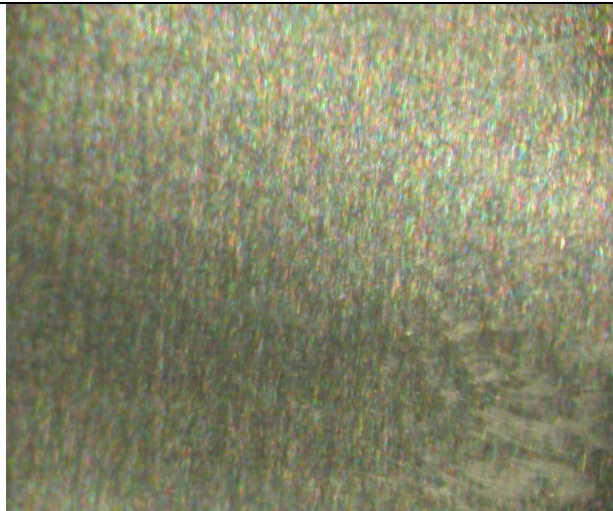
2.1.5.3 Nickel foil with MACC electrolyte

(a) Cyclic voltammogram

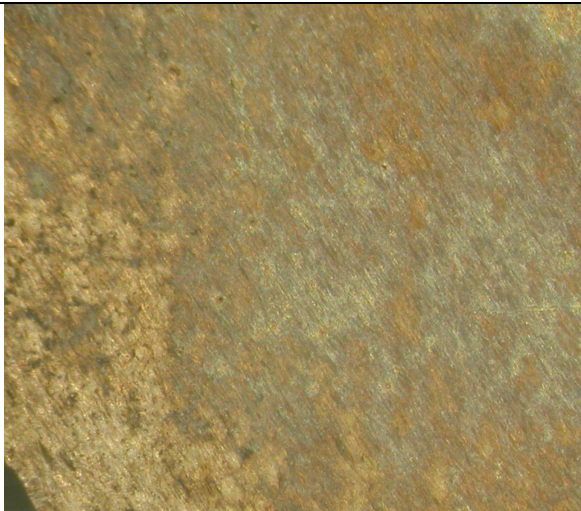


(b) Optical images

Before Measurement



After Measurement



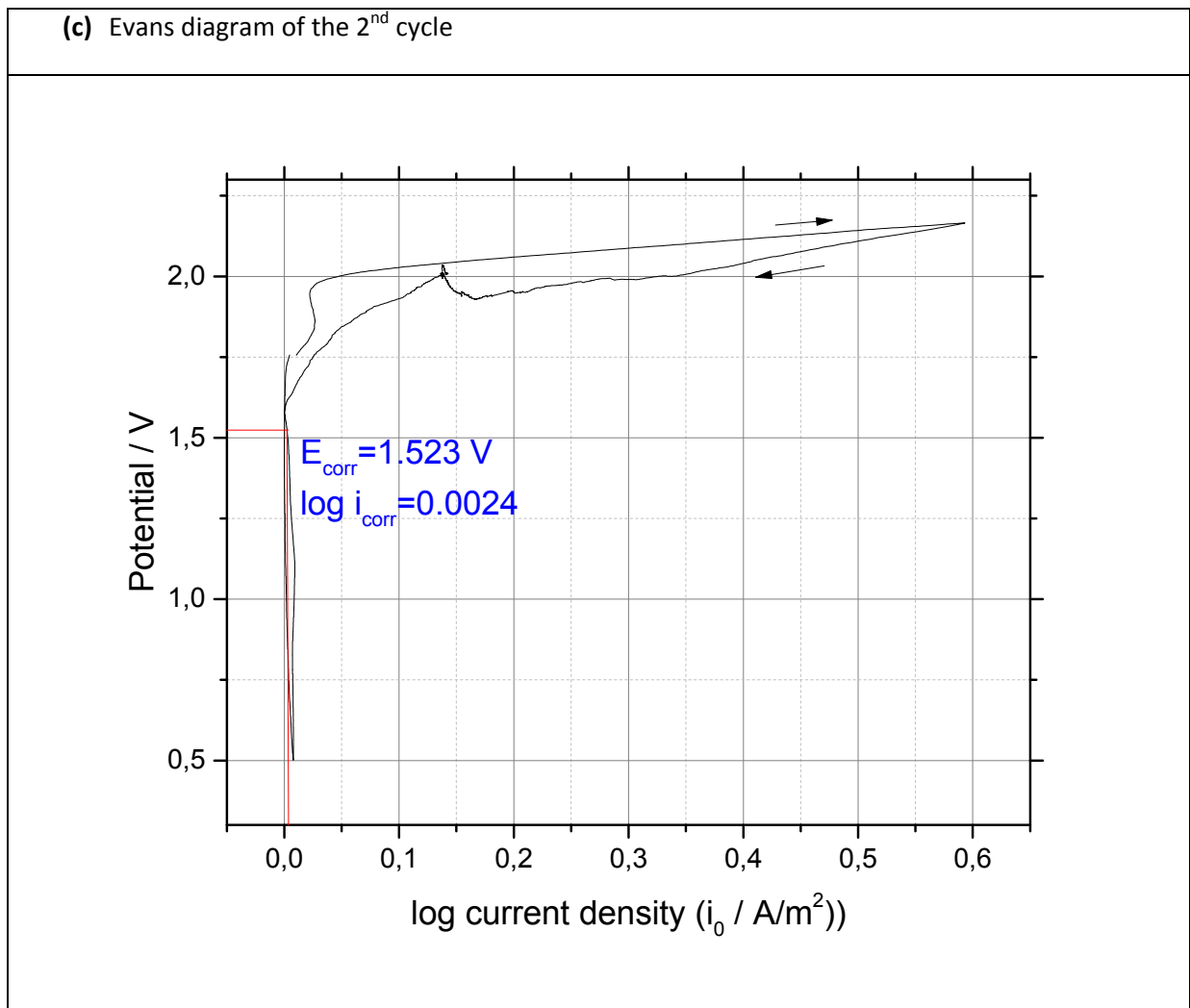


**Figure 37:** (a) Cyclic voltammogram, (b) optical microscope images and (c) Evans diagram of nickel foil with MACC electrolyte

Both carbon based materials showed relatively good corrosion resistance but nickel dissolved quickly above at about 2V. As the figure 37 a) cyclic voltammogram shows that Ni could not reach 3V. Therefore nickel is not suitable as a current collector in this electrolyte.

## 2.2 Electrochemical performance of cathode materials

In this part, several cathode materials were investigated with the selected current collectors. Some of them are synthesized materials and some are commercial materials. Unfortunately, most of the materials are electrochemically inactive for Mg-intercalation. Hereby, only the best results are illustrated.

### 2.1.2 Electrodes preparation

The electrodes were prepared by two different methods. Slurry coating method was used for foils and dry electrode technique was applied for meshes. As an ingredient, the only difference was that in slurry polyvinylidene fluoride (PVDF) as a polymer binder and in dry electrodes polytetrafluoroethylene (PTFE) was utilized.

#### 2.2.1.1 Slurry

Slurry was prepared with 75 wt %  $\alpha\text{MnO}_2$  (99,8%, Erachem Comilog, Inc.), 15 wt% conductive carbon black (Timcal) and 10 wt % PVDF. At first, the active material and the carbon black were pulverized 30 minutes with 2 repetitions by the planetary ball mill. The slurry was made by suspending the mixture in 1-methyl-2-pyrrolidinone (NMP) and was cast on the graphite foil (current collector) using an adjustable micrometer film applicator. The same procedure was examined on Ni and carbon textile, but the best performance was obtained with graphite. After drying in an oven overnight, the electrodes were cut and vacuum dried at 120 °C for 12 hours. Coin cells were used, with Mg foil (Alfa Aesar) as counter and reference electrodes, 0.2 M Mg-HMDS in tetrahydrofuran as an electrolyte, and a Whatsmann© separator. All cells were assembled in an Ar-filled glove box and electrochemical properties were measured by using a potentiostat (MACCOR) for the charge- discharge tests and EClab Biologic multichannel potentiostat for the cyclic voltammogram.



### 2.2.1.2 Dry electrode

As it is previously mentioned, the main difference to slurry technique is the type of polymer binder. The electrodes were pressed into pellets by a pressing tool. All other procedures for manufacturing of the cell are the same.

### 2.1.4 Comparison of results with literature

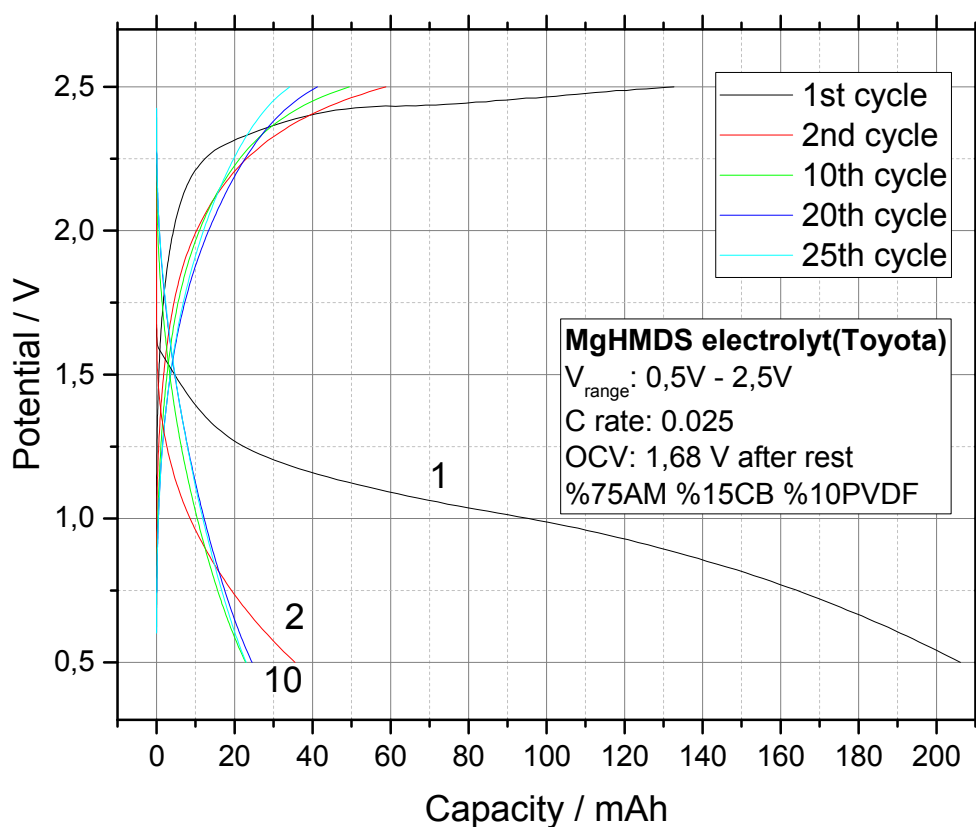


**Figure 38:** Charge-discharge test of  $\alpha$ -MnO<sub>2</sub> at 0.025 C rate

The first discharge (Mg insertion) yielded a capacity of about 205 mAh g<sup>-1</sup>. The first charge capacity was 140 mAh g<sup>-1</sup> with a coulombic efficiency of 69%. The first charge and discharge curves show clear plateaus but the following discharge and recharge curves do not show

clear plateaus. As in Figure 8 illustrated, Zhang et al. described that  $\alpha\text{MnO}_2$  provides a specific capacity  $\sim 280$  mAh/g during the 1st discharge cycle using Mg-HMDS electrolyte [43]. Significant capacity loss for hollandite  $\text{MnO}_2$  has also been observed with nearly 50% capacity lost between the first and second cycles. However, the capacity loss is nearly 80% in the measurement shown in Fig. 35. The first reason for the capacity loss can be the instability of the crystal structure because of the Jahn-Teller distortion [58]. Another possibility for the capacity loss might be the dissolution of Mn into the electrolyte. Furthermore, the morphology and particle size also have significant influences on the performance of  $\text{Mg}^{2+}$  insertion. Zhang et al. mentioned that  $\alpha\text{-MnO}_2$  with 20 nm average particle size showed 280 mAh/g while 100 nm particles only showed 170 mAh/g for the discharge capacity in the 1<sup>st</sup> cycle [43].

## 4 CONCLUSION

---

One fundamental problem for high voltage (>3V) magnesium battery operation is the corrosion of current collectors. For this reason, in this thesis corrosion tests were carried out for different materials for the current collectors. The electrochemical stability of current collectors in three types of protic organic solvents was analyzed. In the first part, electrochemical behaviors of ten different current collectors were investigated with the promising APC electrolyte. From the results of cyclic voltammograms, the most stable current collectors; glassy carbon (reference), nickel, graphite foil and carbon textile 2 were selected and stability tests were also carried out by chronoamperometry method. The potential of the working electrode was hold and the current was measured versus time. The observed current drop was interpreted as the formation of a passivation film on the surface of the current collector. Then the selected current collectors (Ni, graphite and carbon textile 2) were also electrochemically examined with Mg-HMDS and MACC electrolyte. Ni showed better stability with APC electrolyte than with Mg-HMDS and MACC electrolytes. As a second step of the experiments, several cells with different electrolytes, current collectors and cathode materials were electrochemically analyzed; however, only the best one was presented. The positive electrodes for the magnesium cells with  $\alpha$ -MnO<sub>2</sub> as active material were prepared with the selected current collectors. Two types of coating techniques, slurry and dry electrode preparation were implemented. The best result was obtained with the graphite foil current collector which was coated with  $\alpha$ -MnO<sub>2</sub> as an active material. However, the cell did not show good cyclic stability as significant capacity loss was observed.

## References

- [1] Linden, D.; Reddy, T. B. *Handbook of Batteries*, 4th ed.; McGraw-Hill: New York, **2011**, Ch.9.
- [2] Yoo, H.-D.; Shterenberg, I.; Gofer, Y.; Gershinshy, G.; Pour, N.; Aurbach, D. *Energy Environ. Sci.* **2013**, *6*, 2265.
- [3] Xu, K. *Chem. Rev.* **2004**, *104*, 4303.
- [4] Y.Nishi, in: M. Wahikara, O. Yamamoto (Eds.), *Li-ion Batteries*, Wiley/VCH, Weinheim, **1998** (Chapter 18) and references therein.
- [5] Zu C.-X.; Li H.; *Energy Environ. Sci.* **2011**, *4*, 2614–2624.
- [6] Scrosati B.; Hassoun J.; Sun Y., *Energy Environ. Sci.*, **2011**, *4*, 3287–3295.
- [7] Crowther O.; West A. C.; *J. Electrochem. Soc.*, **2008**, *155*, A806–A811.
- [8] Chan C. K.; Peng H.; Liu G.; McIlwrath K.; Zhang X. F.; Huggins R. A.; Cui Y.; *Nat. Nanotechnol.*, **2008**, *3*, 31–35.
- [9] Yamaki J.; Tobishima S.; *Handbook of battery materials*, ed. Besenhard, J. O., Wiley-VCH Verlag GmbH, Weinheim, 1st ed., **2007**, ch. 15, pp. 339–357.
- [10] Aurbach D.; Cohen Y.; Moshkovich M.; *Electrochem. Solid-State Lett.*, **2001**, *4*, A113–A116.
- [11] Aurbach, D.; Suresh, G. S.; Levi, E.; Mitelman, A.; Mizrahi, O.; Chusid, O.; Brunelli, M. *Adv. Mater.* **2007**, *19*, 4260.
- [12] Aydinol M.K.; Ceder G.J., *J. Electrochem. Soc.*, *144*, **1997**, 3832
- [13] Gregory, T. D.; Hoffman, R. J.; Winterton, R. C. *J. Electrochem Soc.* **1990**, *137*, 775.
- [14] Amir N.; Vestfrid Y.; Chusid O.; Gofer Y.; Aurbach D.; *J. Power Sources* **2007**, *174*, 1234-1240.
- [15] Aurbach D.; Gofer Y.; Lu Z.; Schechter A.; Chusid O.; Gizbar H.; Cohen Y.; Ashkenazi V.; Moshkovich M.; Turgeman R.; E. Levi, **2001**, *J. Power Sources* *97–8*.
- [16] Aurbach, D.; Weissman, I.; Gofer, Y.; Levi, E. *Chem. Rec.* **2003**, *3*, 61.
- [17] Lu Z.; Schechter A.; Moshkovich M.; Aurbach D.; *J. Electroanal. Chem.* **466** **1999**, 203.
- [18] Gregory Thomas D.; Hoffman Ronald J.; Winterton R.C.; *J. Electrochem. Soc* **1990**, *137*, 775-780.
- [19] Aurbach D.; Moshkovich M.; Schechter A.; Turgeman R.; *Electrochem. Solid-State*

*Lett.* **3** **2000**, 31-34.

[20] Mizrahi O.; Amir N.; Pollak E.; Chusid O.; Marks V.; Gottlieb H.; Larush L.; Zinigrad E.; Aurbach, D.; *J. Electrochem. Soc.* **155** **2008**, A103 - A109

[21] Aurbach, D.; Gizbar, H.; Schechter, A.; Chusid, O.; Gottlieb, H. E.; Gofer, Y.; Goldberg, I. *J. Electrochem. Soc.* **2002**, *149*, A115.

[22] AIT Austrian Institute of Technology, Projektdokumentation, FFG Projektnummer 840457

[23] Aurbach D.; Lu Z.; Schechter A.; Gofer Y.; Gizbar C.; Turgeman R.; Cohen Y.; Moshkovich M.; Levi E., *Nature (London)*, **2000**, 407, 724.

[24] Kim, H. S.; Arthur, T. S.; Allred, G. D.; Zajicek, J.; Newman, J. G.; Rodnyansky, A. E.; Oliver, A. G.; Boggess, W. C.; Muldoon, J. *Nat. Commun.* **2011**, *2*, 427.

[25] Zhao-Karger, Z.; Zhao, X.; Fuhr, O.; Fichtner, M. *RSC Adv.* **2013**, *3*, 16330.

[26] Liebenow C., Yang Z.; Lobitz P.; *Electrochem. Commun.*, **2000**, 2,641–645.

[27] Liu, T.; Shao, Y.; Li, G.; Gu, M.; Hu, J.; Xu, S.; Nie, Z.; Chen, X.; Wang, C.; Liu, J. *J. Mater. Chem. A* **2014**, *2*, 3430.

[28] Muldoon J.; Bucur C. B.; Oliver A. G.; Sugimoto T.; Matsui M.; Kim H. S.; Allred G. D.; Zajicek J.; Kotani Y., *Energy Environ. Sci.*, **2012**, *5*, 5941.

[29] Doe, R. E.; Han, R.; Hwang, J.; Gmitter, A. J.; Shterenberg, I.; Yoo, H. D.; Pour, N.; Aurbach, D. *Novel, Electrolyte Solutions Comprising Fully Inorganic Salts with High Anodic Stability for Rechargeable Magnesium Batteries*. *Chem. Commun.* **2014**, *50*, 243– 245.

[30] Vestfried Y.; Chusid O.; Goffer Y.; Aped P.; Aurbach D.; *Organometallics*, **2007**, *26*, 3130–3137.

[31] Vestfried Y.; Levi M. D.; Gofer Y.; Aurbach, D.; *J. Electroanal. Chem.*, **2005**, *576*, 183–195.

[32] Mohtadi R.; Mizuno F.; *Beilstein J. Nanotechnol.* **2014**, *5*, 1291–1311.

[33] Lu, Z.; Schechter, A.; Moshkovich, M.; Aurbach, D. *J. Electroanal. Chem.* **1999**, *466*, 203.

[34] Aurbach D.; Weissman I.; Gofer Y.; Levi E.; *Chem. Rec.* **2003**, *3*, 61.

[35] Levi E.; Mitelman A.; Aurbach D.; Brunelli M.; *Chem. Mater.* **19** **2007**, 5131–5142.

[36] Peng B.; Liang J.; Tao Z.; Chen J.; *J. Mater. Chem.* **19** **2009**, 2877.

[37] Levi E.; Gershinsky G.; Aurbach D.; Isnard O.; *Inorg. Chem.* **48** **2009** 8751–8758.

[38] Feng Z. Z.; Nuli Y.; Wang J. L.; Yang J.; *J. Electrochem. Soc.*, **2006**, *153*, C689.

- [39] Kumagai, N.; Komaba, S.; Sakai, H.; Kumagai, N. *J. Power Sources* **2001**, 97–98, 515.
- [40] Lee H.Y.; Goodenough J.B.; *J. Solid State Chem.* 144, **1999**, 220–223.
- [41] Devaraj S.; Munichandraiah N.; *J. Phys. Chem. C* 112, **2008**, 4406–4417.
- [42] Zhang R.; Yu X.; Nam K-W.; Ling C.; Arthur T.S.; Song W.;  *$\alpha$ -MnO<sub>2</sub> as a cathode material for rechargeable Mg batteries. *Electrochem Commun** **2012**, 23, 110–3.
- [43] Song Wei, Arthur Timothy Sean, Bucur Claudiu, Matsui Masaki, Muldoon John, Singh Nikhilendra, et al., *High voltage rechargeable magnesium cell*, **2013**.
- [44] ASTM G15, Standard Terminology Relating to Corrosion and Corrosion Testing, *Annual Book of Standards*, ASTM, Philadelphia, **1993**, Ch11.
- [45] Akid Robert, *Corrosion of Engineering Materials*, **2003**, 355, 137-143.
- [46] J. G. N. Thomas, G. Hinds, *The electrochemistry of corrosion*, **2002**.
- [47] Heineman, W. R.; Kissinger, P. T. Large-Amplitude Controlled-Potential Techniques. In *Laboratory Techniques in Electroanalytical Chemistry*; Kissinger, P. T., Heineman, W. R., Eds.; Monographs in Electroanalytical Chemistry and Electrochemistry; Marcel Dekker: New York, NY, **1984**, 51-127.
- [48] Bard Allen J.; Faulkner Larry R.; *Electrochemical Methods: Fundamentals and Applications*, **2001**, 239-242.
- [49] Bard, A. J.; Faulkner, L. R. *Electrochemical Methods*; Wiley: New York, NY, **1980**; Chapter 6.
- [50] <http://de.slideshare.net/BrianMuldoon1/brian-presentation-55439301> , **20.10.2016**.
- [51] Davies T.J.; Banks C.E.; Compton R.G.; *J. Solid State Electrochem.* 9, 797–808, **2005**
- [52] Kissinger P. T.; Heineman W. R.; “Cyclic Voltammetry,” *Journal of Chemical Education*, **1983**, 60, 702.
- [53] Skoog, D.; Holler, F.; Crouch, S. *Principles of Instrumental Analysis* **2007**
- [54] Baboian R.; Sheldon W. Dean; Harvey P. Hack; *Corrosion Tests and Standards: Applications and Interpretation*, **2005**, 235.
- [55] Zhao S.; Wu F.; Yang L.; Gao L.; Burke A.; *A measurement method for determination of dc internal resistance of batteries and supercapacitors. *Electrochemistry Communications**, **2010**, v.12, 242-245.
- [56] Burke A.; Miller J.R.. *Electric Vehicle Capacitor Test Procedures Manual. Idaho National Engineering Laboratory Report*, October **1994**, 7.

- [57] [http://battery.berkeley.edu/Unprotected/9\\_27\\_07\\_PerformanceMetrics2.pdf](http://battery.berkeley.edu/Unprotected/9_27_07_PerformanceMetrics2.pdf) , **22.09.2016**
- [58] Thackeray M.M.; *Progress in Solid State Chemistry* 25, **1997**, 1.
- [59] Hamann C.H.; Hamnett A.; Vielstich W.; *Electrochemistry 2nd Edition*, Wiley-VCH, **2007**, 8.
- [60] Revie R.W.; Uhlig H.H.; *Corrosion and Corrosion Control*, Wiley, **2008**, 221.
- [61] Pollock M., *Grafoil Engineering Design Manual*, **2002**, 33-36